Investigation, Identification and Mitigation of Harmonic Distortions in Power Systems

by

Yang Wang

A thesis submitted in partial fulfillment of the requirements for the degree of

Doctor of Philosophy

in

Energy Systems

Department of Electrical and Computer Engineering
University of Alberta

Abstract

Harmonic distortion has always been an important power quality concern for utilities and customers. In recent years, a wide variety of harmonic-producing loads, ranging from home appliances to industrial equipment, is being connected to power systems due to rapid advancement in power electronic technology. These harmonic sources can be grouped into two categories – distributed harmonic sources and concentrated harmonic sources.

Distributed harmonic sources are associated with small power-electronic-based loads such as home appliances and office equipment. They are located randomly in distribution systems. Based on extensive field measurements and analysis, this thesis reveals the harmonic distortion characteristics in current distribution systems, especially those supplying residential customers. A main impact of increased harmonic sources is the system-capacitor resonance. This thesis further proposes a scheme to damp harmonic resonance for multiple switchable capacitors using a shared damping block. This damping block is designed in such a way that it will provide adequate damping capability for all possible on/off combinations of the capacitors involved. Performance and effectiveness of the proposed scheme are demonstrated through the comparative study on actual capacitor application cases.

Concentrated harmonic sources are those industrial and commercial facilities that contain a large amount of nonlinear loads. When a harmonic problem occurs in a system with several such facilities as suspects, the first step is to determine

which loads cause the harmonic problem. The second part of this thesis presents two measurement-based methods that can quantify the respective harmonic contributions of multiple concentrated harmonic sources to a harmonic problem. The first method is based on multiple linear regression (MLR). The second method advances the MLR-based method by including synchronized harmonic phasor data and by adopting independent component analysis (ICA). Performances of these methods have been demonstrated using simulation verifications, lab experiments and field measurements. The proposed methods are expected to become useful tools for power quality management.

Preface

Chapter 2 of this thesis has been published as Y. Wang, J. Yong, Y. Sun, W. Xu and D. Wong, "Characteristics of Harmonic Distortions in Residential Distribution Systems," in *IEEE Transactions on Power Delivery*, vol. 32, no. 3, pp. 1495-1504, June 2017. I was responsible for the field measurement, data analysis and the manuscript composition. Dr. Jing Yong and Dr. Yuanyuan Sun were responsible for the data analysis and the manuscript composition. Dr. Wilsun Xu supervised the work. Daniel Wong provided feedbacks to improve the manuscript.

Chapter 3 of this thesis is ready to submit as Y. Wang and W. Xu, “A Shared Damping Scheme for Multiple Switchable Capacitors”, to be submitted.

Chapter 4 of this thesis has been published as Y. Wang, H. E. Mazin, W. Xu and B. Huang, "Estimating Harmonic Impact of Individual Loads Using Multiple Linear Regression Analysis", in *International Transactions on Electrical Energy Systems*, vol. 26, no. 4, pp. 809-824, Apr. 2016. I proposed the idea, conducted the verification studies and composed the manuscript. Dr. Hooman E. Mazin initiated the research and helped me improve the simulation code. Dr. Wilsun Xu supervised the work. Dr. Biao Huang provided the supervisions on the statistical algorithms.

Chapter 5 of this thesis has been published as Y. Wang, W. Xu, J. Yong and K. Chen, "Estimating Harmonic Impact of Individual Loads Using Harmonic Phasor Data", in *International Transactions on Electrical Energy Systems*, accepted on May 7th, 2017, in press. I proposed the idea, conducted the verification studies and composed the manuscript. Dr. Wilsun Xu supervised the work, provided the guidance and revised the manuscript. Dr. Jing Yong provided feedbacks to improve the manuscript. Dr. Kun-Long Chen helped conduct the lab experiment.

Acknowledgement

I would like to express my deepest appreciation to my supervisor, Dr. Wilsun Xu. The joy and enthusiasm he has for his research was contagious and motivated me to transfer form master to Ph.D. program. I appreciate all his contributions of time, ideas, and funding to make my Ph.D. experience productive and stimulating. I will always be proud to say I had the privilege of being his student, and I hope to have learned enough to succeed in my future career.

It is an honor for me to extend my thanks to other professors from my PhD examining committee, Dr. Hao Liang, Dr. Greg Kish, Dr. Jose Marti, and Dr. Horacio Marquez, for reviewing my thesis and providing invaluable comments.

I also thank all my friends and colleagues in the PDS-LAB for their help and company. Special thanks go to Dr. Jing Yong for her selfless help during various stages of this project.

Finally and most importantly, I would like to express my gratitude for my parents Longye Wang and Yachun Yang, who have always been patient, supportive and caring.

Contents

List of Tables

List of Figures

List of Symbols

h	Harmonic order
I_h	h-th harmonic current
I_{hi}	h-th harmonic current measured at the PCC of Load i
I_{hiU}	h-th system harmonic current seen at the PCC of Load i
I_{hiL}	h-th load harmonic current seen at the PCC of Load i
$I_{h,ST}$	h-th service transformer harmonic current
$I_{h,Sub}$	h-th substation (feeder) harmonic current
I_L	The maximum load current
I_F	The fundamental current
V_h	h-th harmonic voltage
V_{hX}	h-th harmonic voltage at Bus X
V_{hXi}	h-th harmonic voltage at Bus X induced by Load i
V_{hX0}	h-th background harmonic voltage at Bus X
V_{hXi-f}	Projection of V_{hXi} on V_{hX}
β_{hiX}	The phase angle between V_{hXi} and V_{hX}
φ_h	Phase angle of h-th harmonic current
φ_{FV}	Phase angle of the fundamental voltage
$\varphi_{I_{h,ST}}$	Phase angle of h-th service transformer harmonic current
$\varphi_{I_{h,Sub}}$	Phase angle of h-th feeder harmonic current
ρ_h	The normalized in-phase component of the h-th harmonic
$C_{(.)}$	Capacitor
$L_{(.)}$	Inductor
$R_{(.)}$	Resistor

$X_{(.)}$	Reactance
$f_{(.)}$	Frequency
$P_{(.)}$	Active power
$Q_{(.)}$	Reactive power
$Z_{(.)}$	Impedance
Z_{hXi}	h-th harmonic transfer impedance between Load i and Bus X
Z_{hiU}	h-th system harmonic impedance seen at the PCC of Load i
Z_{hiL}	h-th load harmonic impedance seen at the PCC of Load i
$\omega_{(.)}$	Angular frequency
ω_F	Fundamental angular frequency
ω_T	Tuning angular frequency
x	Explanatory variables
y	Responsible variables
r	Correlation coefficient
r^2	Coefficient of determination

List of Abbreviations

PQ	Power Quality
LV	Low Voltage
MV	Medium Voltage
HV	High Voltage
PCC	Point of Common Coupling
DFT	Discrete Fourier Transform
FFT	Fast Fourier Transform
MLR	Multiple Linear Regression
MSE	Mean Square Error
ICA	Independent Component Analysis
IDD	Individual Demand Distortion
TDD	Total Demand Distortion
CT	Current Transformer
IHD	Individual Harmonic Distortion
THD	Total Harmonic Distortion
3^{rd}HP	Third Order High Pass
HAR	Harmonic Amplification Ratio
CI	Confidence Interval
HSE	Harmonic State Estimation
HC	Harmonic Contribution
GPS	Global Positioning System
SPM	Synchronized Phasor Measurement
PMU	Phasor Measurement Unit
BSS	Blind Source Separation

Chapter 1

Introduction

Power systems are designed to operate at one frequency, either 50Hz or 60Hz. However, certain type of loads such as power-electronic-based devices produce currents at frequencies that are integer multiple of the fundamental frequency called harmonic currents. When harmonics are combined with the fundamental frequency component, waveform distortions are caused. Harmonic distortions adversely affect both power system components and customers' devices. Therefore, it has always been one of the main power quality concerns since the adoption of alternating current for electric energy transmission. Nowadays, driven by the desire to have more energy efficient equipment and greater control of equipment operation, utility customers are increasingly adopting power-electronic-based devices for industrial, commercial or residential purposes. This trend has increased the concerns about harmonic distortions, which can become considerable and exceed today's allowable limits.

In this introductory chapter, an overview of the harmonics in the modern power systems is presented. Then, the harmonic problems needed to be addressed in this thesis are discussed. Finally, this chapter presents the scope and outline of this thesis.

1.1 Harmonics in Modern Power Systems

At present, the harmonic distortions in power systems are mainly caused by two types of harmonic sources – concentrated harmonic sources and distributed harmonic sources. Concentrated harmonic sources are those industrial and commercial facilities with large amounts of nonlinear loads such as variable frequency drives, uninterruptable power supplies and switch mode power supplies. These harmonic sources are concentrated and connected to the utility grid through

a point of common coupling (PCC). In the past few decades, concentrated harmonic sources have received a great deal of attention from both industry and research communities due to their excessive harmonic production. A lot of effort, including developing effective harmonic mitigating techniques [1]-[6], establishing reasonable interconnection standards [7]-[9], and designing advanced loads with lower harmonic productions [10]-[13], have been devoted to controlling the harmonic distortion from them. To date, although concentrated harmonic sources are still causing problems due to some practical issues such as ineffective harmonic mitigation and the growth of harmonic loads, the progress is going well with the joint efforts from all communities.

Distributed harmonic sources are associated with small power-electronic-based loads such as home appliances and office equipment. These harmonic sources are located randomly in distribution systems. In recent years, the number of distributed harmonic sources is growing rapidly due to energy efficiency considerations. One of the consequences is the increased harmonic distortions in residential distribution systems and its supply transmission systems. Various literature has been published to analyze and address this issue. Paper [14]-[20] presented harmonic characteristics of conventional home appliances and techniques to assess the impact of multiple random harmonic sources. Paper [21]-[25] developed harmonic models for low voltage (LV) harmonic emitting devices and [26]-[29] proposed the harmonic mitigation method for residential systems. In response to such issue, IEEE recently established a working group to push for the adoption of the IEC 61000-3-2 [30] appliance or device level harmonic limits. Although this is a very effective solution to the problem, the progress has been slow due to the strong resistance of appliance manufacturers.

In spite of the above activities and results, both industry and research communities have some doubts on the severity of harmonic distortions in residential distribution systems since there is no systematic field data to confirm or disapprove the claims. Many believe that the harmonics from various home appliances can largely cancel out among themselves. Others believe that new

generation PWM-switching based home appliances have negligible contributions to harmonics. Unless clarified, such controversies may result in an overlook of harmonic issues in residential distribution systems. There is a definite need to investigate the harmonic distortions in current residential distribution systems using systematic field data.

1.2 Harmonic Resonance Mitigation

A main impact of increased harmonic sources is the system-capacitor resonance. Shunt capacitors are the most commonly used reactive power compensation apparatus in power systems. Connected between a bus and ground, the capacitor injects capacitive reactive power into the system. It can boost the bus voltage, improve power factor, and/or reduce power loss. Although shunt capacitors do not generate harmonics, they provide a network path for possible resonance conditions. Figure 1.1 illustrates the causes of parallel resonance caused by the shunt capacitor. The system impedance seen at the capacitor interconnection location is approximately represented by the transformer impedance. The inductive impedance of the system increases and the capacitive impedance of the capacitor decreases as the frequency increases. A resonance occurs when the capacitor' capacitive impedance is approximately equal to the system's inductive impedance at a particular frequency, such as 300Hz. If the system has a current or voltage source at 300Hz, the resonance can be excited. This situation can lead to significant amplification of the 300Hz voltage/current and eventual damage to the capacitors. There is a high probability that other electrical equipment in the system would also be damaged.

In recent years, the proliferation of harmonic sources significantly increases the possibility and severity of system-capacitor resonance. Many incidents of system-capacitor resonance have been reported in the literature. Paper [31] documented the industry experience on a capacitor resonance case in BC Hydro transmission network. Paper [32][33] presented the harmonic resonance cases associated with the shunt capacitors in medium voltage (MV) distribution systems.

Paper [34] reported a resonance-induced failure of LV shunt capacitors used in the textile industrial.

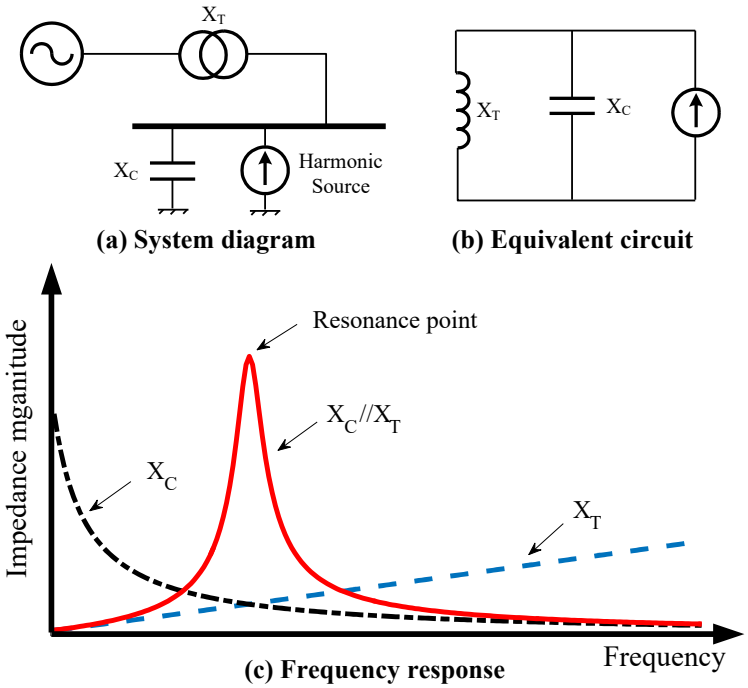

Figure 1.1 Parallel resonance caused by the shunt capacitor

To mitigate the system-capacitor resonance, typical solutions are adding a resonance-mitigation element such as a detuned inductor to the shunt capacitor [35]-[39]. However, such elements are developed for individual capacitors. It is common that the application of shunt capacitors involves multiple switchable capacitor banks. Capacitors are switched on or off according to the reactive power requirement of the system. Therefore, each of the switchable capacitors requires a resonance-mitigation element. The cost and space requirements for such resonance-mitigation methods increase with the number of switchable capacitors. In view of this situation, there is a need to research cost-effective resonance-mitigation methods for multiple switchable capacitors.

1.3 Harmonic Source Identification

Besides of the harmonic resonance, there are many situations that the high

levels of harmonic distortions are caused by harmonic sources themselves [40]-[44]. When a harmonic problem occurs in a system with several concentrated harmonic sources as suspects, the first step is to determine which loads cause the problem. Appropriate actions can be taken by the utility or the customer only after the major harmonic source is identified correctly. Such harmonic source identification problem can be generally described by using the diagram shown in Figure 1.2. Typically, a harmonic problem is reported at Bus X by a customer. The host utility company is aware that the system contains several concentrated harmonic sources with large harmonic-producing capability. Examples are Loads A, B and C. The utility company has reasonable grounds to believe that the harmonic problem at Bus X is caused by either or all of Loads A, B and C.

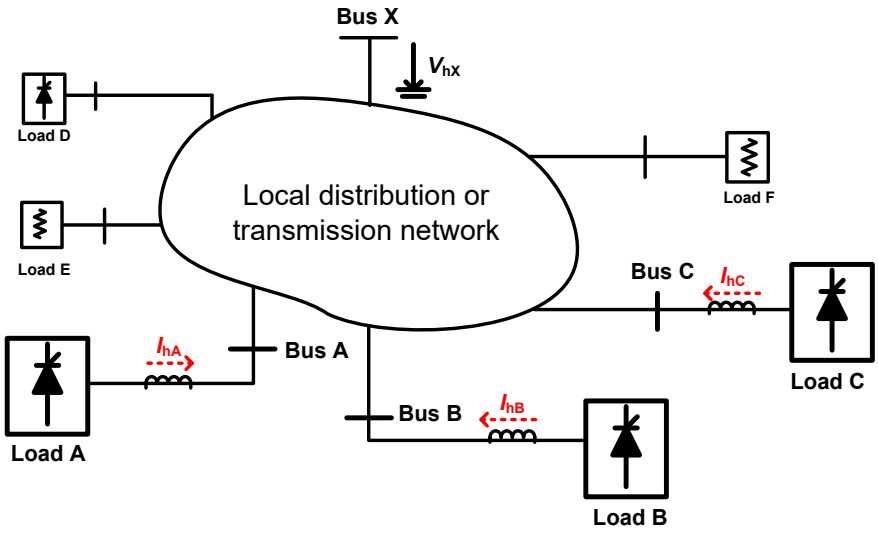

Figure 1.2 A generic diagram for harmonic source identification problem

The objective is to determine which load is making the most significant contribution to the harmonic problem at Bus X. Mathematically, the problem can be formulated by using (1.1),

$$F(X) = f(A) + f(B) + f(C) + f(S) \tag{1.1}$$

where $F(X)$ is an index that represents the harmonic problem at Bus X, $f(A)$, $f(B)$ and $f(C)$ indicate the contribution of each load to $F(X)$, $f(S)$ is the contribution from the rest of the harmonic sources in the system that are not measured. The

objective here is to quantify $f(A)$, $f(B)$, $f(C)$ and $f(S)$ in order to assign responsibilities and find proper solutions for harmonic mitigation. It should be emphasized that the suspected concentrated harmonic sources are not limited to those industrial or commercial facilities. For example, the harmonic source identification problem shown in Figure 1.3 aims to determine which distribution system contributes most to the harmonic voltage at Bus X. Therefore, the suspects in this case are the distribution systems, which represent the aggregation of the harmonic sources in their downstream.

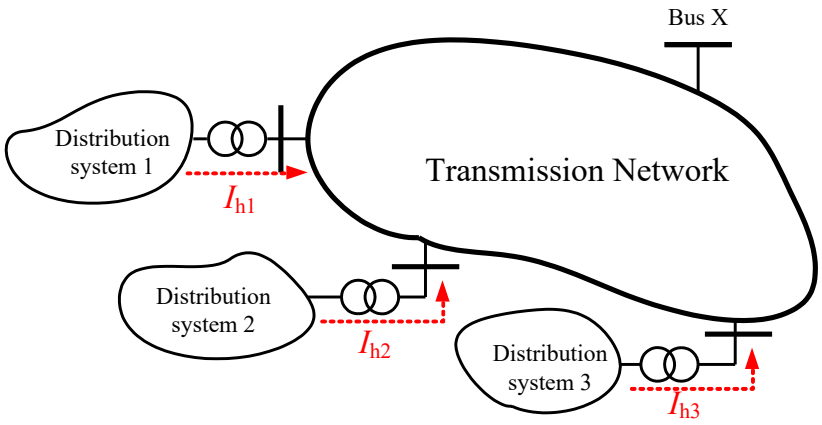

Figure 1.3 Harmonic source identification problem in transmission system.

Previous studies have suggested some solutions for harmonic source identification [45]-[49]. However, most of them are model-based. Such methods are theoretically sound, but not very useful in practice since the adequate system model at the harmonic frequency of interest is normally not attainable. Accordingly, measurement-based methods are a better option for this problem. Due to increased installation of power quality monitors in power systems and the increased capabilities of such monitors, measurement-based methods are more likely to provide useful solutions. In other words, the emerging hardware platform has made them not only theoretically attractive, but also practically sound.

1.4 Thesis Scope and Outline

The scope of this thesis is to investigate, identify and mitigate harmonic

distortions in power systems. More specifically, this thesis aims to solve the following problems:

(1) What are the harmonic distortion characteristics in current residential distribution systems? Are the harmonic distortions caused by massive home appliances truly a concern for the utility and customers?

(2) How to cost-effectively mitigate harmonic resonance for multiple switchable capacitors?

(3) When a harmonic problem occurs in a system with several concentrated harmonic sources as suspects, how to timely and accurately identify the major source that causes the problem?

In order to address the concerns highlighted in the above questions, this thesis introduces several new methodologies and also conducts supporting technical studies. The following paragraphs summarize the organization of the thesis and describe the main topics and research discussed in each chapter.

Chapter 2 investigates the harmonic distortion characteristics in residential distribution systems based on extensive field measurements, ranging from multiple homes, multiple service transformers and multiple feeders. Statistical methods are applied to those data to find out the magnitude and phase angle distribution of harmonic currents. The results at different system locations are compared with each other to show the degree of harmonic addition/cancellation. The harmonic addition/cancellation effects are further quantified by conducting synchronized phasor measurements at two locations of one feeder. Furthermore, a comparative study on the harmonic distortion characteristics of residential, commercial and industrial feeders is conducted to show the severity of harmonic distortions in residential distribution system. Finally, some existing power quality issues in residential distribution systems are discussed.

A main impact of increased harmonic sources is the system-capacitor resonance. Chapter 3 further proposes a scheme to mitigate harmonic resonance

for multiple switchable capacitors. In the proposed scheme, multiple switchable capacitors share one damping block. This damping block is designed in such a way that it will provide adequate damping capability for all possible on/off combinations of the capacitors involved. The chapter first develops the design method to realize the proposed scheme. Comparative studies on actual capacitor application cases are then conducted to evaluate its performance. Finally, as the proposed design method does not require any system information, a standard set values of component parameters are calculated for direct industry use.

Chapter 4 and Chapter 5 focus on the harmonic source identification problem. In Chapter 4, a magnitude-data-based method is proposed. The basic idea is to use multiple linear regression (MLR) technique to study the cause-and-effect relationship between the harmonic current magnitude of a customer and the harmonic voltage magnitude of the concern. Simulation and field case studies are presented in this chapter to show the effectiveness of the MLR-based method. Additionally, some practical considerations such as the fluctuation of background harmonic voltage are fully considered.

Chapter 5 further improves the research in Chapter 4. An independent-component-analysis (ICA)-based method is proposed for harmonic source identification. This method utilizes the same information as the MLR-based method, but requires the data to be synchronized phasor measurements. The simulation verification and the lab experiment are presented in this chapter to demonstrate the feasibility of the ICA-based method. Moreover, comparative studies between the MLR-based method and the ICA-based method are conducted to show the strength and weakness of two methods.

Finally, this thesis's main conclusions and suggestions for future research in this field are summarized in Chapter 6.

Chapter 2

Characteristics of Harmonic Distortions in Residential Distribution Systems

A dramatic penetration of modern nonlinear electronic devices into the regularly used home appliances has resulted in increased harmonic distortions in residential distribution systems. Unless appropriately addressed, such noticeable increase of harmonic pollutions might potentially cause several problems for utility companies and customers. Unlike the industrial or commercial cases, residential harmonic sources are randomly dispersed through the whole system. Each of the several distributed nonlinear loads individually creates harmonic currents that propagate through the feeders collectively causing different degrees of harmonic distortions along a distribution feeder. This unique random and distributed nature makes it difficult to understand and evaluate general harmonic characteristics in residential distribution systems. In recent years, with the efforts of several field measurement activities, a large volume of data has been collected from different locations and periods. In this chapter, systematic analysis for these data are presented for the purpose to reveal general harmonic distortion characteristics of residential distribution systems.

The chapter is organized as follows. Section 2.1 describes the field measurement activities. Section 2.2 presents the magnitude characteristics, phase angle distributions of harmonic currents injected from residential houses. Section 2.3 presents the magnitude characteristics, phase angle distributions of harmonic currents flowing in service transformers. Section 2.4 presents the magnitude characteristics, phase angle distributions of harmonic currents of residential feeders at substation locations. Section 2.5 shows the comparative results of multiple system locations. Section 2.6 and Section 2.7 analyze the characteristics of harmonic addition and voltage induction, respectively.

2.1 Field Measurements

In North America, the residential homes are always served by single-phase two-winding transformers which are called service transformers. Typically, each service transformer provides power to 10 to 15 single detached homes, as shown in Figure 2.1. The harmonics originate from nonlinear loads at homes in a random manner; propagate through service transformers to the distribution feeder. The feeder harmonic currents may penetrate into the transmission systems through substation transformers. Extensive field measurements were conducted at various locations of the system.

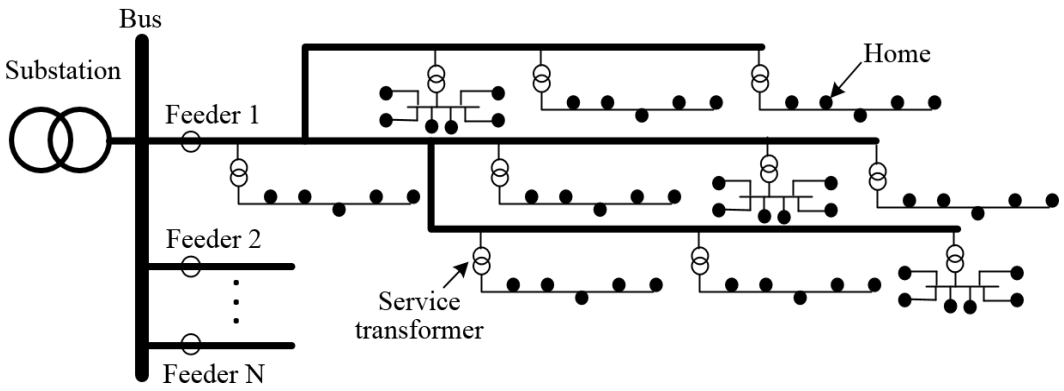

Figure 2.1 A generic schematic of a residential distribution feeder in North America.

2.1.1 Features of Residential Distribution Systems

The configuration of the residential service transformer in North America is shown in Figure 2.2. The secondary winding of the service transformer is split into two parts by the grounded neutral wire. The home appliances can be supplied by either 120V or 240V according to their rated voltages. Since the both sides of the service transformer are grounded, all harmonics generated by home appliances can penetrate into the MV system. In comparison with this common type residential service transformer, the three-phase service transformer with delta to grounded wye connection, usually supplying large commercial building or industry, is able to trap most of triple harmonics. From this point of view, the residential distribution systems may encounter more severe harmonic problems.

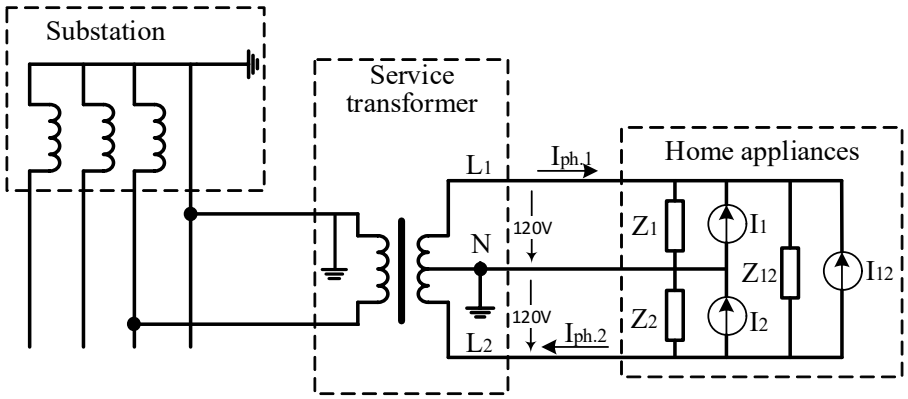

Figure 2.2 Configuration of the service transformer in North America

The measured sites supply typical suburban residential areas in cities of Canada and can be somewhat representative of actual situations in North America. Many homes have similar modern appliances, which can be classified as resistive, motor-driven and electronic devices. The resistive devices include incandescent lamps, heaters, toasters, rice cookers, ovens, kettles and so on. The motor-driven devices include washers, dishwashers, dryers, fridges, fans, gas-furnace, vacuum cleaners, and tread mills. The electronic devices include TVs, computers, microwave oven and LED lights etc. These are natural harmonic sources. In recent years, some of the resistive and motor-driven devices, especially the motor-driven type, have been added with a power-electronic front end for energy efficiency purposes. They also become harmonic sources. The main difference is that there are few air conditioning loads, space heating loads, distributed generations and active devices in the measured systems.

2.1.2 Measurement Locations and Periods

Measurement locations are the service panels of homes, secondary sides of service transformers, and substation-end of residential feeders. Both current and voltage waveforms are recorded. A total of 7 homes, 8 service transformers and 10 residential feeders supplied from different substations were measured. The measurements were conducted overall a few years from 2009 to 2015 due to the challenges in arranging simultaneous measurement campaign. Each measurement

action lasts for one week to several weeks. Our recent sporadic measurements confirmed that the results are still representative. The data recording settings are summarized in Table 2.1. In Table 2.1, labels H, T and F represent home, transformer and feeder. The following number denotes the numbering of each measured location. Measurements for some industrial and commercial feeders were also conducted for comparison.

Table 2.1 Measurement resolutions

Location	Samples per cycle	Cycles per snapshot	Snapshots per minute	Analyzed Snapshots
H_1, 6, 7	256	6	60	6 cycles per 1s.
H_2, 4	256	6	12	6 cycles per 5s.
H_3	256	70	1	6 cycles per 1min.
H_5	256	3	60	3 cycles per 1min.
T_1	64	Gapless recording		90 cycles per 1min
T _2~8	256	6	20	6 cycles per 1min
F_1	256	6	20	6 cycles per 1min
F_2, 3, 4	256	12	5	
F_5, 6	256	6	60	
F_7, 9	256	6	5	
F_8,10	128	6	10	

To make the investigation results more representative, we selected feeders with different load demands. The demand information of measured residential feeders, as well as some commercial and industrial feeders for comparison are shown in Table 2.2.

Table 2.2 Power demand (three phase) of measured feeders

Type	Residential							
Feeder	F_1	F_2	F_3	F_4	F_5	F_6	F_7	F_8
V (kV)	25	14.4	14.4	14.4	25	25	25	25
Pd (MW)	11.9	14.5	10.9	14.0	19.0	15.9	4.0	13.7
Type	Residential		Commercial			Industrial		
Feeder	F_9	F_10	F_11	F_12	F_13	F_14	F_15	
V (kV)	25	25	14.4	14.4	14.4	25	25	
Pd (MW)	11.6	3.7	23.7	18.9	18.9	8.1	12.5	

2.1.3 Measurement Instruments and Data Process

The voltage and current measurements were taken at both MV and LV sides of distribution systems. The current and voltage at MV levels were collected via current and voltage transformers. The signals were then input to power quality monitors through Fluke's voltage and current probs. Only the fundamental component of voltage is used in this investigation for providing reference phase angle for harmonic currents. Since the MV level current transformers (CTs) and probes have good performance on both the magnitude and phase angle for low order harmonic measurement [50], the measurement accuracy therefore can be guaranteed.

The data were analyzed by using discrete fourier transform (DFT). The window selection is according to the analyzed snapshots described in Table 2.1. To eliminate the phase drift caused by varying fundamental frequency of the system, the harmonic phasor angles were shifted using the fundamental voltage angle as $\varphi_h=\varphi_h-h*\varphi_{FV}$, where φ_h is the h-th harmonic current phasor angle, φ_{FV} is the fundamental voltage angle and h is the harmonic order [51].

2.1.4 Indices for Representing the Harmonic Characterization

Generally, the residential loads vary significantly during a day in a pattern that almost repeats itself every day. Therefore, this study focuses on a 24-hour current pattern. In this report, the magnitude ($|I_h|$) and phase angle (φ_h) of harmonics are used to describe the behavior of each order (h) of harmonic current during a day. The following individual demand distortion (*IDD*) and total demand distortion (*TDD*) indices as defined in (2.1) and (2.2) are employed to represent the harmonic distortion levels.

$$IDD_h(\%) = \frac{|I_h|}{|I_L|} \times 100 \tag{2.1}$$

$$TDD(\%) = \frac{\sqrt{\sum_{h=2}^{15} |I_h|^2}}{|I_L|} \times 100 \tag{2.2}$$

where I_L is the maximum moving average load current (with a moving average window of 15 minutes) for the 24 hour period and I_h is the h-th harmonic current. The TDD includes both even and odd harmonics up to the 15th harmonic component. The *IDD* or *TDD* factor is similar to *IHD* or *THD*, defined in (2.3) and (2.4), except that the distortion is expressed as a percentage of maximum load current, rather than the fundamental component of the same instant (I_F). In fact, the *IDD* or *TDD* indices are more meaningful in specific light load cases where a small fundamental frequency current might result in a large *IHD* or *THD* values.

$$IHD_h(\%) = \frac{|I_h|}{|I_F|} \times 100 \tag{2.3}$$

$$THD(\%) = \frac{\sqrt{\sum_{h=2}^{15} |I_h|^2}}{|I_F|} \times 100 \tag{2.4}$$

In order to quantify the harmonic distortion level of each case, the average and 95th percentile *IDD* (*TDD*) are used. The average *IDD* (*TDD*) is simply the mean of 24-hour *IDD* (*TDD*) data. The 95th percentile is defined as the maximum level that is higher than the index for 95% of the time. This index can be extracted from the cumulative distribution function of the variable of interest, e.g. *IDD* (*TDD*). Therefore, simultaneous presentation of both average and the 95th percentile *IDD* (*TDD*) reveals the statistical distribution of harmonic distortion levels.

For the harmonic phase angles, the mean and standard deviation are adopted to represent the phase angle distribution for each order of harmonic during the 24-hour period. Such indices help to estimate the likelihood of harmonic addition or cancellation from different loads.

2.2 Harmonic Current Characteristics of Individual Houses

The currents of seven houses were measured and analyzed. This section refers to each house by Home 1 ~ Home 7. The measurements were performed at the power panel of each house by recording the data for five days during Jan. 2009 to

Nov. 2010. For all measurements, phase A-to-neutral voltage and two phase currents were collected and then the two phase currents were combined together to determine the total load current of each individual house. Magnitude and phase angle of harmonic currents were obtained by processing the data through standard fast fourier transform (FFT). The fundamental component waveform of phase A voltage was selected as the reference for the phase angles of harmonic currents.

The results for Home 7 will be presented as an example to show the harmonic characteristics of an individual house. Then, the overall harmonic-producing behavior of different houses will be investigated through a comparison of all the seven house measurements.

2.2.1 Harmonic Characteristics of a Sample House

As a sample day, data for Home 7 measurement on a weekday (3/29/2010) was analyzed and the results are shown in Figure 2.3 to Figure 2.7 from both magnitude and phase angle perspectives.

- Figure 2.3 shows the 24-hour patterns of active power and *TDD*.
- Figure 2.4 presents the 24-hour variation pattern of individual harmonic current magnitudes.
- Figure 2.5 shows the average and the 95th percentile *IDD* and *TDD*.
- Figure 2.6 presents the 24-hour pattern of individual harmonic phase angles.
- Figure 2.7 presents the probability density curves of harmonic current phase angle.

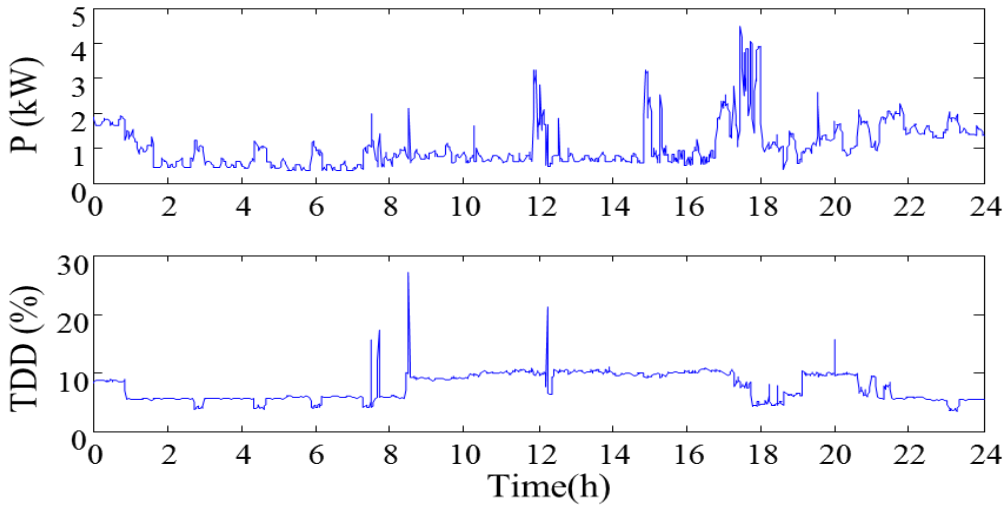

Figure 2.3 Active power and TDD 24-hour pattern (weekday)

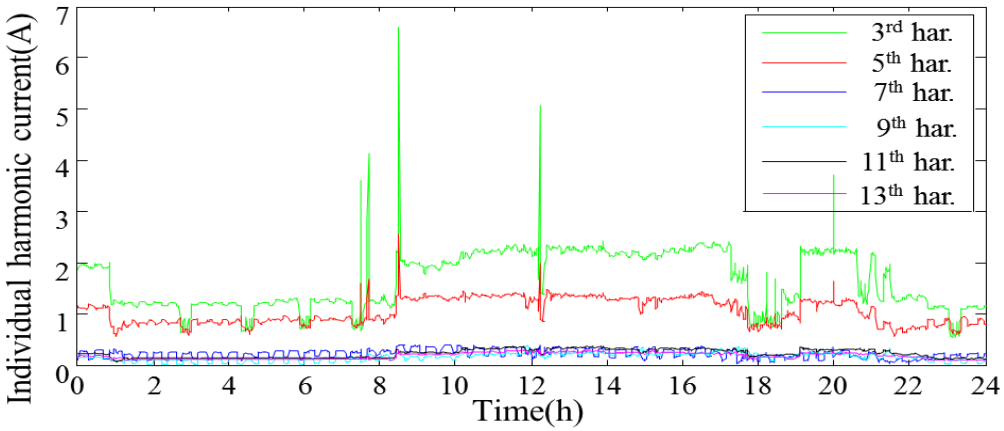

Figure 2.4 Individual harmonic current 24-hour pattern (weekday)

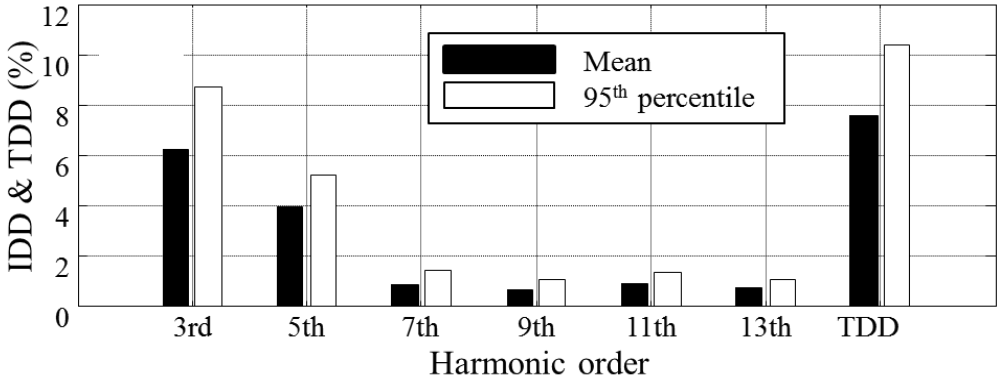

Figure 2.5 Average and 95th percentile IDD and TDD (weekday)

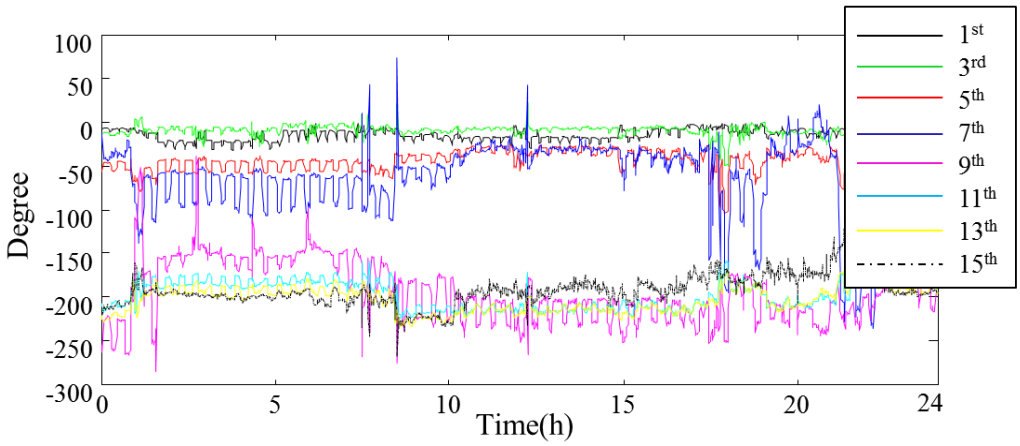

Figure 2.6 Harmonic current phase angle 24-hour pattern (weekday)

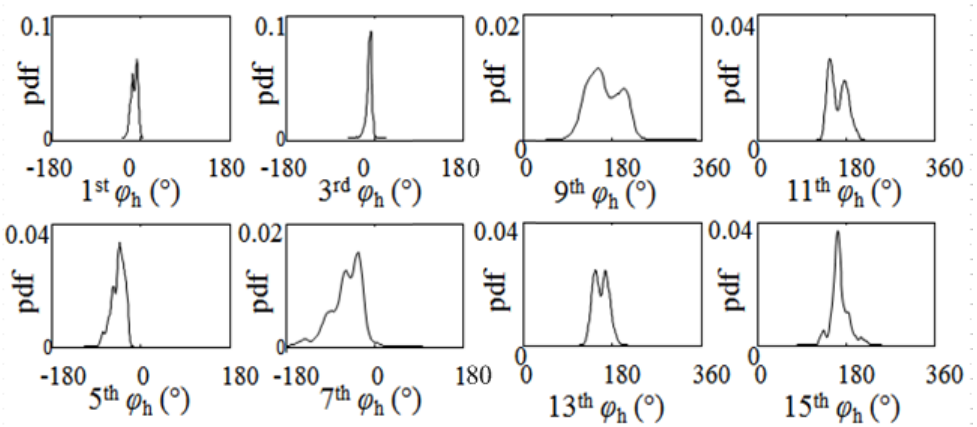

Figure 2.7 Probability density curves of harmonic current phase angle

The observations from the above figures suggest that:

- The *TDD* level has somewhat correlation with the active power, especially during overnight (light load duration), but its overall variation extent is milder than that of active power. It implies that the loads causing significant load variation consist of less nonlinear loads.

- The 3rd and 5th harmonics dominate the harmonic content, and therefore they have a similar 24-hour variation pattern as the *TDD*.

- The phase angles of the most harmonic components, especially the 3rd and 5th ones, are almost time/load independent and concentrated in a very narrow phase-angle range. It implies the probability of add-up (rather than cancelation)

of harmonics from different loads, as the loads are different from one time segment to another.

2.2.2 Harmonic Characteristics of Multiple Houses

The harmonic characteristics might vary considerably from one house to another. A comparison between results of different houses was made to determine differences of harmonics behaviour among the houses.

- Figure 2.8 presents the comparison on the 95th percentile *IDD* and *TDD* of seven houses.
- Figure 2.9 shows the comparisons of mean values and standard deviations of harmonic phase angles, respectively.
- Figure 2.10 provides a phasor-based comparison of 3rd, 5th and 7th harmonic currents of the seven houses. The magnitude and angle of each presented phasor vector is determined on the basis of the daily 95th percentile index and mean value, respectively.

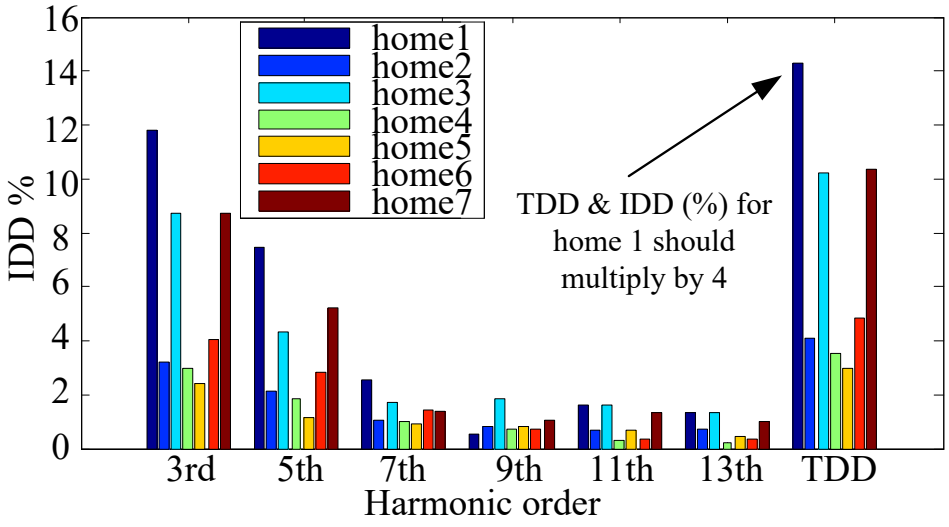

Figure 2.8 The 95th percentile IDD and TDD (IDD & TDD of Home 1 is divided by 4 to fit inside the figure)

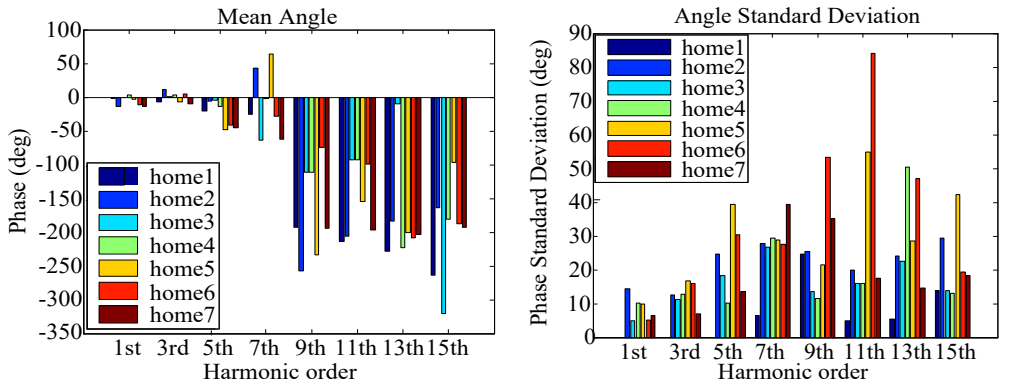

(a) Mean phase angle (b) Phase Angle Standard Deviation

Figure 2.9 Phase angle comparison

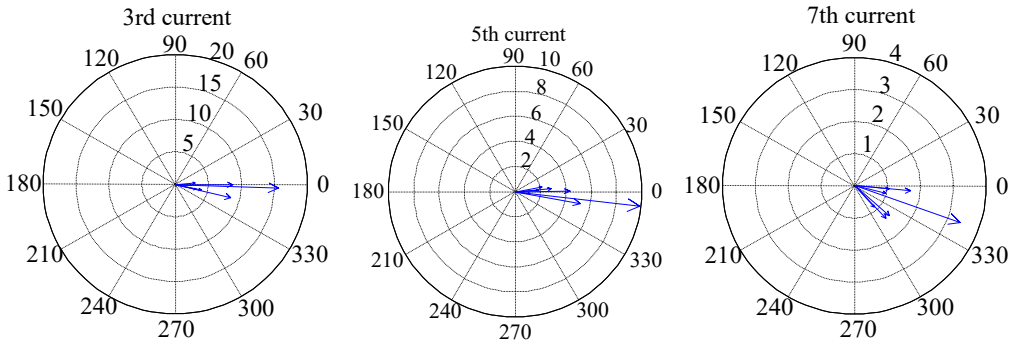

Figure 2.10 Harmonic phasor diagram (the longest arrow in 3rd and 5th harmonics is divided by 3 to fit inside the diagrams)

These comparisons indicate that:

- The 3rd and 5th harmonics are the dominant harmonic components for all houses.
- The phase angles of most harmonics, especially the 3rd, 5th and 7th, are concentrated in a very narrow range. The standard deviations are less than 40 degrees for the 3rd, 5th and 7th harmonics. Therefore, the aggregated harmonic magnitude of different houses can be approximately considered as the pure add-up of the same harmonic order magnitude of individual house by a diversity factor close to 1.
- The diversity degree of harmonic phase angle increases for the higher

harmonic order.

- The harmonic *IDD* varies significantly from one house to another. No harmonic-free house was found. However, some houses can generate extremely high harmonics such as Home 1 in this measurement. The IDD and TDD indices of Home 1 is even larger than the total summation of the same indices associated with the other six houses.

2.3 Harmonic Current Characteristics of Service Transformers

The voltages and currents of total eight service transformers serving residential loads were measured at their secondary sides for more than one week for each transformer during Nov. 2008 and July ~ Aug. 2014. In this section, they are referred as Transformer 1 ~ Transformer 8. For all measurements, the two phase-to-neutral voltages and the two-phase currents were collected. The total load current of each individual transformer was determined by adding the two-phase currents together. The data was processed by using standard FFT. The fundamental component waveform of phase A voltage was used as the reference to compute phase angles of harmonic currents.

The measurement of Transformer 1 is selected as an example to show the harmonic characteristic of an individual service transformer. Then, the results for all eight transformers will be compared in this section to reveal the differences in harmonic characteristics.

2.3.1 Harmonic Characteristics of a Sample Transformer

The current at secondary side of Transformer 1, measured on a weekday (7/30/2014), was analyzed and the harmonic characteristics are presented in the following figures.

- Figure 2.11 shows the 24-hour profile of active power and *TDD*.
- Figure 2.12 presents the 24-hour variation pattern of individual harmonic

magnitudes.

- Figure 2.13 shows the average and the 95th percentile *IDD* and *TDD*.
- Figure 2.14 presents the 24-hour variation pattern of individual harmonic phase angles.
- Figure 2.15 presents the probability density curves of harmonic current phase angle.

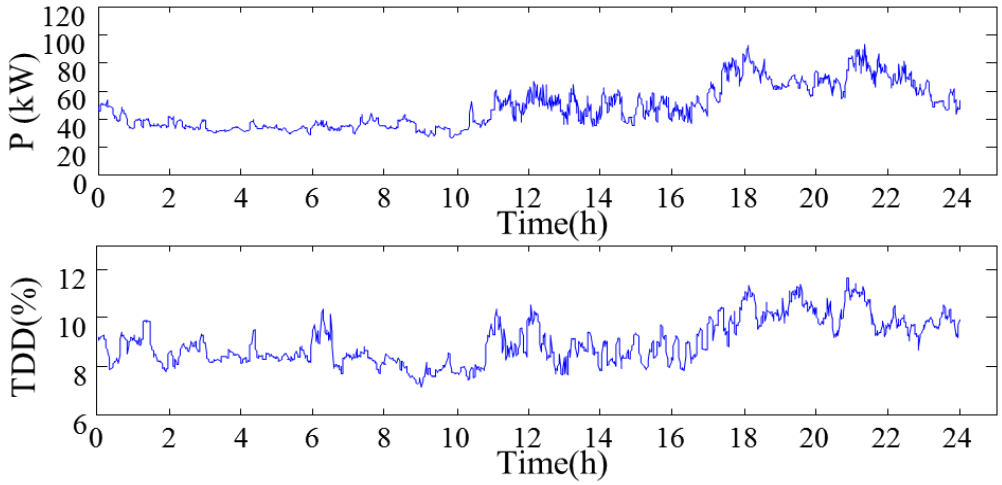

Figure 2.11 Active power and TDD 24-hour pattern (weekday)

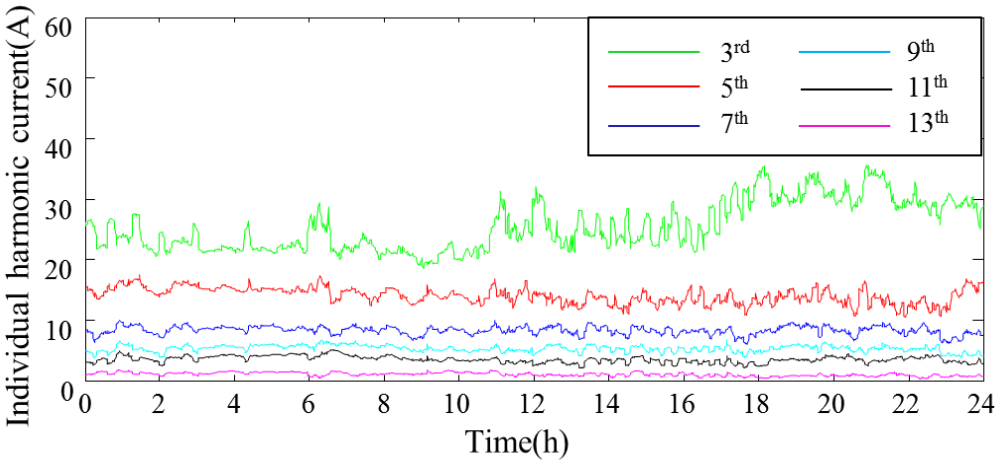

Figure 2.12 Individual harmonic current 24-hour pattern (weekday)

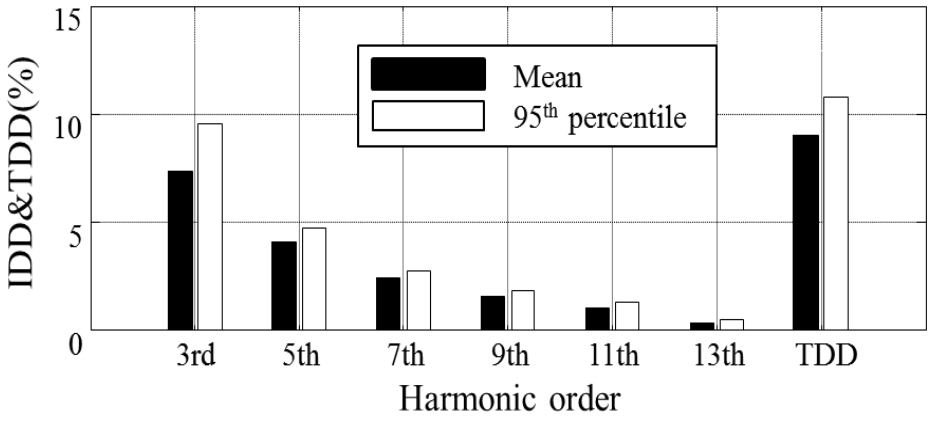

Figure 2.13 Average and the 95th percentile *IDD* and *TDD* (weekday)

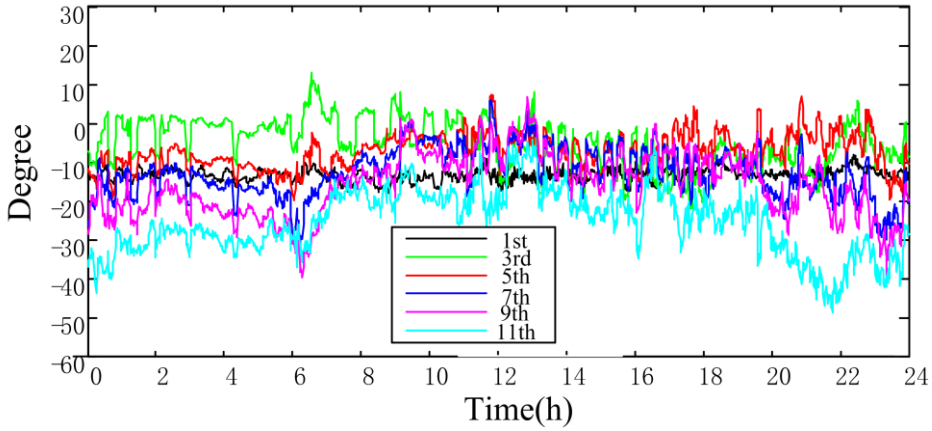

Figure 2.14 Harmonic current phase angle (φh) 24-hour pattern (weekday)

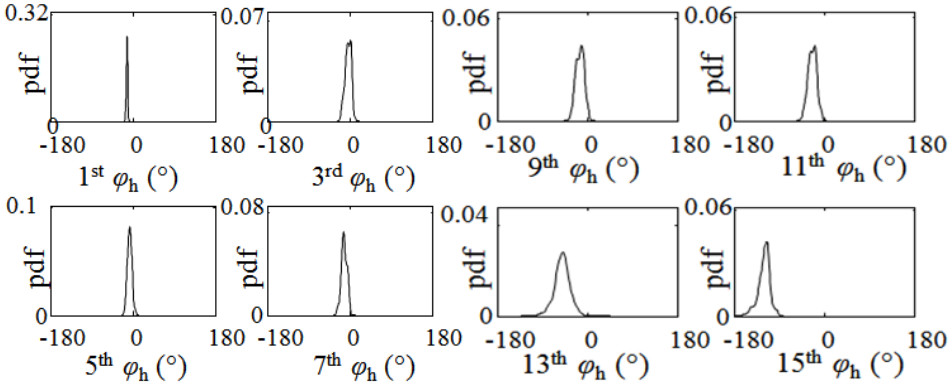

Figure 2.15 Harmonic current phase angle probability density curves (weekday)

The observation from those figures suggest that:

- The *TDD* level has some correlation with the active power. The higher the

active power, the more severe the harmonic distortion is. The overall *TDD* distribution extent is milder than that of the active power variation.

- The 3rd harmonic component is the main contributor to the *TDD* and it dominates the 24-hour pattern of *TDD*.

- The phase angles of the most low order harmonics are almost time/load independent and concentrated in a very narrow phase-angle range. Once again, it implies the likelihood of addition (rather than cancellation) of harmonics from different loads.

2.3.2 Harmonic Characteristics of Multiple Transformers

The harmonic characteristics of all the eight measured service transformers feeding residential loads are summarized in Figure 2.16 to Figure 2.18.

- Figure 2.16 presents the comparisons of *IDD* and *TDD*.

- Figure 2.17 shows the comparisons of mean values and standard deviations of harmonic phase angles, respectively.

- Figure 2.18 provides a phasor-based comparison of 3rd, 5th and 7th harmonic currents of the eight service transformers. The magnitude and angle of each presented phasor vector is determined by the daily 95th percentile index and mean value, respectively.

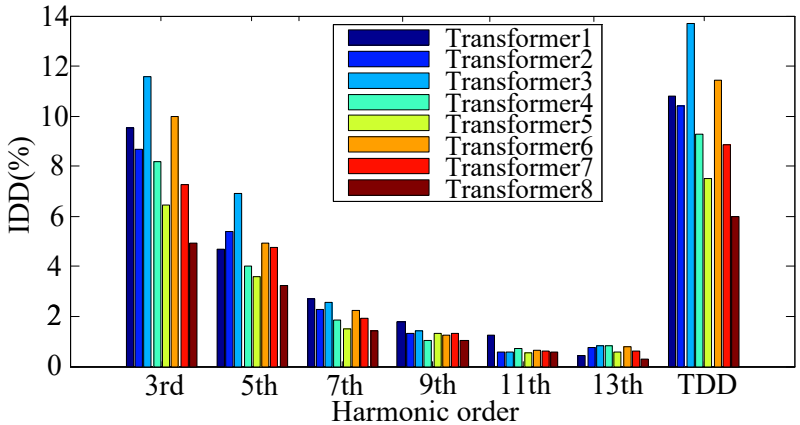

Figure 2.16 The 95th percentile IDD and TDD

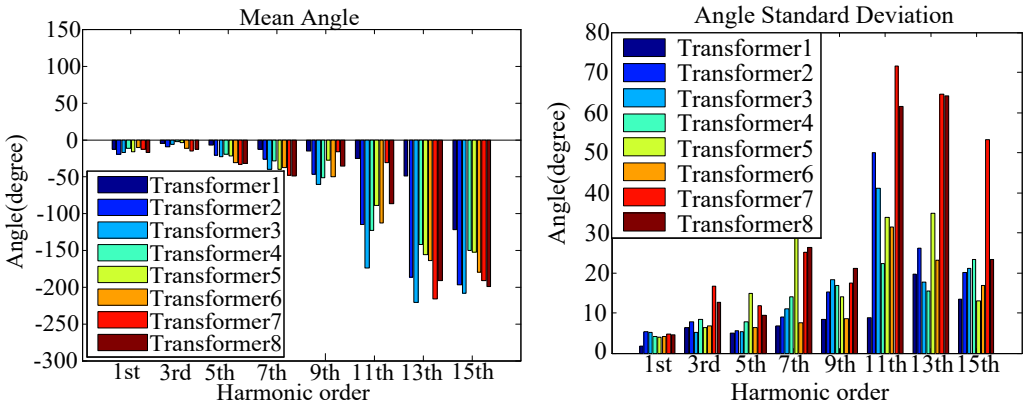

(a) Mean phase angle (b) Phase Angle Standard Deviation

Figure 2.17 Phase angle comparison

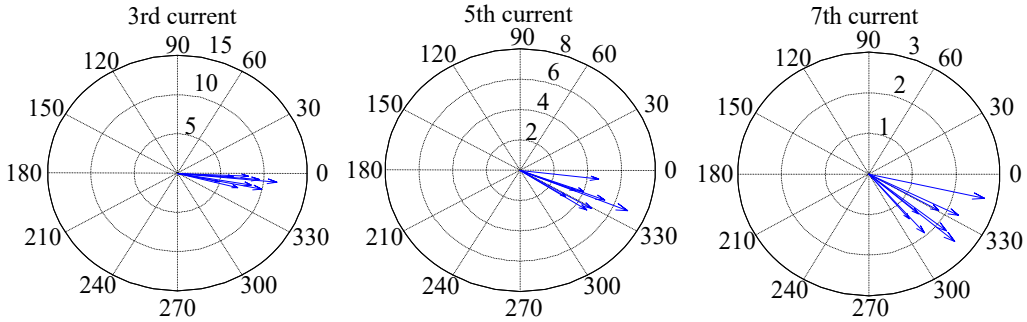

Figure 2.18 Phasor diagrams for eight service transformers

The comparisons reveal that:

- The 3rd harmonic is the greatest contributor to the current distortion of transformers and the value of IDD decreases with the increase of harmonic order by somehow following an exponential trend.
- The harmonic *IDD* varies moderately from one transformer to another. No harmonic-free transformer was observed.
- The phase angles of most harmonics, especially the 3rd, 5th, 7th and 9th harmonics, are concentrated in a very narrow range. The standard deviations are less than 30 degrees for the 3rd, 5th, 7th and 9th harmonics. It implies that the aggregative harmonic magnitude of different transformers can easily add up, i.e. the likelihood of cancellation is very small.

2.3.3 Correlation Between Fundamental Frequency Currents and Harmonic Frequency Currents

Active power and the third harmonic *IDD* 24-hour profiles in Figure 2.11 and Figure 2.12 demonstrated considerable variation similarities. Further analysis was performed to understand this correlation. The relationships of the 3rd harmonic and fundamental frequency currents of the 8 transformers are shown in Figure 2.19. In the scatter plots of this figure, each blue point represents one measurement instance and the correlation red lines are fitted for each plot. It can be seen that the 3rd harmonic magnitude is generally larger at the increased fundamental current.

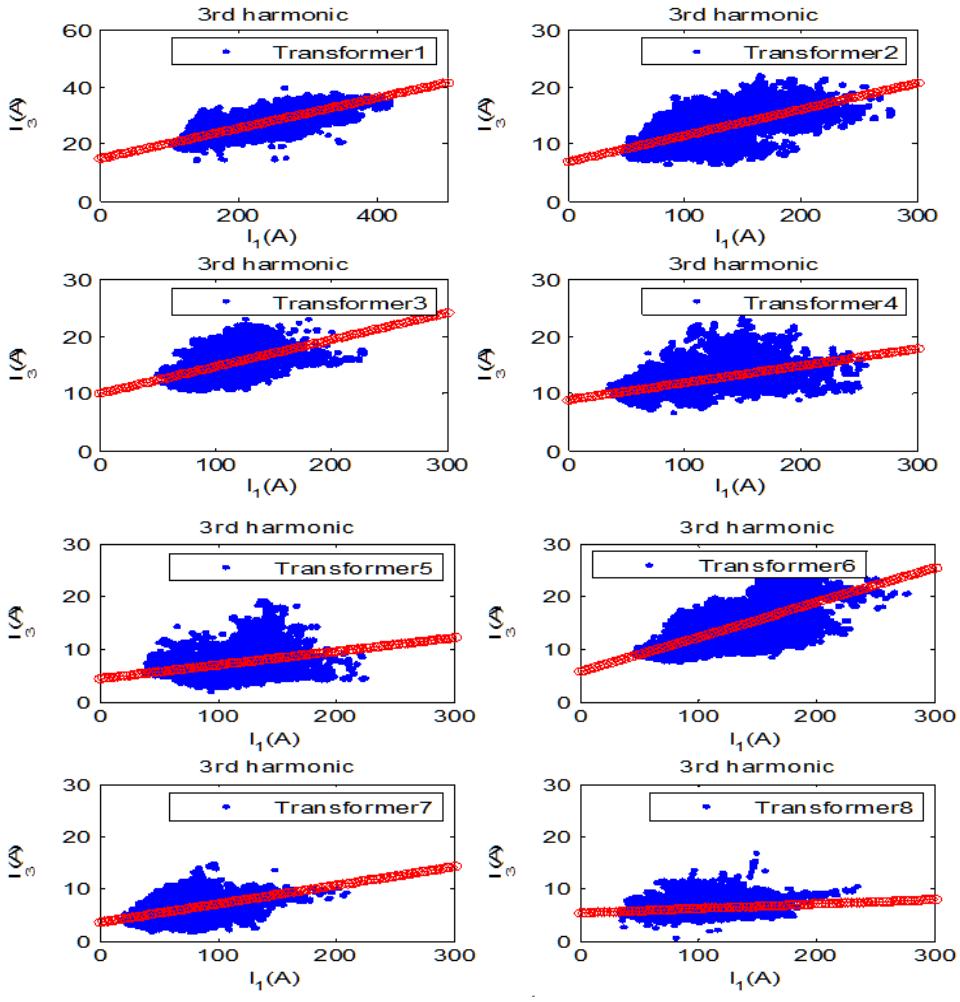

Figure 2.19 Magnitude correlation between 3rd harmonic and fundamental frequency current

The correlation coefficients between the 3rd harmonic and the fundamental frequency component for the eight transformers are listed in Table 2.3. In all cases, the 3rd harmonic exhibits a positive correlation with the fundamental component. Two of the measured transformers present relatively strong correlation between I_3 and I_1, while four of them present a moderate correlation and two transformers present relatively weak correlation between I_3 and I_1. However, the observed correlation coefficients are still not high enough to indicate that the 3rd harmonic current can be directly predicted by the fundamental frequency current.

Table 2.3 Correlation coefficients between the 3rd harmonic current and the fundamental frequency current for all 8 transformers

Transformer	1	2	3	4	5	6	7	8
Correlation coefficient	0.85	0.69	0.54	0.52	0.32	0.71	0.48	0.19

The correlation coefficients of the 3rd, 5th, 7th and 9th harmonics to the fundamental frequency component are also presented in Figure 2.20. It suggests that the no harmonic other than the 3rd one has consistent positive or negative correlation with the fundamental frequency current.

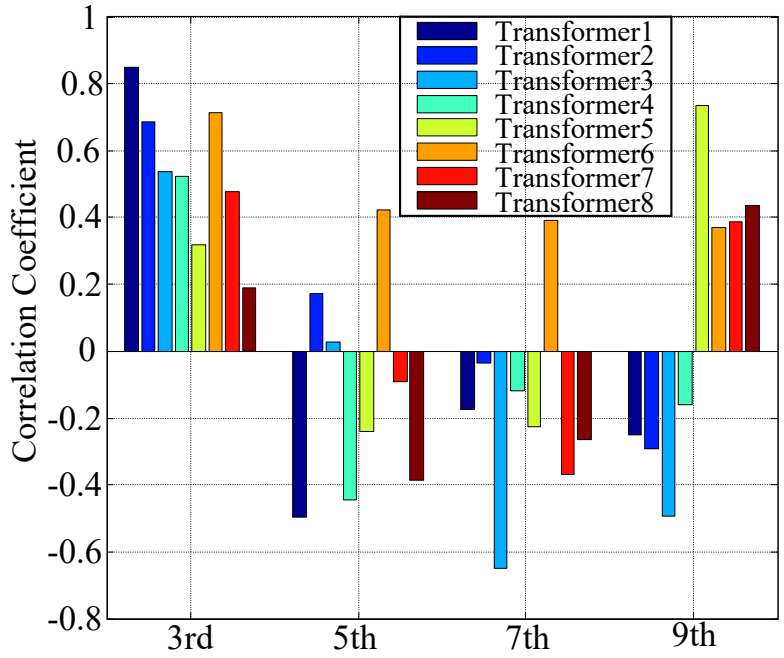

Figure 2.20 Correlation coefficients of the 3rd, 5th, 7th, and 9th harmonics to the fundamental frequency current

2.4 Harmonic Current Characteristics of Residential Feeders

This section presents the measurement results for nine residential and one mixed-load feeders owned by different utilities. Voltage and current have been measured at the substation for all these feeders at different periods (longer than one week) in Nov. ~ Dec. 2008, July 2009, Oct. ~ Nov. 2008 and April 2011. This section refers to the feeders as Feeder 1 ~ Feeder 10, in which Feeder 1 indicates a mixed-load feeder. The supplied load by this feeder approximately consists of 37% industrial, 23% residential and 23% commercial types. Voltage and current were measured for the three phases of each feeder at substation. The data was processed by using standard FFT. The phase angles of harmonic currents are derived with the reference to the phase angle of fundamental component of corresponding phase voltage.

The result of Feeder 10 measurement is presented as an example to show the harmonic characteristics of residential feeders. Then, a general comparison of all ten feeder results is provided in this section to investigate the harmonic characteristic differences. Only measurements of phase A are presented in this report. The sequence components will also be studied to catch any significant observation that might be offered by the results of the other two phases.

2.4.1 Harmonic Characteristics of a Sample Feeder

This section presents the results for Feeder 10 on a weekday 4/7/2011. Phase harmonic currents are considered as well as the sequence characteristics of fundamental and harmonic components. The harmonic characteristics of phase current (phase A) are presented in the following figures.

- Figure 2.21 shows the 24-hour profiles of active power and *TDD*.
- Figure 2.22 presents the 24-hour variation pattern of individual harmonic magnitudes.
- Figure 2.23 shows the average and the 95th percentile *IDD* and *TDD*.

- Figure 2.24 presents the 24-hour variation pattern of individual harmonic current phase angles.
- Figure 2.25 exhibits the probability density curves of harmonic current phase angles.

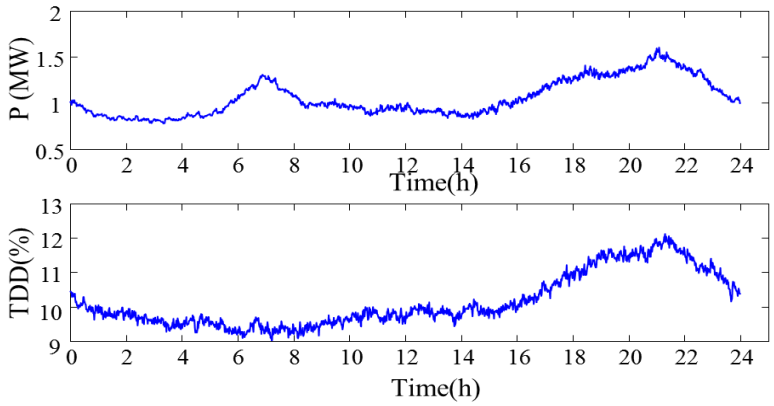

Figure 2.21 Active power and TDD 24-hour pattern (weekday)

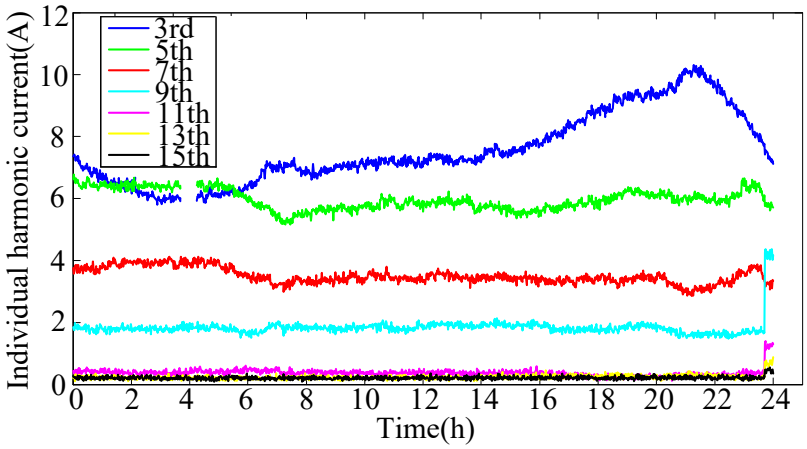

Figure 2.22 Individual harmonic current 24-hour pattern (weekday)

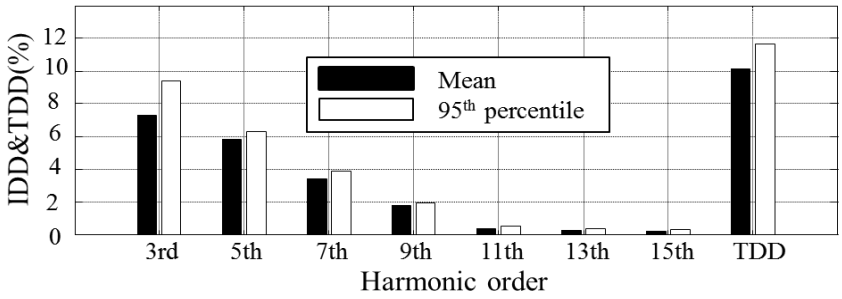

Figure 2.23 Average and the 95th percentile IDD and TDD (weekday)

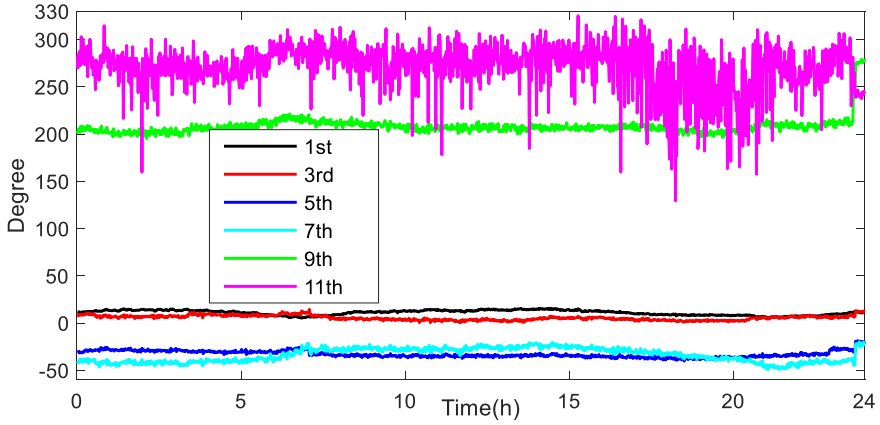

Figure 2.24 Harmonic current phase angle 24-hour pattern (weekday)

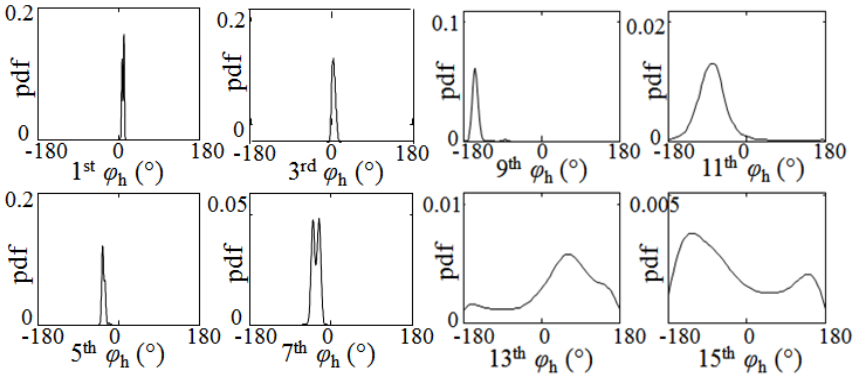

Figure 2.25 Harmonic current phase angle probability density curve (weekday)

The observations from the above figures suggest that:

- The *TDD* level has a correlation with the active power. The higher active power, the higher the harmonic distortion is. However, the overall *TDD* variation extent is milder than that of the active power.
- The 3rd harmonic component is the main contributor to the *TDD* and it dominates the 24-hour pattern of *TDD*.
- The harmonic magnitudes, except the 3rd one, are almost independent of load and time.
- The phase angles of most harmonic components, especially the 3rd, 5th, 7th and 9th, are almost time/load independent and are concentrated in a very narrow range. Such observation implies the likelihood of harmonics addition from

different loads.

The sequence components of different harmonic currents are derived and presented in Table 2.4. The results suggest that the three-phase fundamental and the low order harmonic currents follow a classic dominant sequence characteristic as shown in the last column of Table 2.4.

Table 2.4 Sequence characteristics of harmonic currents

	Sequence Actual Value (A)			Sequence Normalized Value (%)			Dominant sequence characteristics
	Zero	Positive	Negative	Zero	Positive	Negative	
1st	6.28	59.37	7.96	10.58	100.00	13.41	Positive
3rd	6.22	0.72	0.74	100.00	11.58	11.90	Zero
5th	0.44	0.57	5.01	8.78	11.38	100.00	Negative
7th	0.42	3.22	0.21	13.04	100.00	6.52	Positive
9th	1.81	0.25	0.24	100.00	13.81	13.26	Zero
11th	0.18	0.15	0.33	54.55	45.46	100.00	---
13th	0.17	0.21	0.16	80.95	100.00	76.19	---

2.4.2 Harmonic Characteristics of Multiple Feeders

In this section, the harmonic characteristics of all measured feeders are compared. The 95th percentile *IDD* and *TDD* of the 10 feeders are presented in Figure 2.26. It is observed that

- The *IDD* and *TDD* vary in a large range from one feeder to the other.
- The 3rd and 5th harmonics are the main contributors to the *TDD*. For the residential feeders (Feeder 2 ~ Feeder 10), the 3rd harmonic is the most significant one, whereas for the mixed load feeder (Feeder 1), the 5th harmonic is found to be the most significant one.
- The harmonic magnitude decreases with the increase of harmonic order by approximately following an exponential trend with the exception of Feeder 1 which supplies mixed loads.
- The residential feeders show higher harmonic current distortion levels than the

mixed load feeder.

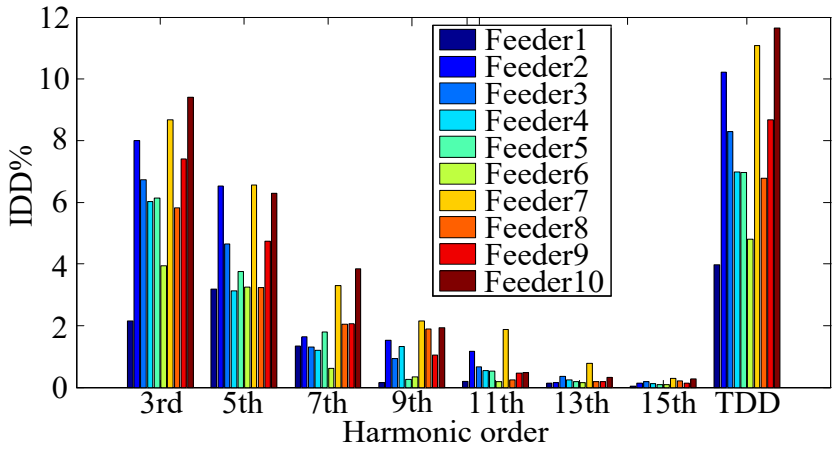

Figure 2.26 Harmonic IDD and TDD of all feeders

2.5 Comparison of Harmonic Characteristics at Different System Locations

The results of various measurements conducted at different system locations have been investigated so far in this chapter. Several similarities of harmonic characteristics were observed. It is therefore necessary to compare the results associated with the different locations (house, transformer and feeder) to each other. Additionally, the results are compared with other distribution systems and IEEE limits to reveal the severity of the problem.

2.5.1 Comparison of *IDD* and *TDD*

The comparison of *IDD*s and *TDD*s measured at seven homes, eight service transformers and ten distribution feeders is shown in Figure 2.27.

- At different system locations, harmonic distortion levels are very similar to each other. This observation once again confirms that the harmonic cancellation among residential loads is not significant.

- The *IDD* may be represented as a function of harmonic order h in the form of $IDD=1/h^{\alpha}$, where the average α for homes, service transformers and feeders

are approximate 2.0, 2.0 and 2.3, respectively.

- Harmonic currents of main concern are the 3rd and 5th. Other harmonics reduce rapidly with increased harmonic order.

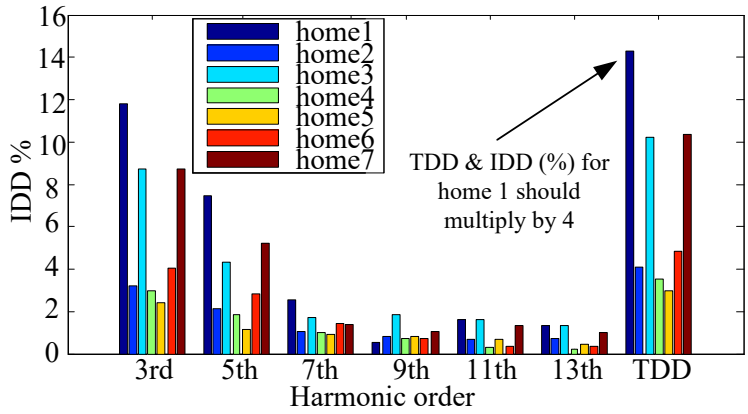

(a) Home

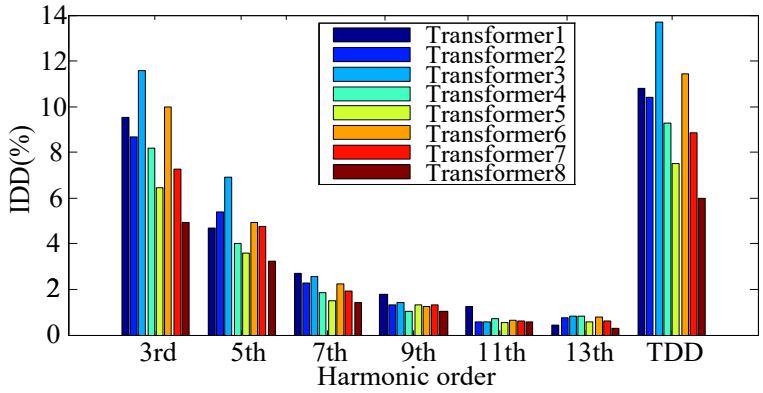

(b) Service transformer

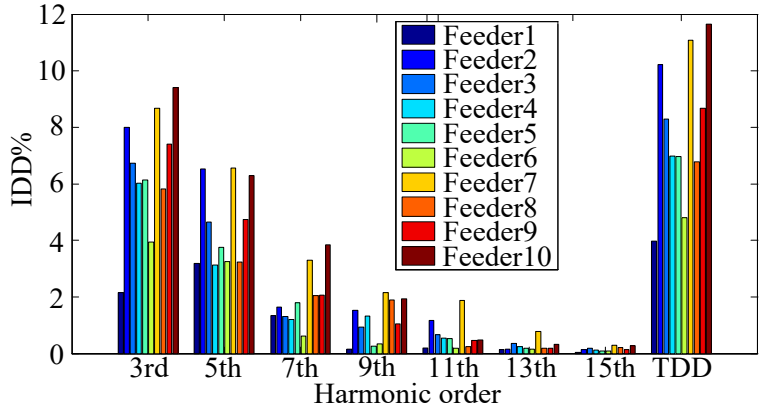

(c) Feeder

Figure 2.27 Comparison of IDD and TDD at different locations

2.5.2 Comparison of Harmonic Phase Angle Distributions

The comparison of harmonic phase-angle distribution and its standard deviation measured at homes and service transformers is shown in Figure 2.28. The following conclusions can be drawn from these observations.

- The mean angle value of low order harmonics (3rd to 7th harmonics) of homes can be either lagging or leading. However, the angles of high order harmonics consistently show a lagging characteristic.

- The standard deviations of harmonic angles of either home or service transformer are quite similar and are distributed in a very narrow range, especially for low order harmonics. This observation suggests that the lower order harmonics of different homes can be added up directly without a significant error to estimate system harmonic levels.

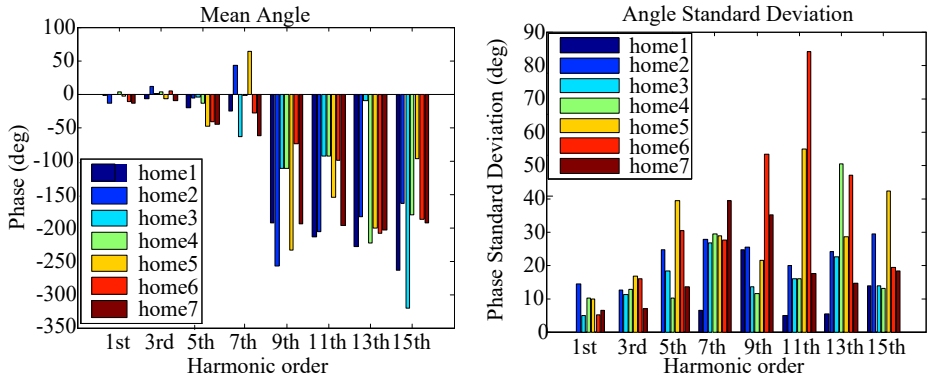

(a) Home

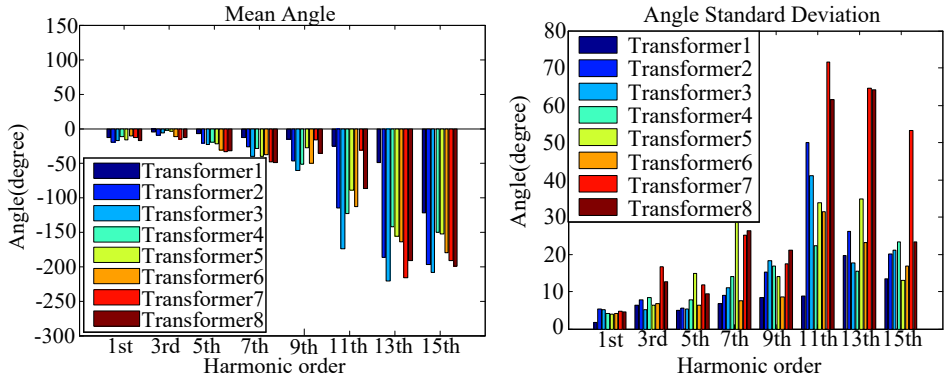

(b) Service transformer

Figure 2.28 Comparison of phase angle characteristics

2.5.3 Comparison with Harmonic Limits

The substation information for the ten measured feeders is presented in Table 2.5. This data is used to determine whether the harmonic distortion levels of actual residential feeders satisfy the standard requirements. For this purpose, the phase A current distortion levels of all ten feeders are compared with the limits recommended by IEEE Std. 519. The results are shown in Table 2.6.

Table 2.5 Substation and load information for the 10 measured feeders

Feeder	System Impedance (ohm)	I_{SC}(kA)	I_L(kA)	I_{SC}/I_L
Feeder 1	0.86+j2.75	5.01	0.28	18
Feeder 2	0.073+ j0.85	9.78	0.60	16
Feeder 3			0.47	20
Feeder 4	0.09+ j0.97	8.48	0.62	14
Feeder 5	0.17 + j2.13	6.78	0.46	15
Feeder 6			0.38	18
Feeder 7			0.08	85
Feeder 8	0.17 + j2.13	6.78	0.30	23
Feeder 9			0.28	24
Feeder 10			0.10	68

Table 2.6 Feeder harmonic currents (% of I_L) compared with IEEE 519 Std. limits

I_{SC}/I_L	Harmonic order	3	5	7	9	11	13	15	TDD
<20	limits (% of I_L)	4	4	4	4	2	2	2	5
	Feeder 1	2.15	3.19	1.33	0.15	0.20	0.14	0.05	3.98
	Feeder 2	8.00	6.52	1.63	1.53	1.16	0.15	0.13	10.22
	Feeder 3	6.72	4.64	1.32	0.94	0.67	0.35	0.18	8.30
	Feeder 4	6.03	3.12	1.20	1.32	0.54	0.25	0.11	6.97
	Feeder 5	6.14	3.76	1.80	0.26	0.52	0.18	0.09	6.97
	Feeder 6	3.93	3.25	0.62	0.33	0.19	0.15	0.09	4.80
20<50	limits (% of I_L)	7	7	7	7	3.5	3.5	3.5	8
	Feeder 8	5.82	3.24	2.04	1.89	0.25	0.18	0.22	6.79
	Feeder 9	7.40	4.74	2.06	1.04	0.46	0.18	0.14	8.67
50<100	limits (% of I_L)	10	10	10	10	4.5	4.5	4.5	12
	Feeder 7	8.67	6.56	3.29	2.16	1.87	0.77	0.29	11.09
	Feeder 10	9.41	6.30	3.84	1.93	0.48	0.32	0.28	11.64

In Table 2.6, the highlighted cells indicate the cases exceeding the IEEE limits. As per the standard, the limits are obtained according to the ratio of system short-circuit capacity to the load (in amperes), I_{SC}/I_L, and the harmonic order. The higher the I_{SC}/I_L, the milder the harmonic distortion limit is. Apparently, the feeders, supplied from lower MVA system, are at higher risk of exceeding the

harmonic limits. Violation of current TDD limit is observed for five feeders. However, individual IDD limits are only exceeded for 3rd and 5th harmonics. In fact, all cases of *TDD* limit violations result from substantially high levels of 3rd (and somehow 5th). For example, the 3rd harmonic distortion of Feeder 2 exceeds the limit by two times. Such observations confirm the severity of 3rd and 5th harmonics produced by residential loads. The results imply that about 50% residential feeders may exceed the limits in one form or another.

In practice, this situation creates a significant challenge for utilities in term of responsibility for harmonic mitigation. A neighborhood in a distribution system usually contains hundreds of service transformers supplying thousands of homes as shown in Figure 2.29. If such a neighborhood were owned by a single owner similar as an industry facility, the neighborhood would not be able to pass the harmonic current limit check at its "PCC". The reality is that there is no single ownership for a residential neighborhood. The supply company may have to take the responsibility.

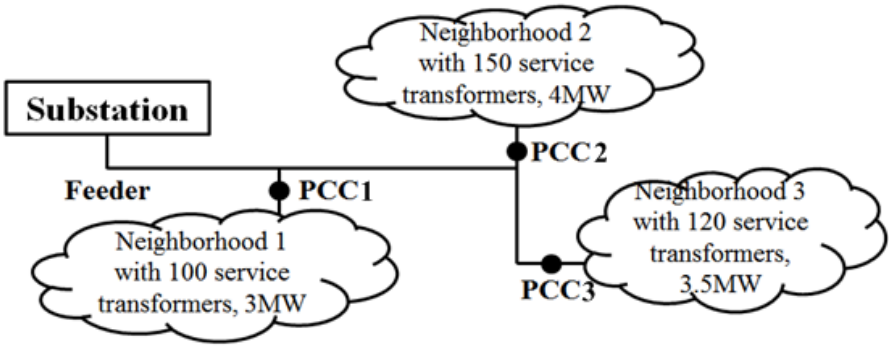

Figure 2.29 A residential feeder supplying three neighborhoods

2.5.4 Harmonic Characteristics of Different Load Types

In this subsection, the harmonic characteristics of a typical residential feeder (Feeder 10) are compared with those of typical industrial/commercial feeders to investigate the differences among the three types of feeders. The industrial feeder is numbered as Feeder 15. It supplies a gas compressing plant which is operating for the whole day constantly. The 24 hour measurements were conducted on Oct. 29th to Nov. 4th 2009. The commercial feeder is numbered as Feeder 11. The 24-

hour measurements took place from June 17th to 19th, 2009. Figure 2.30 shows the comparison of active power and *TDD* 24-hour patterns among three types of feeders. The comparison of *IDD* mean and 95th percentile values among the residential, commercial and industrial feeders are depicted in Figure 2.31.

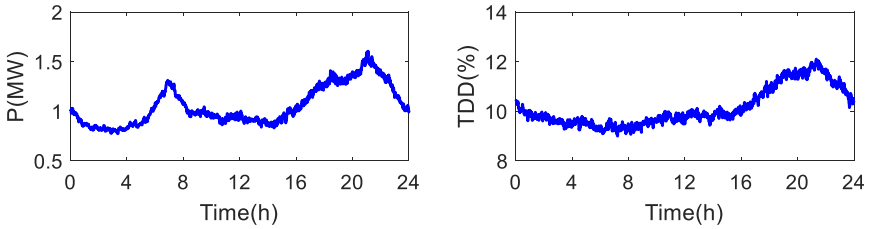

(a) Feeder 10 (residential feeder)

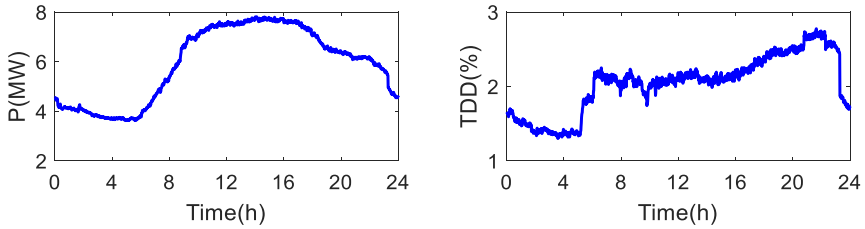

(b) Feeder 11 (commercial feeder)

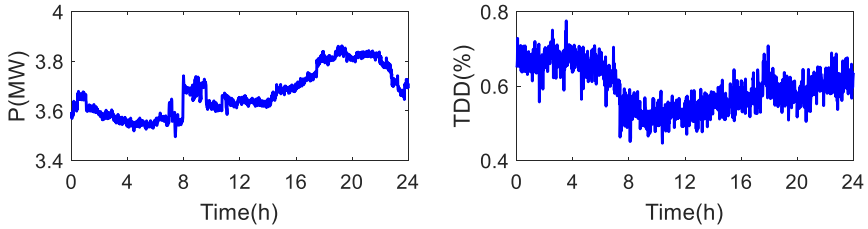

(c) Feeder 15 (industrial feeder)

Figure 2.30 Active power and *TDD* 24-hour pattern of phase A

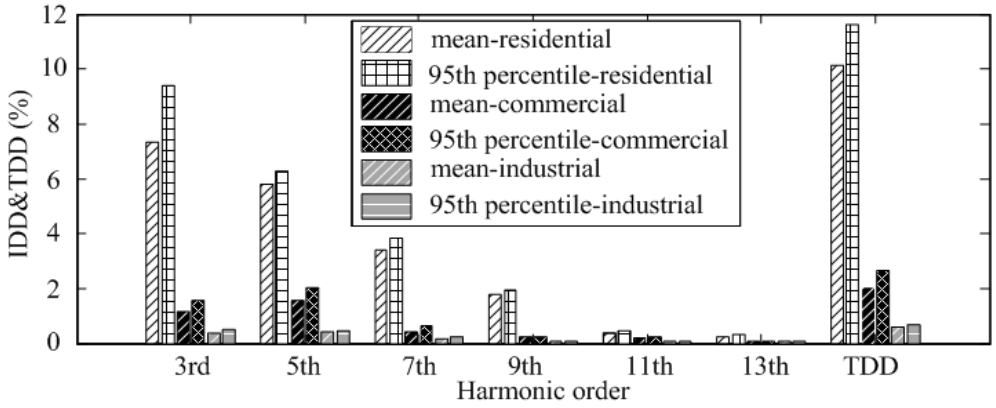

Figure 2.31 *IDD* and *TDD* characteristics of three types of loads

The following conclusions can be drawn:

- Industrial feeder shows a smaller variation of active power and *TDD* in comparison with residential and commercial feeders as expected from its different working duty.
- The 3rd, 5th *IDD*s and *TDD* levels of industrial and commercial feeders are much lower than that of the residential feeder. It further confirms that residential loads can be a significant harmonic source.
- The harmonic spectra are quite different for the three load types. For residential loads the most significant ones are the 3rd and 5th harmonics. For the measured industrial and commercial feeders, there are very little 3rd harmonics.

2.6 Characteristics of Harmonic Addition

The phase angle results have shown that the low order harmonic currents have phase angles that do not vary a lot. Therefore, the harmonics from different homes or service transformers tend to add up and accumulate in the MV feeders. To confirm and quantify this postulation, synchronized phasor measurement (SPM) was conducted for one feeder. This is done by using two global positioning system (GPS) synchronized power quality monitors. One monitor is placed at the feeder sending end located inside a substation. Another is placed at the secondary side of a service transformer. Detailed information about SPM can be found in Section 5.1.

The phasor diagram of h-th feeder harmonic current ($I_{h,Sub}$) at the substation and the service transformer current ($I_{h,ST}$) is depicted in Figure 2.32. As illustrated in this figure, the service transformer current can be separated into two components using the substation current as the reference. One component is called in-phase component. This component completely contributes to the feeder current at the substation location. The other component is called quadrature

component. This component has no contribution to the substation current since it is perpendicular to the substation current.

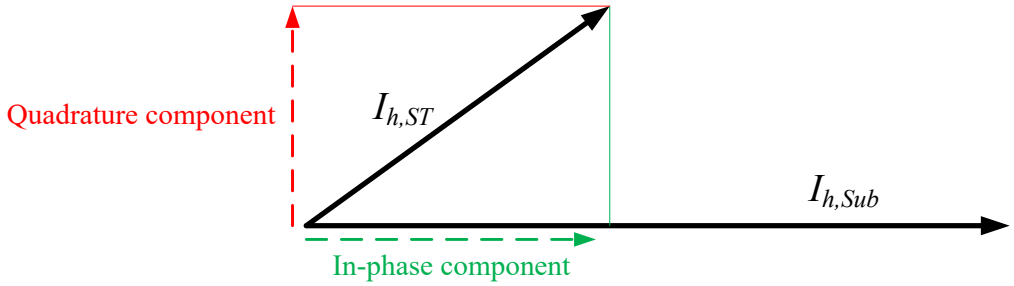

Figure 2.32 The phasor diagram of the substation current and the service transformer current

To quantify the degree of harmonic addition, the normalized in-phase component of the h-th service transformer current $I_{h,ST}$ is determined according to (2.5). This component represents the portion of $I_{h,ST}$ that directly adds to the h-th feeder current $I_{h,Sub}$. The normalized in-phase component, ρ_h , is in the range of -100% to +100%. If ρ_h is above zero, it indicates that $I_{h,ST}$ adds to the feeder current. ρ_h <0 represents harmonic cancellation.

$$\rho_h = \frac{I_{h,ST\_in-phase}}{I_{h,ST}} = \cos(\varphi_{I_{h,ST}} - \varphi_{I_{h,Sub}}) \times 100\% \qquad (2.5)$$

2.6.1 Characteristics of 3rd Harmonic Current

The 24-hour phase-angle variations of the 3rd harmonic currents measured at the substation and the service transformer are presented in Figure 2.33. The results show that the angle patterns are not completely random and the average angle differences are about 47 degree. This difference can be explained by the voltage phase angle variation along the feeder. The longer the distance, the larger the phase angle difference is expected to be. However, this level of measured harmonic phase angle difference at the two locations is not large enough to cause harmonic cancellation.

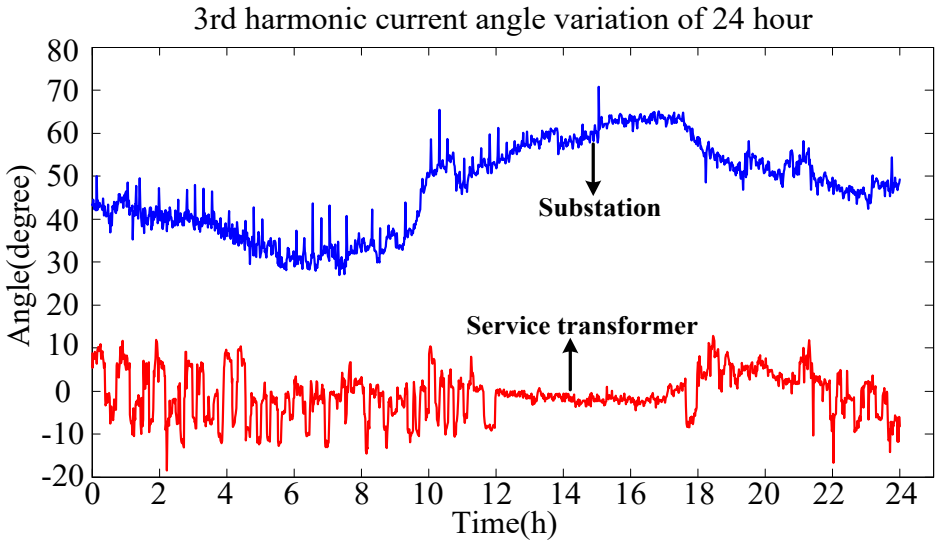

Figure 2.33 The 24-hour phase-angle variation of the 3rd harmonic current

The percentage of the in-phase component of the 3rd harmonic (ρ_3) in 24 hours is shown in Figure 2.34. The probability distribution of ρ_3 is illustrated in Figure 2.35. The results clearly show that the 3rd harmonics from service transformer always adds to the feeder current. There is no period of harmonic cancellation.

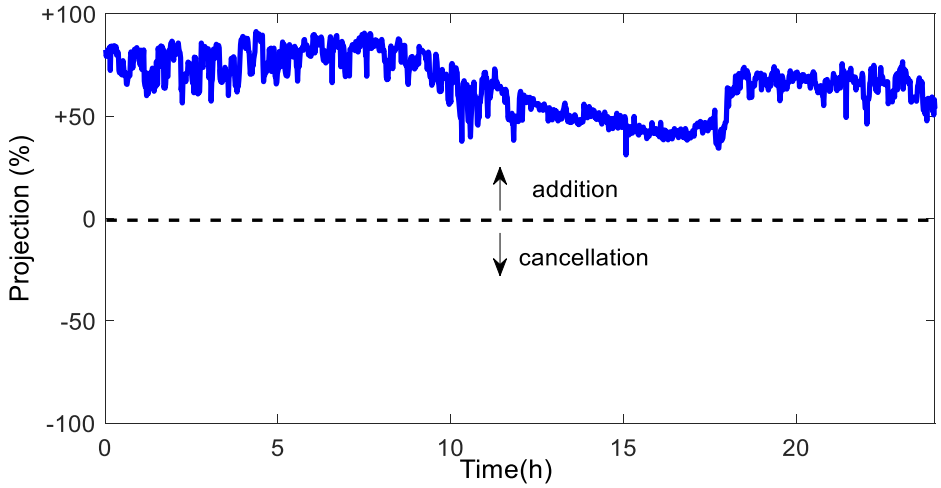

Figure 2.34 The percentage of the in-phase component of $I_{3,ST}$ in 24 hours

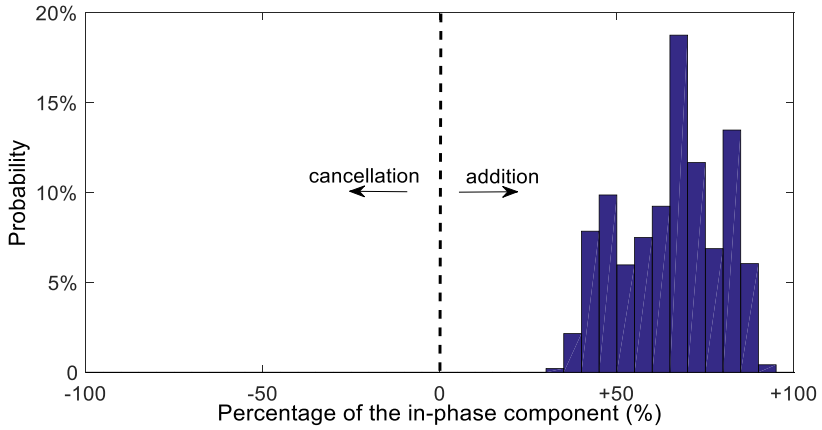

Figure 2.35 Probability distribution of the percentage of in-phase component of $I_{3,ST}$

2.6.2 Characteristics of Other Harmonic Currents

Figure 2.36 presents the 95% confidence interval of normalized in-phase component for various harmonics. It shows that for low harmonic orders (3rd to 11th), $I_{h,ST}$ has an addition effect on $I_{h,Sub}$ during the whole day. This finding further explains why harmonics from individual residential loads can have a large impact on increasing feeder harmonic current distortion levels. However, the contribution becomes unpredictable for high order harmonics, as their contributions change significantly during the whole day. The possible reason is that the change of the fundamental voltage along the feeder has a significant impact on the phase angle of the high order harmonic currents, but less impact for the low order harmonics.

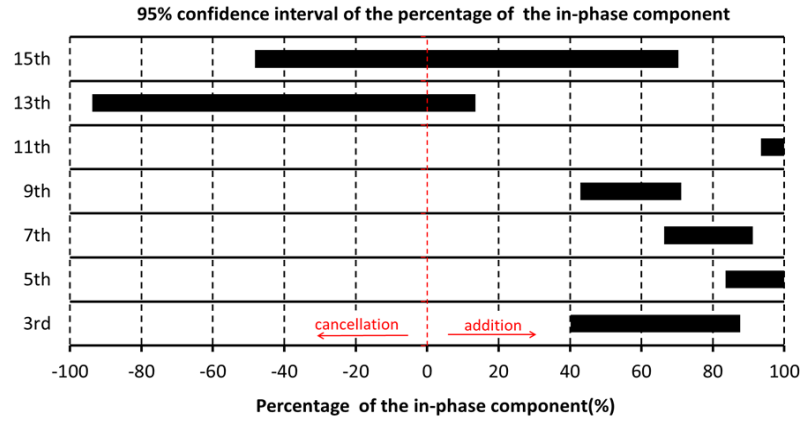

Figure 2.36 The 95% confidence interval of the percentage of the in-phase component for different harmonics

2.7 Harmonic Voltage Induction

One of the negative effects of harmonics is the inductive coupling to nearby conductive structures such as telephone lines and pipelines etc., which could lead to telephone interference or pipeline corrosion [7][52]. The level of induced voltage is dependent on the zero sequence currents of the power line, the frequencies of the currents and the distances between power lines and conductive structure of interest.

Inductive coupling measurements have also been conducted for residential feeders. The induced voltage is measured on a pair of unused telephone line running in parallel with a residential feeder. If the telephone line is not available, probe wires were used as a substitute. The zero sequence harmonic currents of the feeders are also determined.

2.7.1 Induced Voltages

The amount of induced voltage in a telephone line or a probe wire is affected by the length of parallelism. It is not useful to examine the actual value of the induced voltage. Instead, the percentage voltage normalized to the fundamental frequency component is used. The result can show the degree of voltage induction caused by harmonics in comparison with that caused by the fundamental frequency current. Note that inductive coordination standards were developed for the fundamental frequency current first.

The normalized induced voltages are shown in Figure 2.37. The results show that residential feeders can induce significant 3^{rd} and 9^{th} harmonic voltages on the nearby conductors. The induced voltages at 3^{rd} and 9^{th} harmonics can be as high as 6 to 10 times of the fundamental frequency. As a result, the harmonic voltage induction could be a concern for cases where the induction level at the fundamental frequency is closely regulated.

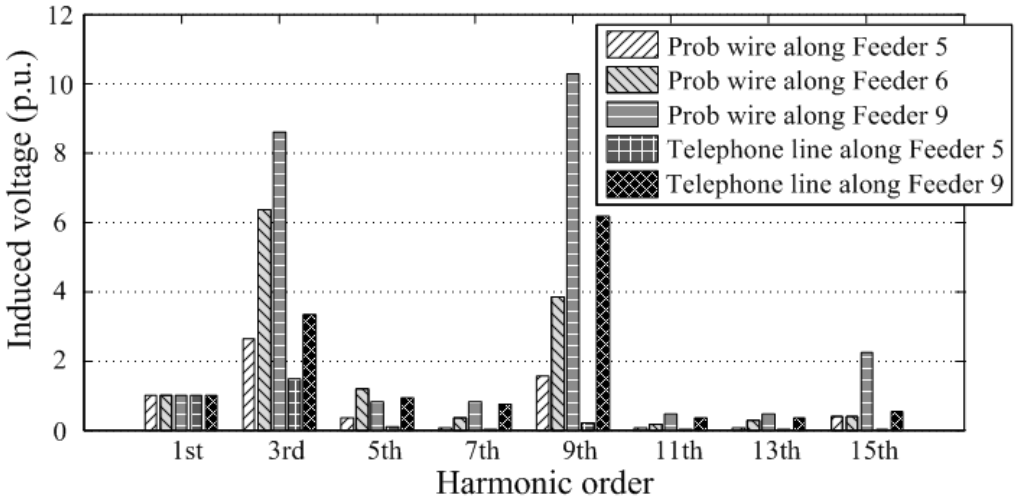

Figure 2.37 Harmonic spectrum of induced voltage.

2.7.2 Zero Sequence Current Level

Except for very short-distance separated installation schemes, such as on joint-use poles, the induced voltage from a feeder to nearby conductors is mainly caused by the zero sequence currents in the feeder. The zero sequence harmonic currents of measured feeders are shown in Figure 2.38.

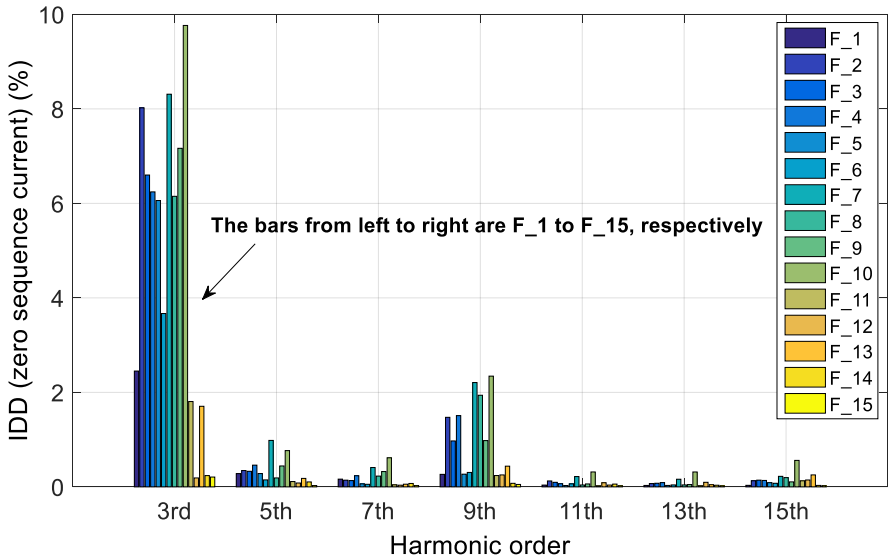

Figure 2.38 Zero sequence harmonic current *IDD* of different feeders

In this figure, F_1 is a mixed load feeder, F_2~F_10 are the residential feeders, F_11~F_13 are the commercial feeders, and F_14~F_15 are the industrial feeders.

It is clearly observed that the residential feeders exhibit much higher zero sequence 3rd harmonic currents compared to commercial and industrial feeders. This is the main cause of significant induced 3rd harmonic voltage observed on probe wires and telephone lines.

The comparison of Figure 2.37 and Figure 2.38 suggests that the 3rd harmonic zero sequence component is much larger than the 9th and 15th ones, while the induced voltages are comparable between 3rd and 9th harmonics. This phenomenon can be explained by the fact that the strength of induced voltage is proportional to the frequency. The higher the frequency, the greater the induced voltage is.

2.8 Summary

This chapter reveals the harmonic current characteristics of the both MV and LV residential distribution systems in North America based on extensive field measurement data, backed by a cohesive analysis on the results obtained from multiple sites and at various levels of a distribution feeder. The main findings of this investigation are summarized as follows:

- Residential loads, although small individually, can collectively inject higher harmonic currents than comparable commercial and industrial loads. The harmonic magnitude spectra of these three types of loads are quite different. The 3rd harmonic is highly noticeable for residential feeders.

- The main harmonics of concern for residential loads are the 3rd and 5th harmonics. Phase angles of these harmonics do not vary randomly. The possible reason is that different home appliances have similar mechanisms to produce harmonics. For example, many home appliances such as the compact fluorescent lamps, computers, and televisions are diode-bridge converter-based devices. As a result, the harmonics from individual homes appliances add together, creating high distortion levels at the feeder terminal. Some of the feeders can have distortions higher than the IEEE Std. 519 limits.

- Residential feeders can contain rich zero sequence harmonic currents. These harmonics can produce much higher induced voltages in nearby conductive structures. The main harmonic component of concern is the 3^{rd} and 9^{th} harmonic.

In summary, harmonics from home appliances are a significant source of harmonic distortions in modern residential distribution systems. Such noticeable increase of harmonic pollutions might potentially cause several problems for utility companies and customers, such as 1) overloading of utility assets (transformers, cable, capacitors etc.), 2) telephone interference and pipeline corrosion, 3) rising neutral current in the primary feeder, leading to increased neutral to earth voltages, 4) resonance caused capacitor/cable failure. It is, therefore, important for appliance manufacturers to adopt the device level harmonic limits. Before that, the utility companies should pay close attention to the above issues.

Chapter 3

Resonance-Free Scheme for Multiple Switchable Capacitors

A serious concern arising from the proliferation of harmonic sources is the increased possibility of system-capacitor resonance. The result is the amplification of the harmonic voltage and current, which can damage the capacitor and other electrical devices in the system. A cost-effective measure that guarantees the capacitor not to resonate with the system is always desired in the capacitor application. This chapter proposes a new scheme to mitigate the harmonic resonance for multiple switchable capacitors. Performance and usefulness of the developed scheme are evaluated through the comparative study on actual capacitor application cases.

The chapter is organized as follows. Section 3.1 reviews the existing methods to mitigate the system-capacitor resonance. Section 3.2 illustrates the proposed scheme. Section 3.3 develops the design method for the proposed scheme. In Section 3.4, performance and effectiveness of the proposed scheme are demonstrated through comparative studies on actual capacitor application cases. In Section 3.5, the design process is further simplified with a lookup table. This table shows the normalized damping block parameters that can work for all possible capacitor sizes and system impedance values.

3.1 Review on Capacitor Resonance Mitigation

The simplest approach to mitigate the capacitor resonance is to resize or relocate the capacitor [33],[53]-[56]. However, this measure would affect the reactive power compensation of the capacitor if the size or the location changes significantly. Besides, there is no guarantee that the resized or relocated capacitor

will not resonate with the system when the system configuration changes.

To address this issue, the idea of adding a detuned inductor to the shunt capacitor has been proposed [35][36], as shown in Figure 3.1(a). The detuned inductor is designed in such a way that the entire filter exhibits an inductive characteristic at frequencies higher than a detuning frequency such as 2.7^{th} or 4.2^{nd} harmonic frequencies. If the system impedance is also inductive, resonance at harmonic frequencies that are higher than the detuning frequency can be avoided. However, this method does not always work if the system exhibits capacitive impedance at certain frequencies which is normally the case for transmission systems. As a result, some utilities have started to configure transmission voltage shunt capacitors as C-type filters to avoid the resonance [37][38], as shown in Figure 3.1(b). The configuration of a C-type filter exhibits good damping characteristics for frequencies higher than its tuning frequency. Besides, the C-type filter has almost zero losses at the fundamental frequency. The recent study in [39] presents a design method to configure a shunt capacitor as a C-type filter with guaranteed resonance-free performance. The term "resonance-free" means the harmonic amplification caused by the capacitor is guaranteed to be less than the predefined limit under any network impedance conditions.

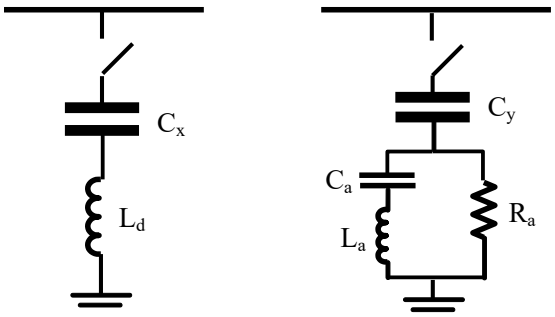

(a) Detuned capacitor (b) C-type filter

Figure 3.1 Typical resonance-mitigation methods for shunt capacitors

For transmission systems, it is common to have more than one switchable capacitor at one location. Each of the capacitors can be switched on or off based on network reactive power demand. In order to mitigate harmonic resonance for

such cases, each of the capacitors requires a C-type damping block to form a C-type filter. The cost and space requirement for implementing these changes increase with the number of switchable capacitors

3.2 Proposed Scheme

This chapter continues the research in [39] and proposes an improved resonance-free scheme for multiple switchable capacitors. The proposed scheme is shown in Figure 3.2. As two switchable capacitors are commonly used at the high voltage (HV) level, Figure 3.2 depicts two switchable capacitors denoted as C_X and C_Y. Both share the same damping block D. It will be shown next that the damping block D, if designed properly, can make all three capacitor energization scenarios (i.e. C_X on, C_Y on and C_X & C_Y both on) not to cause harmonic resonance with the system regardless of the system impedance value.

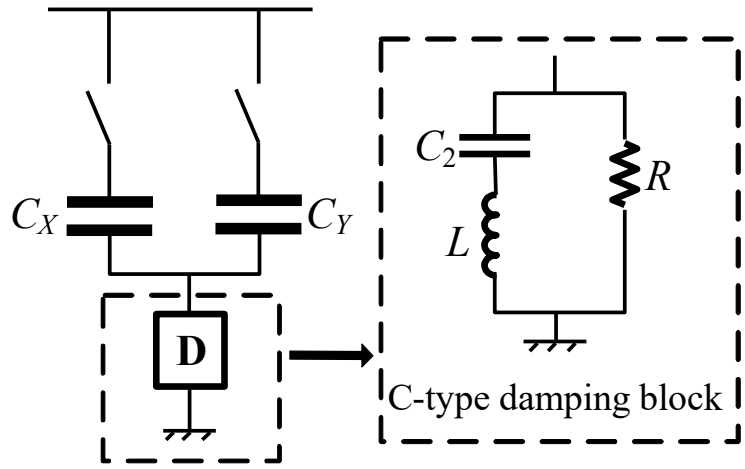

Figure 3.2 The proposed scheme and its C-type damping block

As can be seen from Figure 3.2, the damping block takes the form of the C-type damping block, where C_2 is the auxiliary capacitor, L is the tuning inductor and R is the damping resistor. If the block is series connected with a capacitor, one can easily recognize a C-type filter is formed. The main feature of the C-type damping block is the L-C_2 branch tuned at the fundamental frequency. The frequency response of the C-type damping block can be calculated as (3.1), where X_L is the fundamental frequency impedance of L and h is the harmonic order.

$$Z_D = R_D + jX_D \tag{3.1}$$

where

$$R_D = \frac{R[X_L(h-1/h)]^2}{R^2 + [X_L(h-1/h)]^2} \tag{3.2}$$

$$X_D = \frac{R^2[X_L(h-1/h)]}{R^2 + [X_L(h-1/h)]^2} \tag{3.3}$$

The frequency response of the entire shunt device including the main capacitor (C_X and C_Y) and the C-type damping block can be determined as (3.4),

$$Z_f = Z_{C1} + Z_D = R_D + j(X_D - X_{C1}/h) \tag{3.4}$$

where X_{C1} is the fundamental frequency impedance of the main capacitor in three capacitor energization scenarios, i.e. X_{C1}=[X_{CX}, X_{CY}, X_{CX}||X_{CY}].

According to (3.4), a large X_L and R can increase X_D. Thus, if X_L and R are selected to be sufficiently large, the imaginary part of (3.4) will be dominated by X_D, namely,

$$X_D \gg \frac{\max(X_{C1})}{h} \tag{3.5}$$

Thus, Z_f=Z_{C1}+Z_D≈Z_D, which suggests that the frequency response of the entire shunt device can be approximately determined by its damping block.

When a shunt device of impedance $Z_z(h)$ is connected to the system, the h-th harmonic voltage at the connection bus changes from $V_{pre}(h)$ to $V_{post}(h)$. So, the amplification of harmonic voltage caused by connecting the shunt devices is,

$$HAR(h) = \left| \frac{V_{post}(h)}{V_{pre}(h)} \right| \tag{3.6}$$

where *HAR* stands for harmonic amplification ratio. According to [39], the worst-case amplification of the harmonic voltage is,

$$HAR_{\text{worst}}(h) = \max\left(\frac{V_{post}(h)}{V_{pre}(h)}\right) = \sqrt{1+\left(\frac{X_Z(h)}{R_Z(h)}\right)^2} \tag{3.7}$$

where $X_z(h)$ and $R_z(h)$ are the imaginary and real part of h-th harmonic impedance of the shunt device $Z_z(h)$, respectively. According to [39], such a worst-case occurs for the extreme condition that the system impedance has no resistance and is in perfect resonance with $X_z(h)$. Substitute R_D in (3.2) and X_D in (3.3) as R_Z and X_Z into (3.7) yields

$$HAR_{worst}(h) = \sqrt{1+\left(\frac{X_D(h)}{R_D(h)}\right)^2} = \sqrt{1+\left(\frac{R}{X_L(h-1/h)}\right)^2} \tag{3.8}$$

Eq. (3.8) shows that if a limit of harmonic voltage amplification is selected by a designer such as $HAR_{worst} \leq 1.2$ for $h \geq 5$, the components R and X_L can be selected to meet the following condition:

$$R \leq X_L\sqrt{(h-1/h)^2(HAR_{limit}^2-1)} \leq 3.2X_L \tag{3.9}$$

In other words, the above condition will guarantee a "resonance-free" performance for all three capacitor energization scenarios regardless of the value of the system impedance. Here "resonance-free" is defined as $HAR_{worst}(h)$ less than a designer selected threshold of 1.2.

One can also infer from condition (3.5), if a C-type damping block is designed for the smallest capacitor (in term of reactive power output, i.e. largest X_{C1}), the damping block can provide sufficient damping for all scenarios of higher reactive power output. In other words, the parameter of the C-type damping block in the proposed scheme is mainly determined by the smallest capacitor. For example, for the case involving two switchable capacitors of 10MVar and 15MVar, the parameter of the damping block is mainly determined by the 10MVar capacitor.

The conventional scheme equips each capacitor with a C-type damping block, so two blocks are needed for two capacitors. The main advantage of the proposed scheme is therefore to save one damping block. The space requirement is definitely reduced. However, the cost saving is not straightforward. For example,

the shared damping block shall be rated to carry the current of both capacitors. In comparison, the conventional scheme only requires to rate each damping block for individual capacitors. A detailed comparative analysis on costs will be presented in Section 3.4.

3.3 Design method

To simplify the illustration, the condition (3.5) is used in the previous section to explain the proposed scheme. This condition is a sufficient condition rather than a necessary condition. It will be shown next that the size of the C-type damping block could be much smaller if the block is properly designed. This section proposes the design method to optimize the parameters of the proposed scheme. Without loss of generality, the number of switchable capacitors is assumed to be two. The proposed design method can be easily extended for three or more capacitors.

- **Condition 1:** reactive power support

At the fundamental frequency, the C-type damping block behaves like a short circuit as L and C_2 are tuned at the fundamental frequency. The reactive power output of the entire shunt device is only determined by the main capacitor C_X and C_Y. This feature yields the first design equation:

$$C_X = Q_{FX} / (\omega_F V_r^2), C_Y = Q_{FY} / (\omega_F V_r^2) \tag{3.10}$$

where ω_F is the fundamental angular frequency, V_r is the rated system voltage, Q_{FX} and Q_{FY} are the required reactive power for C_X and C_Y, respectively.

- **Condition 2:** resonance-free condition

The C-type damping block should guarantee all capacitor energization scenarios (i.e. C_X on, C_Y on and C_X & C_Y both on) to be resonance free. This condition leads to the second design equation (3.11).

$$HAR_{\text{worst}}(\omega, C_1, C_2, L, R) \le HAR_{\text{limit}}, \quad \text{for } \omega \ge \omega_T \tag{3.11}$$

where C_1=[C_X, C_Y, C_X||C_Y], ω_T is the tuning frequency which normally can be selected as 3rd or 5th harmonic, and

$$HAR_{\text{worst}}(\omega, C_1, C_2, L, R) = \sqrt{1 + \left(\frac{a_1\omega^4 + b_1\omega^2 - 1}{\omega R C_1 (\omega^2 L C_2 - 1)^2}\right)^2} \tag{3.12}$$

$$\begin{cases} a_1 = R^2 L C_2^{\,2} C_1 - L^2 C_2^2 \\ b_1 = 2LC_2 - R^2 C_1 C_2 - R^2 C_2^2 \end{cases} \tag{3.13}$$

- **Condition 3:** fundamental frequency loss minimization

C_2 and L are tuned at the fundamental frequency to eliminate the fundamental frequency loss, which leads to

$$L = 1/(\omega_F^2 C_2) \tag{3.14}$$

- **Condition 4:** cost minimization

Above three conditions are the basic requirements for the proposed scheme. If only those three constraints are applied, there would be thousands of solutions. As a result, one more condition is required to determine the final parameters. The fourth design condition can be application dependent. In this thesis, the cost minimization is adopted as the fourth design condition. When the required reactive power output is given, the larger inductance of L, the greater of the capacities are needed for both L and C_2. Also, the cost for both L and C_2 are positively correlated with their capacities. If the inductance of L can be reduced to the minimum, the total investment of the C-type damping block is assumed to the least [57]. Therefore, the cost minimization is to minimize the inductance of L.

$$\text{Cost minimization:} \quad \min(L) \tag{3.15}$$

- Design procedure

Among the four design conditions, C_X and C_Y can be determined using (3.10). C_2 can be determined by (3.14) once L is known. Therefore, the problem is basically a two-variable (L and R) optimization problem, which tries to find the minimum L that satisfies the predefined HAR_{limit}. The formulation of the design

problem, complying with the previous constraints, is presented as follows. It should be emphasized that the proposed design method is different with the one in previous work [39]. A comparison of these two design methods are illustrated in Appendix A.

Objective function: $F = \min_{L,R}(L)$

Subject to:

- $C_X = Q_{FX} / (\omega_F V_r^2), C_Y = Q_{FY} / (\omega_F V_r^2)$
- $L = 1/(\omega_F^2 C_2)$
- $HAR_{\text{worst}}(\omega, C_1, C_2, L, R) \le HAR_{\text{limit}}$, for $\omega \ge \omega_T$

This optimization problem must have a solution, which has been explained in Section 3.2. There are many methods to solve this problem. The simplest way is to scan all feasible values of L and R. This is the method adopted here and it is shown in Figure 3.3. Note the proposed scheme guarantees the resonance-free performance for all harmonic frequencies higher than the tuning frequency ω_T. It is prerequisite to solve the frequency ω_e that reaches the maximum HAR_{worst}. If $HAR_{worst}(\omega_e)$ is smaller than HAR_{limit}, the resonance-free performance then can be guaranteed. The method to solve ω_e is presented in Appendix B.1. Furthermore, search ranges of L and R are established in Appendix B.2 to improve the search efficiency.

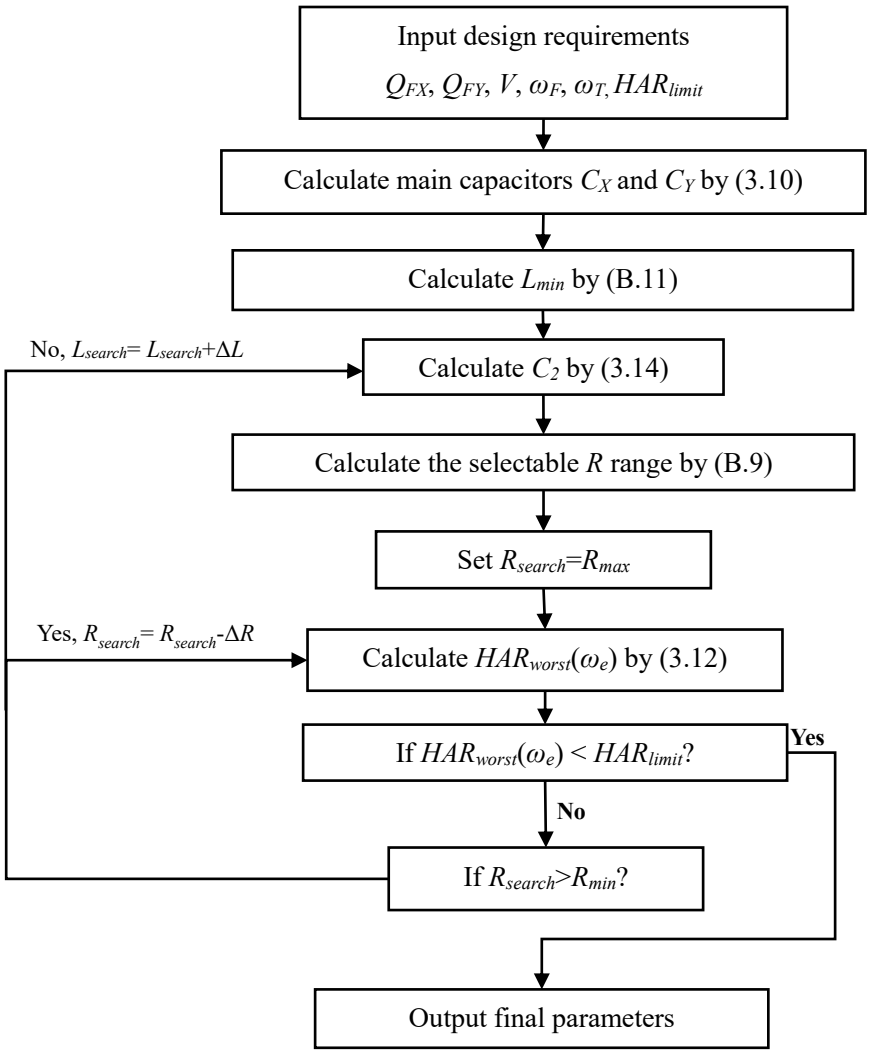

Figure 3.3 Flow chart of the design procedure.

3.4 Comparative Case Study

In this section, case studies are presented for evaluating the effectiveness of the proposed scheme. The performance of the proposed scheme is compared with that of the conventional scheme.

3.4.1 Case Description

Figure 3.4 shows the simplified single line diagram of a part of 240/144kV transmission system in Alberta, Canada. The system has over 1000 transmission voltage buses and a number of shunt capacitors. This study involves two

switchable capacitors to be connected to substation SX. The short circuit capacity at substation SX is 1400MVA. The installed capacitors have two different combinations of reactive power, as shown below.

1) Case #1: two 15MVar capacitors are connected

2) Case #2: one 10MVar capacitor and one 20MVar capacitor are connected.

The background voltage distortion at substation SX is assumed to be 1.5% from 5th to 19th harmonics according to IEEE 519 limit. Two resonance-free scheme options are evaluated. They are:

3) Conventional scheme - two C-type damping blocks are installed for each capacitor.

4) Proposed scheme - one C-type damping block is shared by two capacitors.

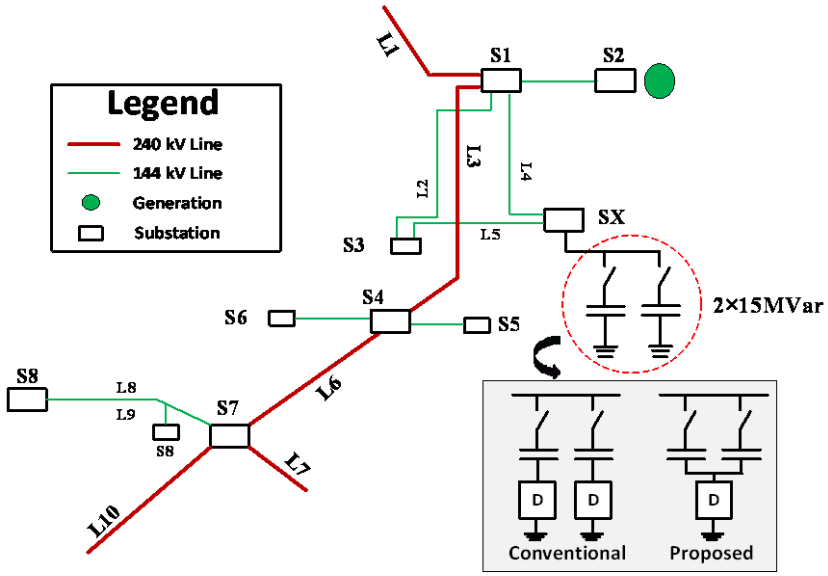

Figure 3.4 System configuration

3.4.2 Performance and Cost Comparison of Case #1

In case #1, two 15MVar capacitors are connected to substation SX. This is the most common situation in practice where two switchable capacitors have equal capacities. There are two capacitor energization scenarios in this case.

1) Scenario #1 – one 15MVar capacitor on,

2) Scenario #2 – two 15MVar capacitors on.

The proposed design methods are applied to determine the parameters for the conventional scheme and the proposed scheme. The resonance-free condition is selected as HAR_{limit}=1.2 and the tuning frequency is f_T=300Hz (i.e., 5th harmonic). This study compares the resonance-mitigation performance, power loss and cost.

a) Resonance-mitigation performance

Figure 3.5 shows the harmonic voltage amplification caused by two schemes. The worst-case ratio is determined by assuming the system impedance has no resistance and is in perfect resonance with the capacitor. The actual amplification ratio is calculated by considering the reference system impedance given by the utility. Two conclusions can be drawn. 1) The proposed scheme can guarantee the resonance-free condition for both two capacitor energization scenarios. Even under the worst system condition, the harmonic amplification caused by the proposed scheme is always below the design limit. 2) The actual harmonic amplification performance is much better than the design limit. According to Figure 3.5, the actual harmonic amplification ratios for most harmonic orders are below 1.0. This suggests that the proposed scheme so designed has large chance to reduce the harmonic distortion level at the installation location.

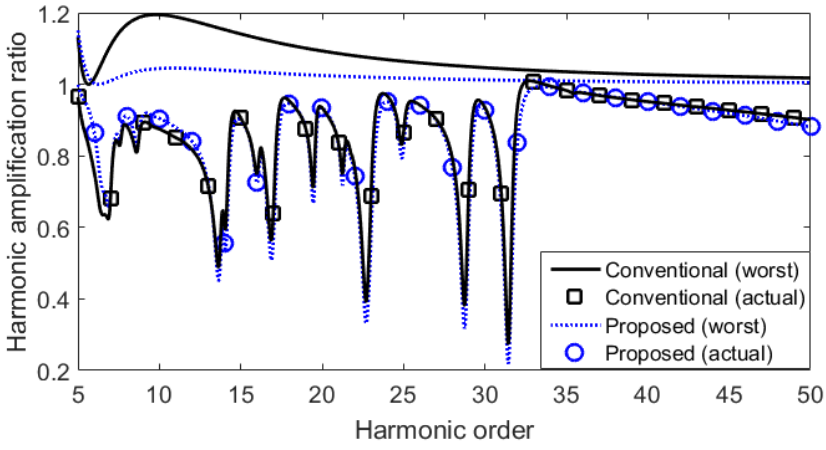

(a) Scenario #1

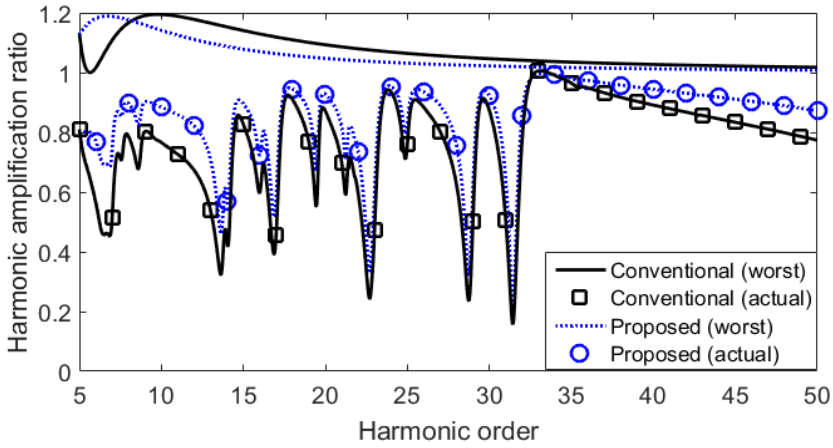

(b) Scenario #2

Figure 3.5 HARs of two schemes (case #1)

Figure 3.6 gives the voltage spectra at substation SX for installation scenarios: 1) no capacitor; 2) pure capacitors; 3) the conventional scheme; and 4) the proposed scheme. As can be seen from these two figures, the pure capacitor could cause significant voltage distortion at this substation, while using the proposed scheme would lead to a slight decrease of the harmonic voltages. The harmonic reduction performance of the proposed scheme is comparable with that of the conventional scheme.

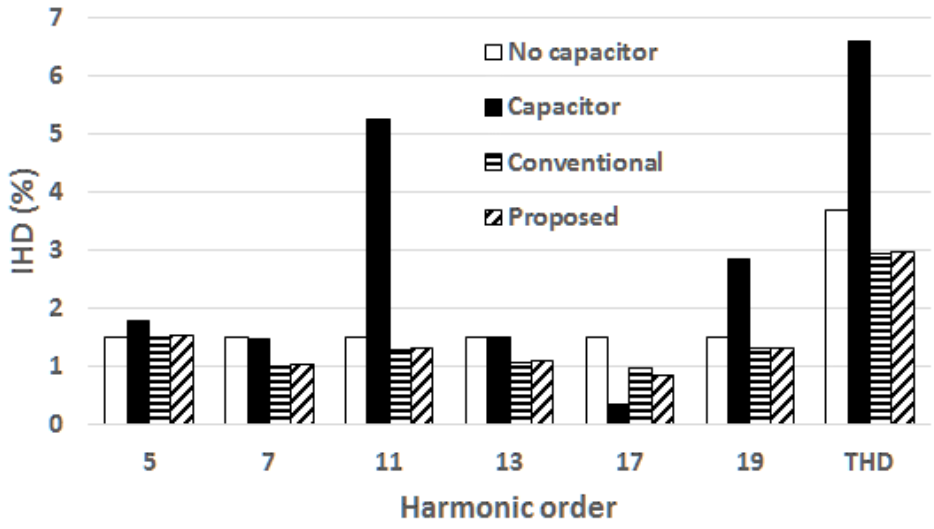

(a) Scenario #1

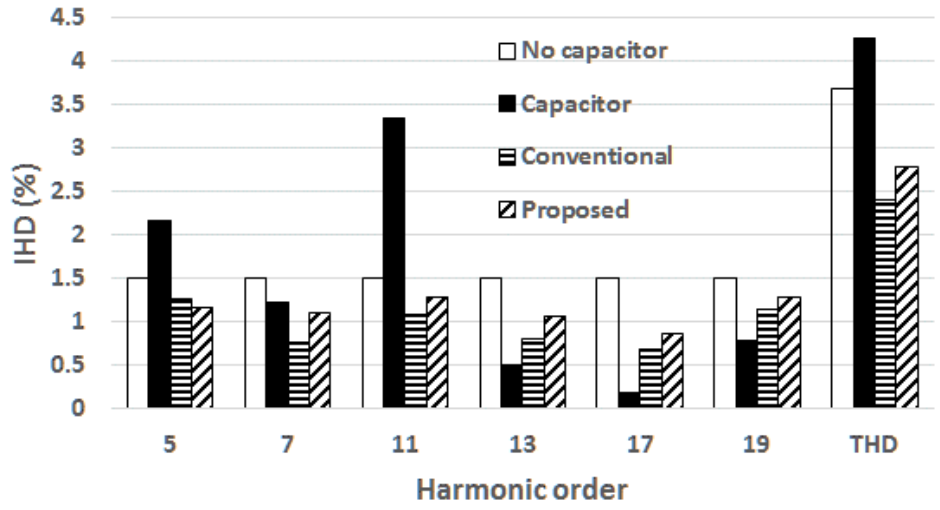

(b) Scenario #2

Figure 3.6 Voltage spectra at SX for different installation scenarios (case #1)

b) Cost comparison

Table 3.1 compares the parameters and loadings of two schemes. The conventional scheme has two same C-type damping blocks, denoted as DP #1 and DP #2 that designed for two 15MVar capacitors (C_X and C_Y). The proposed scheme needs only one C-type damping block, denoted as DP #3. In the table, index "voltage" means the line to line RMS voltage experienced by the corresponding component and index "current" means the current flowing through the corresponding component. The loading value in the table represents the maximum value in two capacitor energization scenarios. According to Table 3.1, the values of R, L, C_2 are roughly same in two schemes. This finding confirms the conjecture in Section 3.2 that the damping block parameters of the proposed scheme are mainly determined by the smallest main capacitor (15MVar). In terms of the loading conditions of two schemes, the fundamental current flowing through the C-type damping block is determined by the main capacitor, so the current flowing through L and C_2 in DP #3 is approximately double of that in DP #1 (or DP #2). The harmonic current flowing through the C-type damping block is mainly determined by the C-type damping block itself. Therefore, the current flowing though R in DP #3 is almost equal to that in DP #1 (or DP #2).

Table 3.1 Comparison of parameters and loadings of two schemes (case #1)

Main capacitor		Conventional (C_X or C_Y)	Proposed (C_X or C_Y)
C_1	Value (uF)	1.92	1.92
	Voltage (kV)	144.12	144.08
	Current (A)	61.66	61.23
C-type damping block		Conventional (DP #1 or DP #2)	Proposed (DP #3)
C_2	Value (uF)	50.20	47.52
	Voltage (kV)	5.51	11.63
	Current (A)	61.35	120.51
L	Value (mH)	140.20	148.10
	Voltage (kV)	8.80	12.70
	Current (A)	61.35	120.51
R	Value (Ω)	627.89	453.72
	Voltage (kV)	6.69	5.66
	Current (A)	6.15	7.21

With the information of parameters and loadings, the cost is then compared for each component:

- C_1: The loadings of C_1 are same in two schemes, so the costs of C_1 are same.
- C_2: The capacity of C_2 in the proposed scheme (DP #3) is approximately double of that in the conventional scheme (DP #1 & DP #2). If the cost of a capacitor is assumed to be approximately proportional to its capacity, the cost of C_2 in the proposed scheme is double of that in the conventional scheme. However, this additional cost is not significant as the per MVar cost of a capacitor is lower than that of the inductor or the resistor.
- L: The inductance of L in DP #3 is roughly equal to that in DP #1 (or DP #2), but the current rating of L in DP #3 is doubled. The manufacturer needs to use a thicker conductor for the inductor in the proposed scheme. However, such change does not significantly increase the cost for a HV air core inductor. According to the quotations from inductor manufacturers, the cost of the inductor in the proposed scheme (DP #3) is 25% lower than the cost of two inductors in the conventional scheme (DP #1 & DP #2).
- R: The loading of R in DP #3 is roughly equal to that in DP #1 (or DP #2). The

proposed scheme saves one resistor, so its expense on *R* is half.

Table 3.2 shows the expenses of two schemes on C-type damping blocks based on the quotations from the manufacturers (the quotations are presented in Appendix C). The relative cost in the table means the per unit cost of the proposed scheme using the cost of the conventional scheme as the base value. As can be seen from the table, the total cost of the proposed scheme is two thirds of that of the conventional scheme. Further cost saving can be expected on the CTs. Since each component in the C-type damping block requires one CT, the proposed scheme saves three CTs.

Table 3.2 Cost of C-type damping blocks in two schemes (case #1)

	Conventional ($)	Proposed ($)	Relative cost (p.u.)
C_2	5,777	12,122	2.10
L	61,510	45,914	0.75
R	76,826	38,376	0.50
Total	144,113	96,413	0.67

Besides of the component cost, other expenses of the scheme, such as the construction cost, the engineering cost and the real estate cost, should also be considered in the cost comparison. According to the facility study report of PJM Interconnection [58], the construction and engineering costs to install a HV capacitor is roughly equal to its equipment cost. Since the proposed scheme saves one C-type damping block, the costs of the site development and the real estate are cut down. Besides, the workload for the engineers to assemble and test the C-type damping block are also reduced. All these cost savings make the proposed scheme more attractive.

c) Power loss comparison

Table 3.3 compares the power loss of two schemes. According to the table, the proposed scheme and the conventional scheme, theoretically, have zero fundamental frequency loss. The harmonic loss of the proposed scheme is lower than that of the conventional scheme in scenario #2. This is because the equivalent harmonic impedance of the entire shunt device is mainly determined

by the C-type damping block. In scenario #2, the conventional scheme with two paralleled C-type damping blocks has smaller harmonic impedances. A smaller shunt impedance results in higher harmonic loss.

Table 3.3 Power loss comparison of two schemes (case #1)

		Conventional		Proposed	
Scenario		#1	#2	#1	#2
Reactive power (MVar)		15.00	30.00	15.00	30.00
Power loss (kW)	Fundamental frequency	0	0	0	0
	Harmonic frequencies	71.23	96.65	70.62	55.24
	Total	71.23	96.65	70.62	55.24
	% loss (of total MVar)	0.24	0.32	0.23	0.18

d) Summary of case #1 study

Through the comparison of resonance-mitigation performance, economic performance and power loss performance, some key findings are summarized for case #1 study.

- The proposed scheme has comparable resonance-mitigation performance as the conventional scheme.
- The component cost of the proposed scheme is lower than two thirds of that of the conventional scheme. Further savings on construction cost and engineering cost can be expected.
- The proposed scheme has lower harmonic loss than that of the conventional scheme.

3.4.3 Performance and Cost Comparison of Case #2

According to the investigation of the HV capacitors in Canada, two switchable capacitors at one bus have equal reactive power capacities in most cases. If not, the ratio of their capacities is normally no bigger than two. Taking this into account, case #2 studies an additional case that one 10MVar capacitor and one

20MVar capacitor are connected to substation SX. There are three capacitor energization scenarios in case #2.

1) Scenario #3 – 10MVar capacitor on,

2) Scenario #4 – 20MVar capacitor on.

3) Scenario #5 – both 10MVar capacitor and 20MVar capacitor on.

The proposed design methods are applied to determine the parameters for the conventional scheme and the proposed scheme. The resonance-free condition is selected as HAR_{limit}=1.2 and the tuning frequency is f_T=300Hz (i.e., 5th harmonic). This study compares the resonance-mitigation performance, power loss and cost.

a) Resonance-mitigation performance

Figure 3.7 shows the harmonic voltage amplification caused by two schemes. As seen from the figure, the proposed scheme can guarantee the resonance-free performance for all three capacitor energization scenarios and its actual harmonic amplification ratios for most harmonic orders are below 1.0.

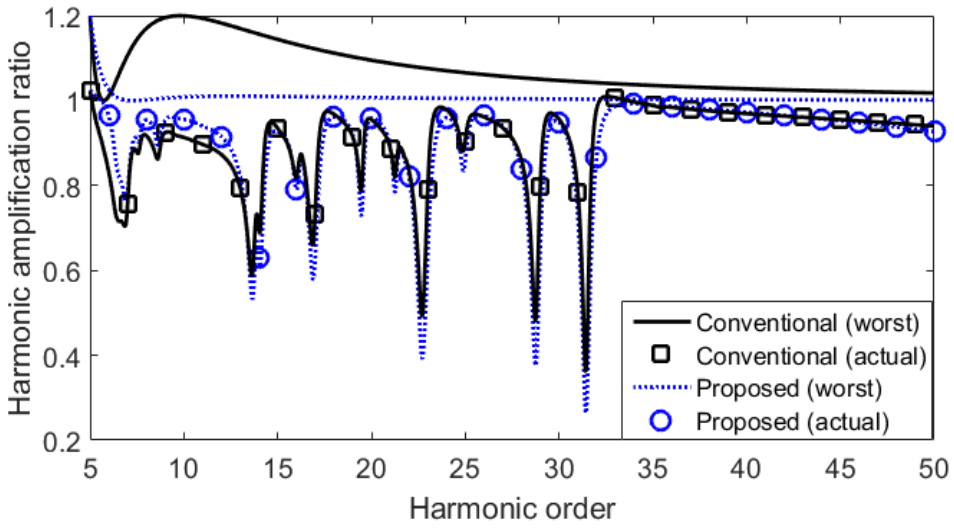

(a) Scenario #3

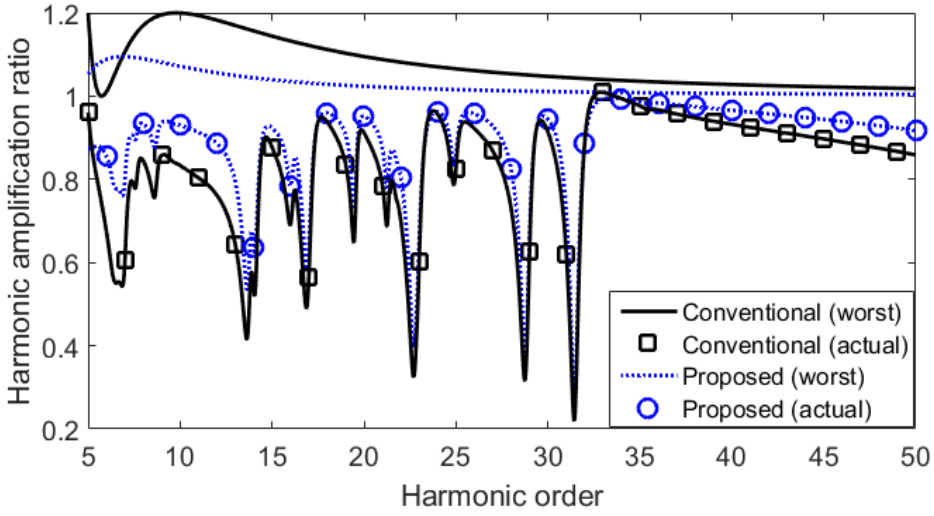

(b) Scenario #4

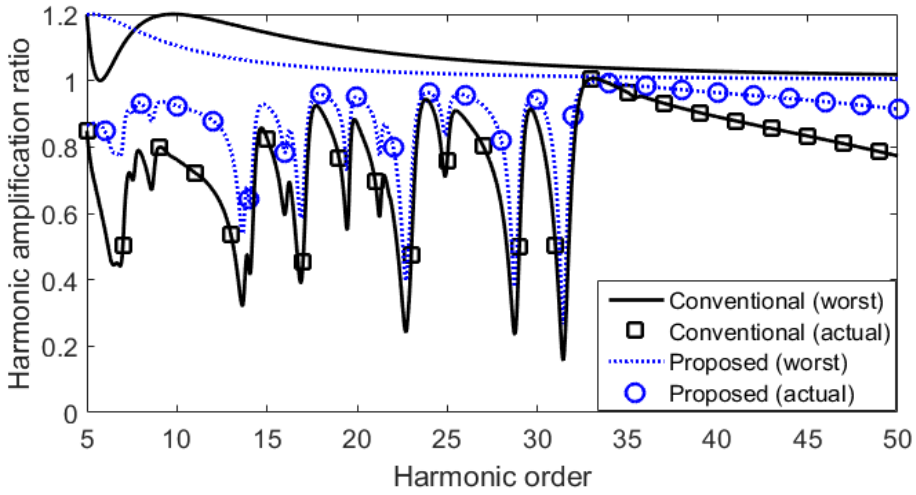

(c) Scenario #5

Figure 3.7 HARs of two schemes (case #2)

Figure 3.8 gives the voltage spectra at substation SX for different installation scenarios: 1) no capacitor; 2) pure capacitors; 3) the conventional scheme; and 4) the proposed scheme. It can be observed that the pure capacitor could lead to severe voltage distortion at this substation, while using the proposed scheme would lead to a slight decrease of the harmonic voltages.

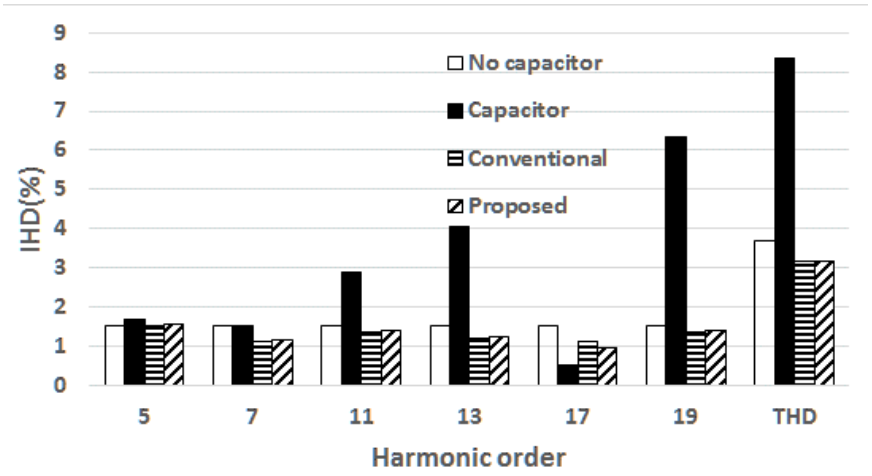

(a) Scenario #3

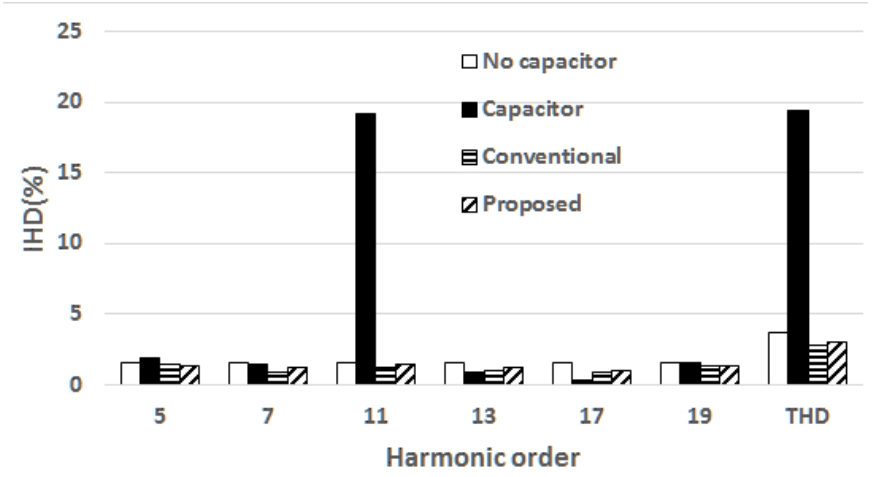

(b) Scenario #4

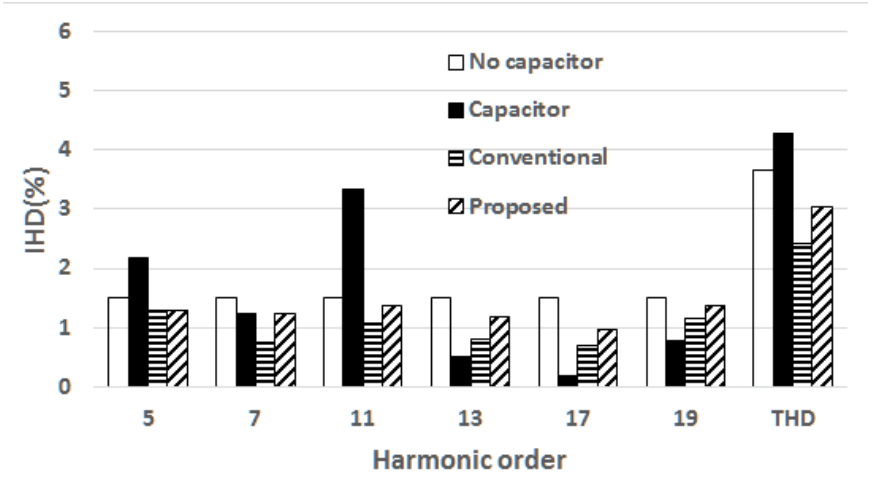

(c) Scenario #5

Figure 3.8 Voltage spectra at SX for different installation scenarios (case #2)

b) Cost comparison

Table 3.4 shows the parameters and loading conditions of two schemes. In this case, the conventional scheme requires two different C-type damping blocks, denoted as DP #4 and DP #5 that designed for the 10MVar capacitor (C_X) and the 20MVar capacitor (C_Y), respectively. The proposed scheme needs only one C-type damping block, denoted as DP #6. According to Table 3.4, the parameters of DP #6 is close to that of DP #4. This finding, again, confirms the conjecture that the parameters of the damping block of the proposed scheme are mainly determined by the smallest main capacitor. In terms of the loading condition, the current flowing through L and C_2 in DP #6 is three times of that in DP #4. This is because L and C_2 in DP #6 need to carry the currents of both main capacitors. The harmonic current flowing through R is mainly determined by the C-type damping block itself, rather than the main capacitor. Consequently, the loading of R in DP #6 is close to that in DP #4.

Table 3.4 Comparison of parameters and loadings of two schemes (case #2)

Main capacitor		Conventional		Proposed	
		C_X	C_Y	C_X	C_Y
C_1	Value (uF)	1.28	2.56	1.28	2.56
	Voltage (kV)	144.13	144.11	144.06	144.01
	Current (A)	41.20	82.02	40.78	80.50
C-type damping block		Conventional		Proposed	
		DP #4	DP #5	DP #6	
C_2	Value (uF)	33.5	66.93	29.3	
	Voltage (kV)	5.51	5.51	18.85	
	Current (A)	40.96	81.65	120.36	
L	Value (mH)	210.3	105.1	240.0	
	Voltage (kV)	9.11	8.49	19.51	
	Current (A)	40.96	81.65	120.36	
R	Value (Ω)	941.8	470.92	573.7	
	Voltage (kV)	7.07	6.29	5.50	
	Current (A)	4.34	7.71	5.54	

With the information of parameters and loadings, the cost is then compared for each component.

- C_1: The loading and cost of main capacitors are same for two schemes.

- C_2: The capacity of C_2 in the proposed scheme is approximately three times of that in the conventional scheme, while the ratio is roughly two in case #1. From this point of view, the relative cost of C_2 becomes higher in case #2.

- L: The capacity of L in the proposed scheme is approximately three times of that in the conventional scheme, while the ratio is roughly two in case #1. Therefore, the relative cost of L also becomes higher in case #2.

- R: The loading of R in DP #6 is roughly equal to that in DP #4. The proposed scheme saves one resistor, so its expense on R is roughly half.

Table 3.5 shows the expenses of two schemes on C-type damping blocks based on the quotations from the manufacturers. As can be seen from the table, the total cost of the proposed scheme increases from $96,413 to $115,453 due to the higher rating of L and C_2. Nevertheless, the total cost of the proposed scheme is still lower than that of the conventional scheme.

Table 3.5 Cost of C-type damping blocks in two schemes (case #2)

	Conventional ($)	Proposed ($)	Relative cost (p.u.)
C_2	5,775	19,639	3.40
L	61,424	58,529	0.95
R	76,508	37,284	0.49
Total	143,707	115,453	0.80

c) Power loss comparison

Table 3.6 compares the power loss of two schemes. According to the table, the proposed scheme and the conventional scheme, theoretically, have zero fundamental frequency loss. The harmonic loss of the proposed scheme is lower than that of the conventional scheme in scenario #4 and scenario #5. This is because the proposed scheme has larger equivalent harmonic impedances in these two scenarios.

Table 3.6 Power loss comparison of two schemes (case #2)

		Conventional			Proposed		
Scenario		#3	#4	#5	#3	#4	#5
Reactive power (MVar)		10.0	20.0	30.0	10.0	20.0	30.0
Power loss (kW)	Fundamental frequency	0	0	0	0	0	0
	Harmonic frequencies	53.1	84.1	96.7	52.7	47.8	42.4
	Total	53.1	84.1	96.7	52.7	47.8	42.4
	% loss (of total MVAr)	0.18	0.28	0.32	0.18	0.16	0.14

d) Summary of case #2 study

Through the comparison of resonance-mitigation performance, economic performance and power loss performance, some key findings are summarized for case #2 study.

- In case #2, the proposed scheme still has comparable resonance-mitigation performance as the conventional scheme.
- The relative cost of the proposed scheme becomes higher in case #2. This finding indicates that the proposed scheme is more cost-effective for the case where switchable capacitors have equal capacities.
- In case #2, the proposed scheme still has lower harmonic loss than that of the conventional scheme.

3.4.4 Sensitivity Study

This subsection presents the sensitivity study results. The studies are related to following parameters: HAR_{limit}, tuning frequency and the background voltage distortion. Since the resonance-free performance must be guaranteed by the proposed scheme, the sensitivity study focuses on the cost performance and the power loss performance.

a) HAR_{limit}

In case #1 and case #2, HAR_{limit} is selected to be 1.2. In practice, HAR_{limit} can

be selected in coordination with IEEE Std. 519 limits. For example, if the voltage total harmonic distortion (THD) before the connection of the capacitor is 1.6%, a selection of HAR_{limit}=1.5 can guarantee voltage THD after the capacitor connection is below 1.6*1.5%. The impact of HAR_{limit} selection on the cost and the power loss are presented in Figure 3.9.

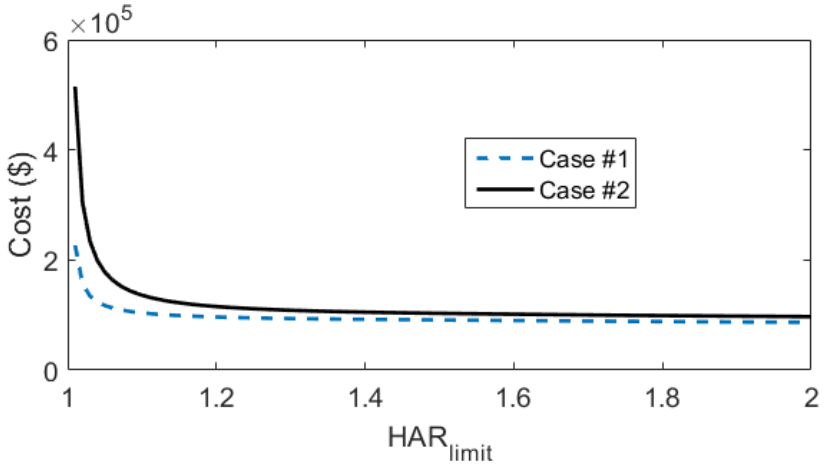

(a) Cost

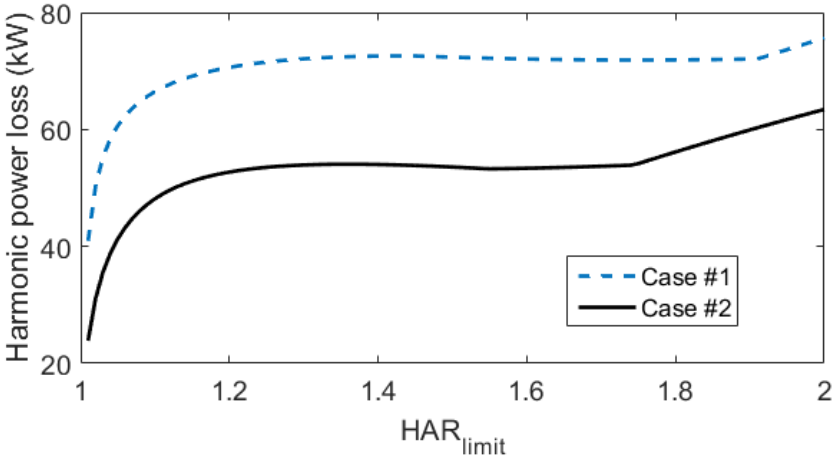

(b) Harmonic loss

Figure 3.9 The impact of HAR_{limit}

According to Figure 3.9(a), the smaller of HAR_{limit}, the higher of the component cost. This is because small HAR_{limit} leads to a design result with large C-type damping block parameters. Consequently, the loading (cost) of L and C_2 are large. The relationship between HAR_{limit} and the cost are nonlinear. It is not

very cost effective to select HAR_{limit} smaller than 1.1, as the C-type damping block parameters/cost would increase rapidly. The situation is opposite for the harmonic loss, as shown in Figure 3.9(b). The smaller of HAR_{limit}, the lower of the harmonic loss. As aforementioned, small HAR_{limit} is achieved by using a C-type damping block with large parameters (equivalent harmonic impedance). When a large harmonic impedance is shunt connected to the system, the harmonic loss becomes small.

b) Tuning frequency

In some cases, the utility may consider to tune the capacitor to the 3rd harmonic to avoid the 3rd harmonic resonance. Table 3.7 shows the performances of two schemes with different tuning frequencies. According to the table, the cost becomes much higher if the capacitor is tuned to the 3rd harmonic instead of the 5th harmonic, especially for the proposed scheme. This is because tuning to the 3rd harmonic requires a C-type damping block with larger parameters. The higher loadings of L and C_2 increase the total component cost. This finding suggests it may be beneficial to tune the capacitor to the 5th harmonic coupled with an undergrounded connection. The harmonic loss becomes lower when the capacitor is tuned to the 3rd harmonic, as equivalent harmonic impedances of the entire shunt device become larger.

Table 3.7 Cost and power loss comparison with different tuning frequency

Case #1				
	Proposed scheme		Conventional scheme	
Tuning frequency	3rd	5th	3rd	5th
Cost ($)	159,074	96,417	167,818	144,113
Power loss (kW)	35.6	70.6	45.4	96.7
Case #2				
	Proposed scheme		Conventional scheme	
Tuning frequency	3rd	5th	3rd	5th
Cost ($)	219,863	115,453	167,745	143,707
Power loss (kW)	28.9	50.7	45.4	96.7

c) Background voltage distortion

In case #1 and case #2, the background voltage distortion is assumed to be

1.5% from 5th to 19th harmonics according to IEEE 519 limit. It is straightforward that the component cost and the harmonic loss will increase with the background voltage distortion. The correlation is shown in Figure 3.10. The results in these two figures are obtained by simultaneously changing the voltage distortion at each harmonic frequency. It should be emphasized that the proposed resonance-free scheme aims to mitigate the capacitor resonance, rather than reduce the system harmonics. If the background voltage distortion is very severe, the utility should take actions to find the cause and take proper mitigating measures to control the harmonic distortion.

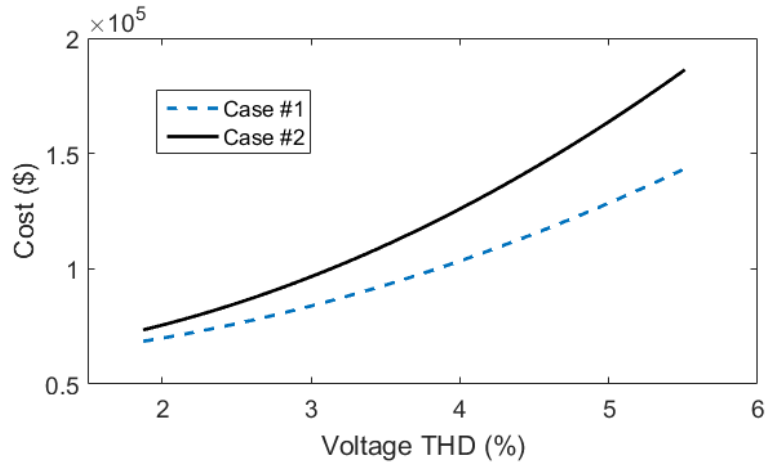

(a) Cost

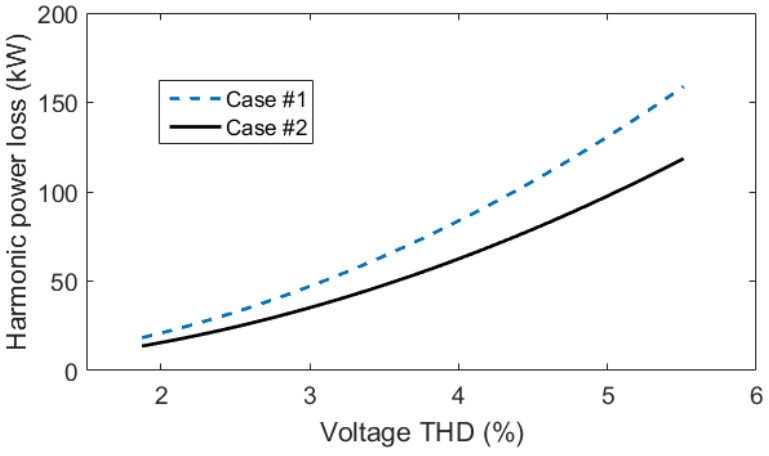

(b) Harmonic loss

Figure 3.10 The impact of background voltage distortion

3.5 Lookup Table for Component Parameters

An important outcome of the proposed resonance-free concept and associated design method is the following: the design results are independent of the system impedances. As a result, a standard set of R, L and C_2 parameters can be pre-calculated for direct use by industry. (This also implies that finding a better algorithm to solve the design equations is not necessary since it will not be used by designers anyway).

For this purpose, sample lookup tables for normalized component parameters have been created and are shown in Table 3.8 and Table 3.9. Two tables list the parameters for the tuning frequency f_1=300Hz (i.e., 5th harmonic) and f_1=180Hz (i.e., 3rd harmonic) under three HAR_{limit} values, respectively. The capacity ratio (Cap_{ratio}) in tables indicates the ratio of the capacity of two capacitors. The value of C_1 in tables is the value of the capacitor with smaller capacity.

Table 3.8 Lookup table for per-unit component parameters (tuning frequency f_1=300Hz)

			Capacity Ratio (Cap_{ratio})		
			1.0	1.5	2.0
HAR_{limit}	1.1	C_1	1.0000	1.0000	1.0000
		C_2	19.9732	18.1783	16.4349
		L	0.0501	0.0550	0.0608
		R	0.2997	0.2797	0.2677
	1.2	C_1	1.0000	1.0000	1.0000
		C_2	24.7646	23.8734	22.9173
		L	0.0404	0.0419	0.0436
		R	0.3282	0.2980	0.2767
	1.5	C_1	1.0000	1.0000	1.0000
		C_2	30.0000	30.0000	29.9851
		L	0.0333	0.0333	0.0334
		R	0.3847	0.3813	0.3472

Table 3.9 Lookup table for per-unit component parameters (tuning frequency f_1=180Hz)

			Capacity Ratio (Cap_{ratio})		
			1.0	1.5	2.0
HAR_{limit}	1.1	C_1	1.0000	1.0000	1.0000
		C_2	6.7244	6.0933	5.4781
		L	0.1487	0.1641	0.1826
		R	0.5044	0.4676	0.4462
	1.2	C_1	1.0000	1.0000	1.0000
		C_2	8.2910	7.9890	7.6521

	L	0.1206	0.1252	0.1307
	R	0.5551	0.5009	0.4623
1.5	C_1	1.0000	1.0000	1.0000
	C_2	9.9977	9.9983	9.9987
	L	0.1000	0.1000	0.1000
	R	0.6214	0.6187	0.5836

The base value for capacitance C_b, inductance L_b and resistance R_b are determined as

$$\begin{cases} C_b = Q_r / (2\pi f_r V_r^2) \\ L_b = V_r^2 / (2\pi f_r Q_r) \\ R_b = V_r^2 / Q_r \end{cases} \tag{3.16}$$

Take case #1 as an example. For this case, V_r=144kV, Q_r=15MVar, f_r=60 Hz, Cap_{ratio}=1. The base value can be determined as C_b=15/(2*π*60*144^2)=1.92e-6F, R_b=144^2/15=1382.4Ω, L_b=144^2/(2*π*60*15)=3.67H. The resonance-free condition is HAR_{limit}=1.2 and f_1=300Hz. Per this requirement, the shaded values in Table 3.8 are located. Multiply these values by C_b, R_b, L_b, the actual values for the components are obtained. It can be easily verified, these actual values for the components are the same as shown in Table 3.1.

3.6 Summary

This chapter has presented a new and effective scheme to mitigate the harmonic resonance for multiple switchable capacitors. The core idea is to allow multiple capacitors to share a common damping block. Compared with the conventional scheme that requires each switchable capacitor to equip a damping block, the main advantage is therefore to eliminate the need for multiple damping blocks. Design method to make the above concept feasible has been developed. It has been shown that design results are independent of the system conditions. As a result, a look-up table of component parameters of the damping block has been calculated for direct industry use.

Comparative analysis on actual capacitor application cases has been

conducted between the proposed scheme and the conventional scheme. The results demonstrate that the proposed scheme can achieve the same performance as the conventional scheme with about 30% cost saving. Depending on the layout of a substation, space saving can also be achieved.

According to [39], the third order high pass (3^{rd}HP) damping block provides a similar damping capability as the C-type damping block. This work also investigated the feasibility of the 3^{rd}HP damping block for the proposed scheme. The corresponding materials are presented in Appendix D.

Chapter 4

A Magnitude-Data-Based Method for Harmonic Source Identification

Besides of the harmonic resonance, there are many situations that the high levels of harmonic distortions are caused by harmonic sources themselves. When a harmonic problem occurs in a system with several concentrated harmonic sources as suspects, the first step is to determine which source causes the problem. Such information is useful for identifying problematic loads, assigning responsibility for harmonic mitigation, and troubleshooting the problem. For this purpose, this chapter proposes a magnitude-data-based method for harmonic source identification. The basic idea is to use multiple linear regression (MLR) technique to study the cause-and-effect relationship between the harmonic current magnitude of a harmonic source and the harmonic voltage or current magnitude of the concern. Simulation study and field measurement are carried out to demonstrate the effectiveness of the proposed method.

The chapter is organized as follows. First, a brief review on the harmonic source identification is presented in Section 4.1. Next, Section 4.2 derives the proposed method. Sections 4.3 evaluates the performance of the proposed method in two different system networks using the simulation study. Section 4.4 discusses practical considerations and their impact on the proposed method. Finally, Section 4.5 shows the field measurement performance.

4.1 Review on Harmonic Source Identification

The most widely researched harmonic source identification method is harmonic state estimation (HSE). HSE involves the estimation of the states of the network using available measurements. The states are normally chosen to be the

voltage magnitudes and phase angles at all buses in the network or the current injections, depending on the method used to carry out HSE. Generally, two classes of HSE can be found in literature: dynamic HSE [45][46] and static HSE [47][48]. For example, an adaptive Kalman filter based technique for dynamic estimate of harmonic injection is proposed in [45]. The proposed method uses two process noise covariant Q models to carry out harmonic estimation and this eliminates the requirement for the calculation of an optimal Q model. In [47], a static HSE problem is formulated as a sparsity maximization problem which is solved efficiently by linear programming. However, all HSE methods require an adequate power system model at the harmonic frequency of interest. This model includes those of the linear and nonlinear loads at various load buses during the period when measurements are available. Such load models are not attainable. In addition, many systems cannot provide redundant measurements at harmonic frequencies, which are required by the state estimation approaches.

As a result, some other harmonic source identification methods have been proposed apart from HSE. In [59], a method based on wavelet transform is proposed to identify the location of the harmonic sources. The method is attractive as it can determine the type of nonlinear loads as well. However, this method is not intended to determine the harmonic contribution of each non-linear load. In [60], a statistical method to identify the harmonic load profile is proposed. The approach is interesting as it does not involve any system information. However, the method can provide accurate results only if the number of measurements is more than the number of harmonic sources in the system. In [49], a method based on the direction of harmonic power flow is proposed to rank the buses in the system to suspected and non-suspected harmonic buses. One drawback of this approach is that it requires the synchronized harmonic voltage phasor measurements at all buses. In practice, it is not cost effective to install power quality monitors at all buses of a power system. In [61], a least-square (LS)-correlation based method is proposed. The basic idea is to study the inter-dependency of the harmonic distortion at a specific bus with the behaviors of some major harmonic loads. The advantage of this technique is that it can

determine the harmonic contribution without any information of the network by utilizing the measurements at a few large suspected loads. However, this method places certain requirements on the data. When more suspected loads are considered, the shortage of valid data for analysis can severely limit the application range of the LS-based method.

4.2 MLR-based Method

Figure 4.1 shows the phasor diagram of the hth harmonic voltage at Bus X (V_{hX}) and its constructive components. As Figure 4.1 shows, V_{hX} can be represented by (4.1), where I_{hi} is the hth harmonic current measured at the PCC of Load i (i=A, B, C), Z_{hXi} is the hth harmonic transfer impedance between Load i and Bus X, V_{hXi} is the hth harmonic voltage at Bus X induced by Load i, $V_{hXi\text{-}f}$ is the projection of V_{hXi} on V_{hX}, and β_{hiX} is the phase angle between V_{hXi} and V_{hX}. To quantify the harmonic contribution of each load on V_{hX}, the ratio between $V_{hXi\text{-}f}$ and V_{hX} is used.

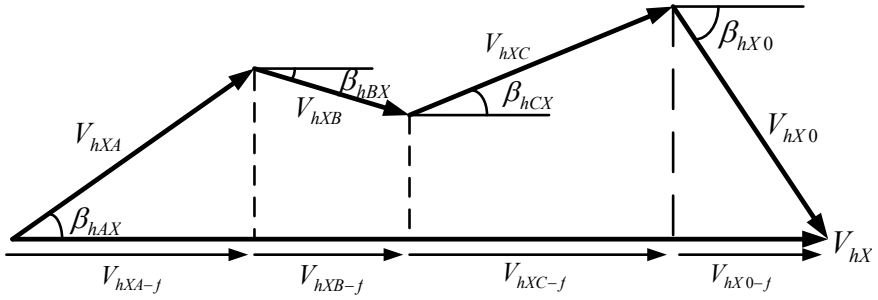

Figure 4.1 Phasor diagram of harmonic voltage at Bus X.

$$\begin{aligned} |V_{hX}| &= |V_{hXA-f}| + |V_{hXB-f}| + |V_{hXC-f}| + |V_{hX0-f}| = \ldots \\ &|I_{hA}||Z_{hXA}|\cos\beta_{hAX} + |I_{hB}||Z_{hXB}|\cos\beta_{hBX} + \ldots \\ &|I_{hC}||Z_{hXC}|\cos\beta_{hCX} + |V_{hX0}|\cos\beta_{hX0} \end{aligned} \tag{4.1}$$

In order to solve the above problem, following assumptions need to be made:

1) The problem attempts to quantify the impact of major known harmonic sources. The impact of minor sources is lumped together as background harmonic voltage V_{hX0}. This voltage is assumed to be proximately constant

during the measurement period. A diagnostic criterion will be explained later to deal with the case where V_{hX0} has significant impact on V_{hX}.

2) The selected data set (k=1,..,n) has an average value of β_{hAX}. This value is labeled as β_{hAX-eq}. If β_{hAX-eq} is used in the above equation instead of $\beta_{hAX}(k)$, an error will appear in the equation. A similar average value will be used for $\beta_{hBX}(k)$ and $\beta_{hCX}(k)$.

With the above assumptions, (4.1) can be rewritten in the form of a linear algebraic equation as shown in (4.2), when large harmonic loads A, B,… M are in the system.

$$\begin{aligned}|V_{hX}(k)| = |V_{hX0}|\cos\beta_{hX0-eq} + |I_{hA}(k)||Z_{hXA}|\cos\beta_{hAX-eq} \\ \cdots + |I_{hM}(k)||Z_{hXM}|\cos\beta_{hMX-eq} + \varepsilon_k,\ k = 1,2,...,n\end{aligned} \tag{4.2}$$

Further defining

$$\begin{cases} B_0 = |V_{hX0}|\cos\beta_{hX0-eq} \\ B_A = |Z_{hXA}|\cos\beta_{hAX-eq} \\ B_B = |Z_{hXB}|\cos\beta_{hBX-eq} \\ \vdots \\ B_M = |Z_{hXM}|\cos\beta_{hMX-eq} \end{cases} \tag{4.3}$$

The following set of equations can be established:

$$y = xB + \varepsilon \tag{4.4}$$

where

$$\begin{aligned} y &= \left[|V_{hX}(1)| \quad |V_{hX}(2)| \quad \cdots \quad |V_{hX}(n)|\right]^T \\ B &= [B_0 \quad B_A \quad \cdots \quad B_M]^T \\ x &= \begin{bmatrix} 1 & |I_{hA}(1)| & |I_{hB}(1)| & \cdots & |I_{hM}(1)| \\ 1 & |I_{hA}(2)| & |I_{hB}(2)| & ... & |I_{hM}(2)| \\ 1 & \vdots & \vdots & ... & \vdots \\ 1 & |I_{hA}(n)| & |I_{hB}(n)| & ... & |I_{hM}(n)| \end{bmatrix} \end{aligned} \tag{4.5}$$

The above manipulation has converted the harmonic source identification

problem to a MLR problem where harmonic currents of suspected loads are explanatory variables (x) and the harmonic voltage is the response variable (y). Using traditional MLR solution techniques, matrix B can be calculated as follows [62] and thus the regression can be achieved:

$$\hat{B} = \left(x^T x\right)^{-1} x^T y \tag{4.6}$$

Based on (4.2) and (4.3), V_{hXi-f}, equals to $|I_{hi}||Z_{hXi}|\cos\beta_{hiX-eq}$ or $|I_{hi}|B_i$. Thus, the harmonic contribution index, defined as the ratio between $|V_{hXi-f}|$ and $|V_{hX}|$, can be calculated as follows:

$$\begin{cases} HC_{load\ A}^{Bus\ X}(k) = \dfrac{|V_{hXA-f}(k)|}{|V_{hX}(k)|} = \dfrac{|I_{hA}(k)|}{|V_{hX}(k)|}\hat{B}_A \times 100\% \\ HC_{load\ B}^{Bus\ X}(k) = \dfrac{|V_{hXB-f}(k)|}{|V_{hX}(k)|} = \dfrac{|I_{hB}(k)|}{|V_{hX}(k)|}\hat{B}_B \times 100\% \\ \vdots \\ HC_{load\ M}^{Bus\ X}(k) = \dfrac{|V_{hXM-f}(k)|}{|V_{hX}(k)|} = \dfrac{|I_{hM}(k)|}{|V_{hX}(k)|}\hat{B}_M \times 100\% \\ HC_{background}^{Bus\ X}(k) = \dfrac{|V_{hX0}(k)|}{|V_{hX}(k)|} = \dfrac{1}{|V_{hX}(k)|}\hat{B}_0 \times 100\% \end{cases} \tag{4.7}$$

Eq. (4.7) calculates the harmonic contribution of each sample in the data set. It is more useful to know the average harmonic contribution over this period. This calculation can be determined using a simple average of the indices as shown in (4.8). Other statistical indices, such as 95% percentile value (the maximum level that is higher than the index for 95% of the time), can be developed as well.

$$HC_{load\ A}^{Bus\ X} = \frac{\sum_{k=1}^{n}|I_{hA}(k)|}{\sum_{k=1}^{n}|V_{hX}(k)|}\hat{B}_A \times 100\% \tag{4.8}$$

4.3 Simulation Verification

The proposed method has been tested in both radial and looped networks. The

radial network under study is constructed based on a real distribution system in Alberta, Canada. The looped network is based on the IEEE 57 bus test system. Both test systems have several harmonic producing loads and their nonlinear portion of loads is modeled using the harmonic current source model. A sample harmonic spectrum table in simulation is presented in Table 4.1. Note that the harmonic spectrum differs from load to load. The entire procedure of the simulation is illustrated in Figure 4.2.

Table 4.1 Sample current spectrum of a suspected load

Harmonic Order	Magnitude (percent)	Relative angle (degree)
1	100	0.00
5	21.34	42.73
7	15.34	76.39
11	7.43	-112.36

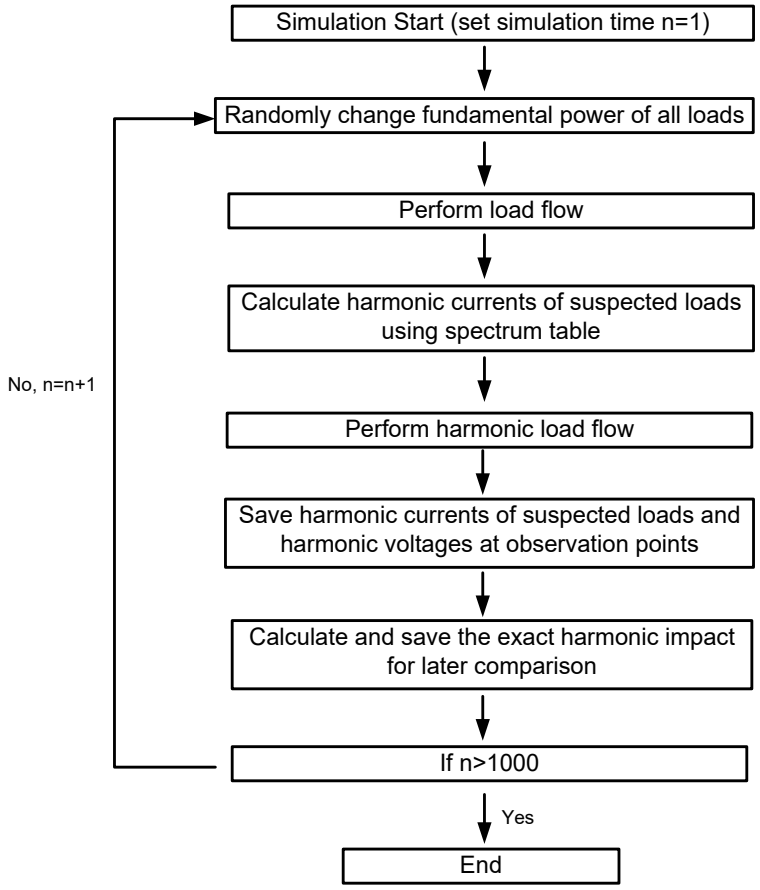

Figure 4.2 Flow chart of the simulation.

During the simulation, the fundamental power of all loads is randomly changed with a maximum fluctuation of 10% to cause the variation in harmonic currents and voltages. A total of 1000 “measurement” samples is produced by this process. It is definite that using more samples could improve the estimation accuracy, but 1000 samples are sufficient according to our sensitivity studies. Each of "measurement" data includes the harmonic current magnitudes of suspected loads and the harmonic voltage magnitudes at observation buses, which are the input data for the proposed method. For this work, the exact or true harmonic contribution can be calculated by harmonic power flow using the network model at the harmonic frequency of interest. Their average values are then used as the benchmark results to check the prediction of the proposed method. The verification procedure for different harmonic orders is exactly same, thus only the 5th harmonic is presented here.

4.3.1 Radial Network

This network contains 24 three-phase nodes, 23 three-phase branches and four voltage regulators. The network is shown in Figure 4.3 and the key information of the system is presented in Table 4.2. Large loads at Bus 2, 6, 15, 17, 19, 23 are known to be harmonic producing loads (suspected loads) and Bus 1, 7, 16, 20 are selected to be the observation bus.

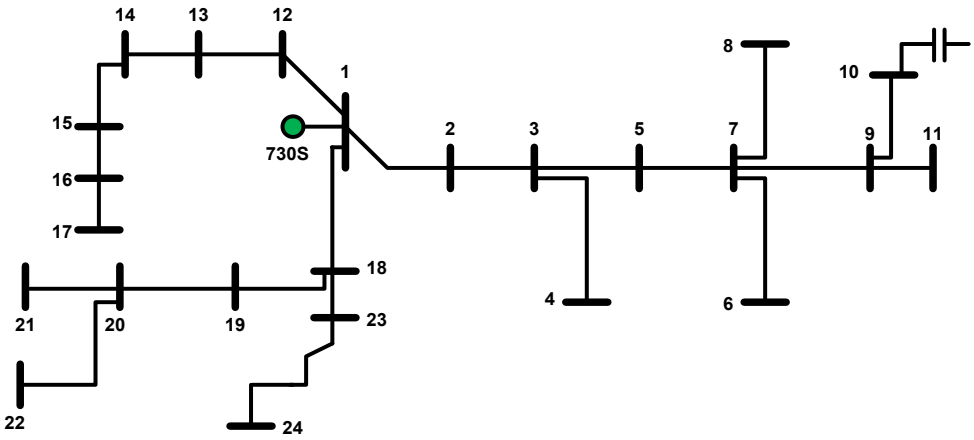

Figure 4.3 Radial network for simulation study.

Table 4.2 Information of the radial network.

Equivalent Source	Voltage(L-L):25kV Z1: 1.03+j3.82 ohms Z0: 0.063+j0.92 ohms			
Load	Bus	2	4	5
	Power (kVA)	430+j141	215+j74	297+j98
	Bus	6	8	10
	Power (kVA)	978+489j	171+j82	147+j48
	Bus	11	12	13
	Power (kVA)	177+j86	173+j57	288+j95
	Bus	14	15	16
	Power (kVA)	336+j110	516+j250	247+j118
	Bus	17	19	21
	Power (kVA)	309+j147	790+j211	432+j103
	Bus	22	23	24
	Power (kVA)	240+j117	523+j227	250+j103
Z_{line}	0.35+0.64j ohms/mile			
Capacitor	Rated Power: 200kVar per phase, Rated voltage:14.4kV			

Figure 4.4 shows the estimated harmonic contribution of suspected loads on Bus 1. Load 6 and 19 are identified to be the major harmonic polluters as they contribute 70% and 60% of the harmonic distortion at Bus 1, respectively. Load 2 and Load 17 have negative impact, which means that they help reduce the harmonic voltage caused by other loads. Similarly, the estimated harmonic contributions of suspected loads on other observation buses are shown in Table 4.3. All estimation results have good agreement with the exact value. Such results demonstrate that the proposed MLR method can accurately quantify the individual harmonic contribution of several large harmonic-producing loads.

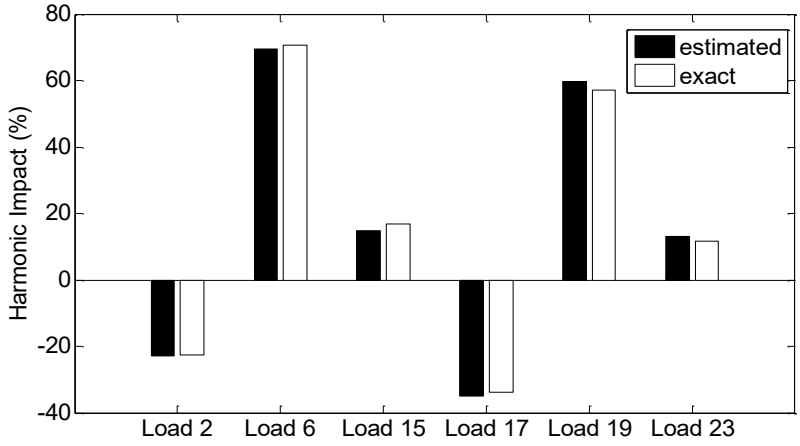

Figure 4.4 Estimated harmonic contribution of suspected loads on Bus 1.

Table 4.3 Estimated harmonic contribution (%) at observation buses (radial network)

		bus 1	bus 7	bus16	bus20
load 2	Estimated	-22.24	-11.59	30.18	-14.49
	Exact	-22.11	-11.59	28.72	-14.09
load 6	Estimated	69.56	92.70	19.15	35.27
	Exact	69.50	92.29	12.69	36.34
load 15	Estimated	14.49	8.99	108.35	5.51
	Exact	16.70	9.90	119.38	6.42
load 17	Estimated	-34.59	-13.55	-3.92	-19.44
	Exact	-33.04	-12.93	0.68	-18.35
load 19	Estimated	59.35	23.15	-9.28	72.96
	Exact	57.00	22.20	-13.67	71.98
load 23	Estimated	13.23	0.81	-44.93	19.03
	Exact	11.95	0.13	-47.80	17.69

4.3.2 Looped Network

Detailed information of this network can be found in [63]. Load 5, 15, 23, 33 and 47 are selected to be harmonic-producing loads. The resultant 5th harmonic distortion at each bus is shown in Figure 4.5. Among them, Bus 1, 25, 33 and 55 experience relatively high harmonic distortion and are selected as observation buses.

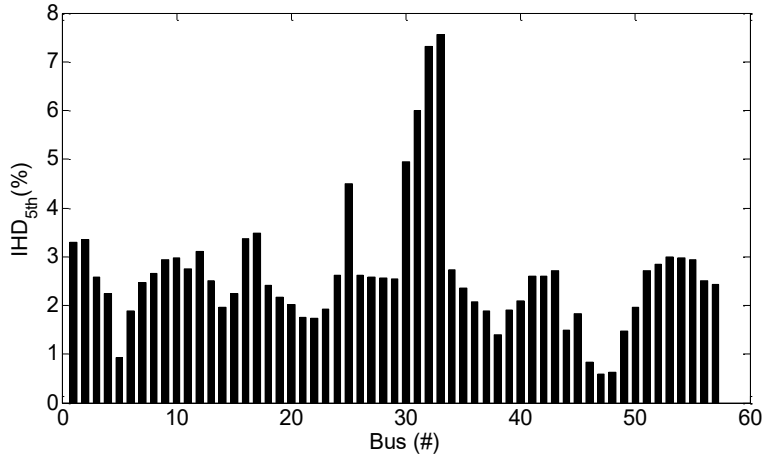

Figure 4.5 Voltage harmonic distortion at each bus.

Figure 4.6 illustrates the estimated harmonic contribution of suspected loads on Bus 1. Load 5 and 47 are identified to be the major harmonic polluters as they are responsible for almost 95% of harmonic distortion at Bus 1. Load 33 has a negative harmonic contribution. This load partially cancels out the harmonic

voltage caused by other loads. Table 4.4 indicates the estimation results of other observation buses. All estimated values and the exact values are congruent.

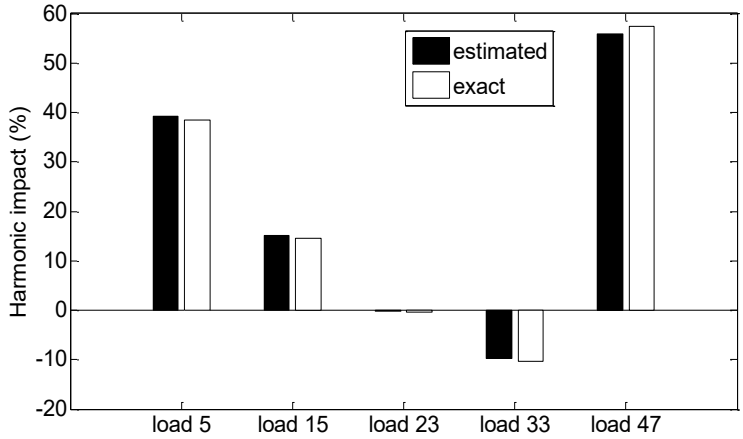

Figure 4.6 Harmonic contribution of suspected loads on Bus 1.

Table 4.4 Estimated harmonic contribution (%) at observation buses (looped network)

		bus 1	bus 25	bus 33	bus55
load 5	estimated	39.14	24.12	17.01	27.41
	exact	38.52	24.43	16.18	27.74
load 15	estimated	15.44	18.76	8.96	25.19
	exact	14.62	19.08	9.09	26.41
load 23	estimated	-0.21	5.85	1.89	-2.55
	exact	-0.31	6.29	1.94	-1.73
load 33	estimated	-9.72	46.73	75.65	-7.12
	exact	-10.33	49.70	77.32	-7.45
load 47	estimated	55.88	-0.25	-4.17	53.86
	exact	57.51	0.50	-4.54	55.02

4.4 Practical Considerations

This section discusses practical considerations and their potential impact on the proposed method. The studied system is the IEEE 57 bus system and the selection of suspected loads is the same as outlined in Section 4.3.2.

4.4.1 Load Impedance

An inherent requirement of using MLR technique is that different explanatory variables are uncorrelated. To meet this condition, suspected loads should be modeled as current sources, as the load impedances would make measured

harmonic currents of different suspected loads correlated. Although a common practice is that most harmonic loads can be approximately modeled as current sources, this assumption may not always be true. A correlation study should be performed to check if there is a correlation between different suspected loads, as shown in (4.9).

$$r(I_i, I_j) < 0.1, \;\; i, j \in [A, B, ..., M] \tag{4.9}$$

The MLR-based method cannot yield reliable results when (4.9) is not satisfied. In the case that the small load impedances are caused by the harmonic filter or the shunt capacitor on the consumer side, two instructions are recommended to make the MLR-based method workable. One is to conduct the measurement when the filter or capacitor is disconnected. Another is to place the metering point between the filter (or capacitor) and consumer.

4.4.2 Background Harmonic Voltage

In simulation study, it is assumed that all harmonic loads are measured and regarded as suspected loads, which means that there is no background harmonic voltage. In practice, only some major harmonic loads are measured, and the rest should be considered as background harmonic loads. The objective of this subsection is to study the impact of background harmonic voltages.

The harmonic loads of three randomly selected buses are considered as unknown harmonic loads. Those unknown harmonic loads create a background harmonic voltage in the system. Various harmonic spectra are applied to those unknown harmonic loads, which results in a change of the magnitude and the phase angle of the background harmonic voltage. Different fluctuation levels are also applied to those unknown harmonic loads, which results in a change of the fluctuation of the background harmonic voltage.

To study the impact of different background harmonic voltages, the mean square error of each estimation result is calculated by (4.10).

$$MSE_{BusX}(\%) = \sqrt{\frac{\sum_{i=1}^{N_{bus}} \left(HC_{loadi}^{BusX} - \tilde{HC}_{loadi}^{BusX} \right)^2}{N_{bus}}} \tag{4.10}$$

where N_{bus} is the number of suspected harmonic loads, and HC_{loadi}^{BusX} and $\tilde{HC}_{loadi}^{BusX}$ are the exact and the estimated harmonic contribution of load i on Bus X, respectively. The impact of background harmonic voltages on Bus 1 is shown in Figure 4.7. The results are presented with respect to the magnitude and fluctuation of the background harmonic voltage. The base value of the magnitude is the harmonic voltage magnitude at Bus 1 induced by suspected loads. The base value of the fluctuation is the fluctuation of suspected loads. For certain magnitude and fluctuation, different phase angles of the background harmonic voltage may lead to some differences in MSE, and the maximum MSE is presented in Figure 4.7.

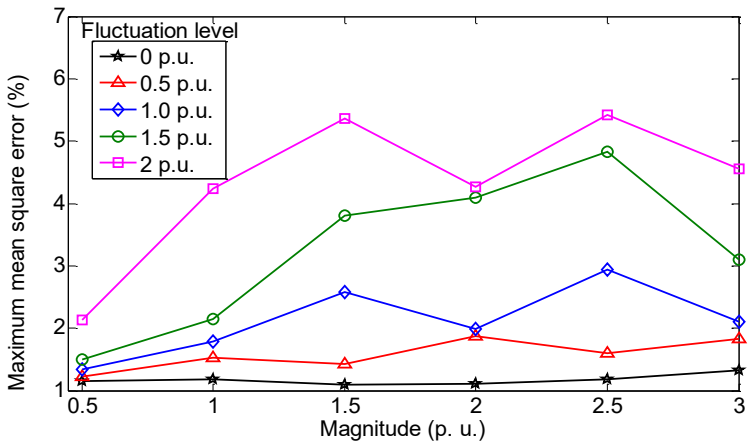

Figure 4.7 Maximum mean square error under different background harmonic voltages.

As seen from Figure 4.7, the proposed method remains accurate as long as the background harmonic voltage is stable. The reason is that a constant background harmonic voltage has been considered in the algorithm. However, if the background harmonic voltage has large fluctuation, the estimation accuracy will degrade. A straightforward method to diagnose the impact of the background harmonic is to use the coefficient of determination r^2 [62], as shown in (4.11),

$$r^2 = \frac{\sum(\hat{y}_i - \bar{y})}{\sum(y_i - \bar{y})} \tag{4.11}$$

where y_i is the measured values of the response variable (y), $\bar{y}$ is the mean value of the response variable (y), and $\hat{y}_i$ is the fitted value of the response variable (y). r^2 is a measure of how well the response variable (y) can be modeled by explanatory variables (x). If the concerned harmonic voltage can be well explained by selected suspected loads and a constant background harmonic, r^2 should be close to 1, and vice versa. In practice, a minimum requirement of 0.9 can be used to filter unreliable results. It should also be emphasized r^2 indicates the overall estimation accuracy, which includes not only the impact of background harmonic voltage, but also the impact of other practical issues, such as the phasor angle change and the measurement error.

If r^2 is greater than 0.9, it means the overall estimation is good. Then we can further calculate the confidence interval of the estimated harmonic contribution to have a better understanding on the possible error range. For example, if the estimated harmonic contribution of a suspected load is 50% and its confidence interval is ±2% for a 95% confidence level. It means that the harmonic contribution of this suspected load is between 48% and 52% with the probability of 95%. Thus, we can conclude that the estimated harmonic contribution is very reliable and the background harmonic voltage has small impact. In a MLR problem, the confidence interval of i-th regression coefficient (B_i) can be calculated as follows [62],

$$CI(\hat{B}_i) = \pm t^{n-p-1}_{(1-\alpha)/2} \cdot \sqrt{\hat{\sigma}^2 \eta_{ii}} \tag{4.12}$$

where $t^{n-p-1}_{(1-\alpha)/2}$ stands for t-distribution with n-p-1 degree of freedom, n is the number of measurements, p is the number of suspected loads, α is the confidence level that usually sets on 95%. $\hat{\sigma}^2 \eta_{ii}$ stands for the variance of $\hat{B}_i$, where $\hat{\sigma}^2$ is the error mean square that equals to $(y'y - \hat{B}'x'y)/(n-p-1)$ and η_{ii} is the i-th diagonal element of $(x'x)^{-1}$. The i-th regression coefficient (B_i) determines the

harmonic contribution of load *i* by (4.8). Therefore, the confidence interval of the estimated harmonic contribution of load *i* can be calculated as:

$$CI_{Load\,i}^{Bus\,X} = \frac{\sum_{k=1}^{n}\left|I_{hi}(k)\right|}{\sum_{k=1}^{n}\left|V_{hX}(k)\right|} CI(\hat{B}_i)\times 100\% \tag{4.13}$$

Table 4.5 shows the correlation between the confidence interval and the estimation accuracy. The values in the table are determined using the estimation results generated in previous sensitivity study of background harmonics. As seen from Table 4.5, the confidence interval of the estimated harmonic contribution directly indicates the range of the estimation error. In practice, a threshold of the confidence interval such as ±5% can be set to filter unreliable results.

Table 4.5 The correlation between the confidence interval and the estimation accuracy

	95% Confidence interval (*CI*) of the estimated harmonic contribution					
	|CI|≤1%		1%＜|*CI*|≤5%		5%＜|*CI*|≤10%	
	Average error	Maximum error	Average error	Maximum error	Average error	Maximum error
load 5	0.59%	1.24%	1.20%	4.24%	2.85%	9.12%
load 15	0.51%	0.90%	1.21%	4.49%	2.91%	10.41%
load 23	0.40%	0.94%	1.29%	5.60%	3.54%	10.45%
load 33	0.61%	1.28%	1.50%	4.89%	3.32%	10.43%
load 47	0.74%	1.58%	1.51%	4.65%	3.90%	11.78%

4.4.3 Load Fluctuation

In the simulation study, all suspected loads are assumed to have the same fluctuation, a maximum 10% of its base value. In a real power system, the fluctuation of different suspected loads cannot be exactly same. This subsection is to study the influence of different load fluctuation. Sensitivity study is carried out by changing the fluctuation level of each suspected harmonic load to 15%, 5% and 1%, respectively. After performing the proposed method, the error of the estimated harmonic contribution of each suspected load on Bus 1 can be calculated. The result is presented in Figure 4.8. It is clear that different load fluctuation normally has little impact on the accuracy of the estimation. However,

if one load is found to be extremely stable over the entire data set, e.g. its fluctuation level is as small as 1%, the harmonic contribution of this load estimated by the proposed method could be less accurate.

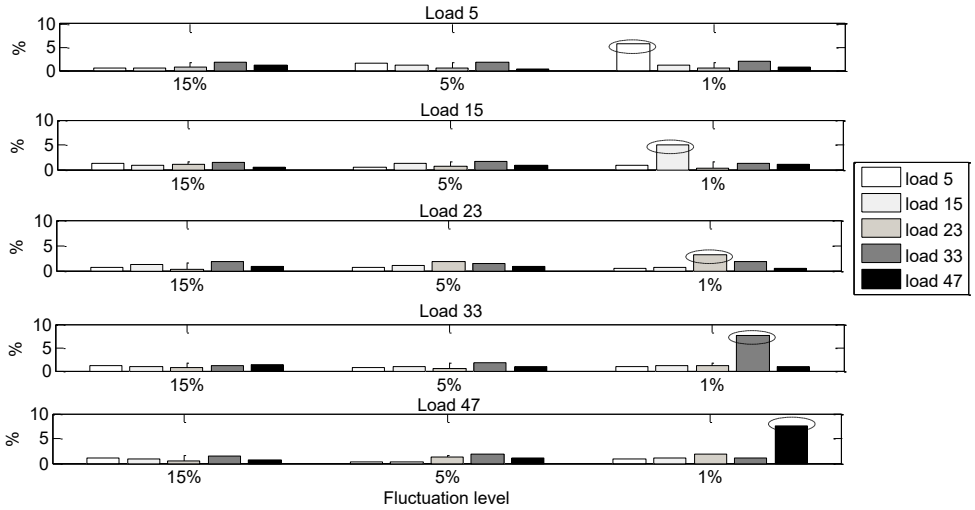

Figure 4.8 Error of the estimated harmonic contribution of suspected loads under different fluctuation levels.

This phenomenon can be explained by the theory of the MLR. In a MLR problem $y=a_1x_1+a_2x_2\ldots+b$, regression coefficients (a_1, $a_2\ldots$) are determined by studying the inter-dependency between the variation of explanatory variables (x_1, $x_2\ldots$) and their response on the response variable (y). If the fluctuation of an explanatory variable, e.g. x_1, is very small, its response on y becomes ambiguous. The MLR algorithm becomes difficult to determine the correlation between x_1 and y, due to the fact that there are always some errors in the regression model. This phenomenon also can be mathematically proved by the confidence interval. If load i has very small fluctuation, η_{ii}, the i-th diagonal element of $(x'x)^{-1}$, becomes large as the determinant of $x'x$ becomes small. Large η_{ii} leads to a large confidence interval of the estimated harmonic contribution, which indicates the unreliability of the estimation. Table 4.6 shows the change of the confidence interval of the estimated harmonic contribution when the suspected load changes its fluctuation. It can be seen that the confidence interval becomes larger when the fluctuation of the load decreases to 1%, which indicates the unreliability (larger

error) of the estimation.

Table 4.6 95% confidence intervals of the estimated harmonic contribution under different fluctuation levels

	Fluctuation level					
	15%		5%		1%	
	Error	CI	Error	CI	Error	CI
load 5	0.42%	±0.73%	1.52%	±2.12%	5.61%	±10.72%
load 15	0.64%	±0.72%	1.07%	±2.14%	4.97%	±10.69%
load 23	0.36%	±0.68%	1.76%	±2.07%	3.23%	±10.82%
load 33	1.19%	±0.68%	1.74%	±2.02%	6.65%	±10.06%
load 47	0.53%	±0.70%	0.84%	±2.15%	6.55%	±10.46%

4.4.4 Method Guideline

The procedures of the MLR-based method can be summarized as follows:

1) Measure the harmonic current magnitudes of suspected loads ($|I_{hA}|$, $|I_{hB}|$,…,$|I_{hM}|$) and the harmonic voltage magnitude of the observation bus ($|V_{hX}|$) over the appropriate time interval

2) Check if $|I_{hA}|$, $|I_{hB}|$,…,$|I_{hM}|$ are uncorrelated using (4.9).

3) If yes, performance MLR to the measured magnitude samples using (4.6).

4) Check if r^2 in (4.11) is greater than 0.9

5) If yes, calculate the harmonic contribution of each load using (4.8)

6) Check if the confidence intervals of the estimated harmonic contribution in (4.13) are within ±5%.

7) If yes, output the results.

4.5 Field Measurement Verification

Additionally, two field cases of the harmonic source identification problem are

also conducted.

4.5.1 Field Case #1

The first case is to determine the 5th harmonic contribution of three ski resorts in the Banff National Park of Canada. These loads are named as A, B and C, as shown in Figure 4.9. Harmonic voltage and current magnitudes collected at the buses and their corresponding loads are shown in Figure 4.10 and Figure 4.11.

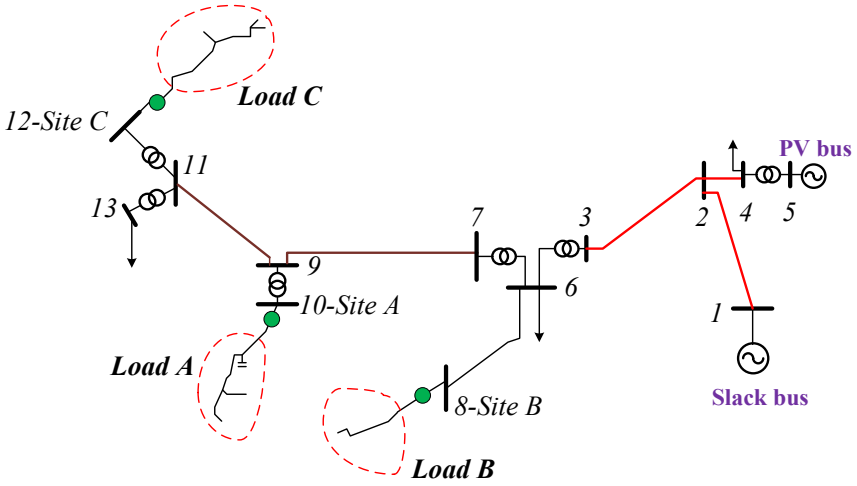

Figure 4.9 Schematic diagram of field case #1.

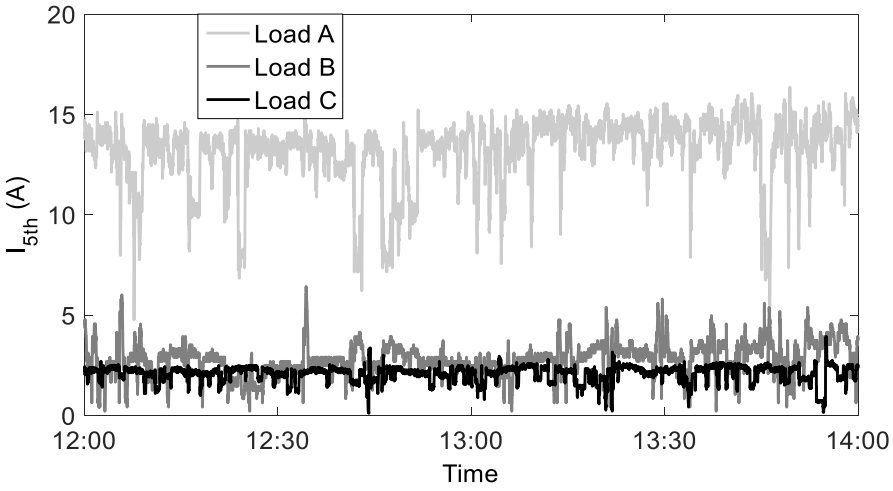

Figure 4.10 Harmonic currents (5th) of three loads.

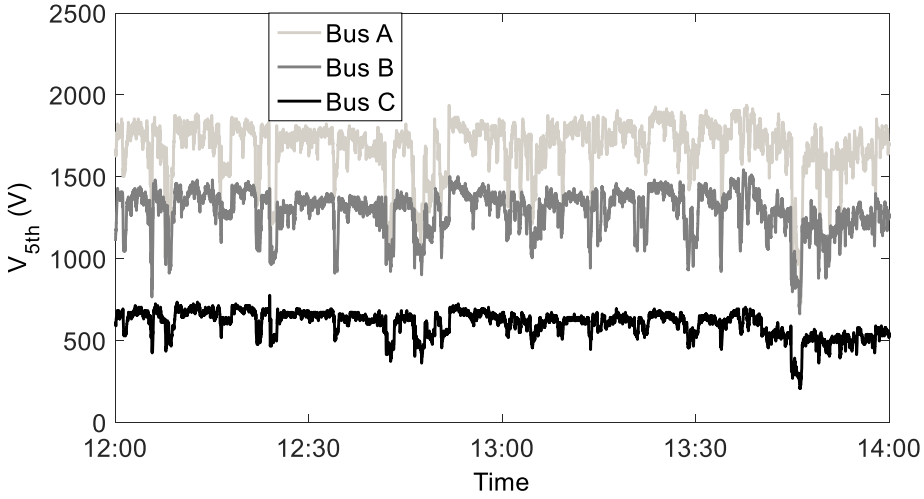

Figure 4.11 Harmonic voltages (5th) at three buses.

The harmonic contributions estimated by the MLR-based method are shown in Table 4.7. The estimations are considered to be reliable as they satisfy the criteria discussed in Section 4.4. To further justify its accuracy, estimation results are compared with the reference value in [61]. Those reference values were determined using the measured harmonic currents and the transfer impedance obtained by intrusive field measurements. Through the comparison, it is found that the findings of the proposed method are consistent with the results determined by the intrusive method. Load A is identified to be the major harmonic polluter as it has a large harmonic contribution on all three buses, while load B has a negative harmonic contribution on three buses, indicating that it helps in reducing the harmonic voltage caused by the other loads. Load C has almost no contribution to the system. Some differences can be observed between the estimated value and the reference value. The reason is that the utilized transfer impedances were only accurate for the short period when the intrusive field measurement was conducted. With load changes, the accuracy of the reference values will deteriorate. This is why they are called "reference values" instead of "actual values" or "exact values".

Table 4.7 Comparison of estimated harmonic contribution and reference harmonic contribution

	Load A		Load B		Load C	
	Reference HC (%)	Estimated HC (%)	Reference HC (%)	Estimated HC (%)	Reference HC (%)	Estimated HC (%)
Bus A	70.2±5.1	74.0	-22.1±6.7	-6.3	4.0±3.1	1.5
Bus B	42.7±4.8	40.6	-0.1±2.1	-3.1	5.4±3.5	1.1
Bus C	59.1±7.6	58.1	-25.6±8.3	-14.3	14.3±7.2	3.0

4.5.2 Field Case #2

The second application is to determine which feeder causes the most significant 5th harmonic voltage at a common bus in a substation. This case involves a 110kV substation with three feeders in Jinan, China. The schematic diagram of the system is shown in Figure 4.12. The measurement lasted for two hours and the measured feeder currents are shown in Figure 4.13.

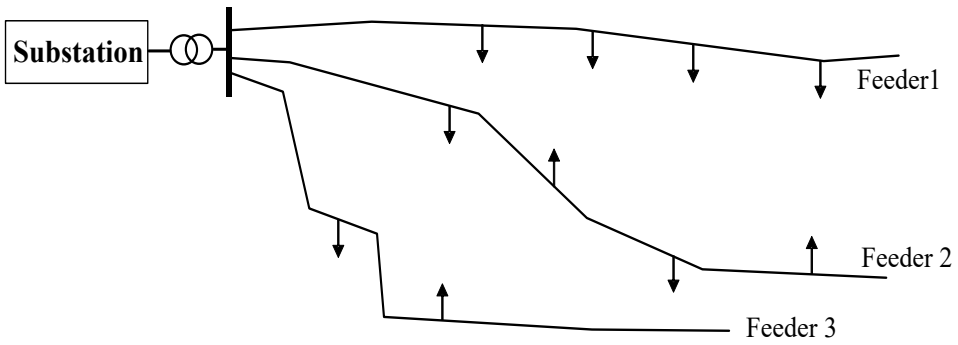

Figure 4.12 Schematic diagram of field case #2.

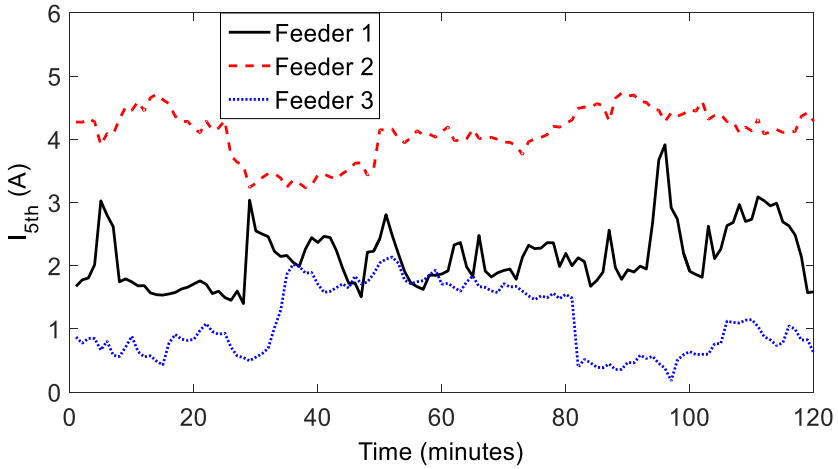

Figure 4.13 Harmonic currents of different feeders.

The harmonic contribution of each feeder calculated by the MLR-based method is shown in Table 4.8. The result reveals that feeder 2 is the main harmonic polluter, as it contributes nearly 94% of the 5th harmonic distortion at this substation. Feeder 1 and 3 almost have zero harmonic contributions. Such difference is due to the magnitude and phase angle differences among the feeder harmonic currents.

Table 4.8 Estimated harmonic contribution (%) for each feeder

HC	feeder 1	feeder 2	feeder 3
Estimated	-1.55	93.6	-4.08
Reference	-3.30	92.9	-3.35

The estimations are considered to be reliable as they satisfy the criteria discussed in Section 4.4. To further calculate the reference value for comparison, we analyzed the equivalent circuit of this system. The reference harmonic contribution of feeder 1 can be calculated as

$$HC_{Feeder1}^{Sub} = \frac{|V_{5-f}|}{|V_{5,Sub}|} = \frac{|V_{5,Sub} \cdot (I_{5,Feeder1} \times Z_{5S})|}{|V_{5,Sub}|^2} \tag{4.14}$$

where V_{5-f} is the projection of $V_{5,Feeder1}$ on $V_{5,Sub}$, $I_{5,Feeder1}$ is the 5th harmonic current of feeder 1 and $V_{5,Sub}$ is the 5th harmonic voltage of the substation. The only unknown variable in (4.14) is the 5th harmonic system impedance Z_{5S}, which is approximately equal to the sum of short circuit network impedance and the last transformer impedance. Hence, the reference value can be calculated with the information provided by the utility company. The result is also shown in Table 4.8.

4.6 Summary

This chapter presented a novel technique to quantify the respective harmonic contributions of multiple concentrated harmonic sources to a harmonic problem. The basic idea is to use multiple linear regression (MLR) technique to study the cause-and-effect relationship between the harmonic current magnitude of suspected harmonic loads and the harmonic voltage magnitude of the concern.

Unlike the harmonic power flow or harmonic state estimation techniques, the proposed method is statistical inference based and does not require network models or extensive measurements. Simulation and field measurement verifications have demonstrated the technical and practical feasibility of the proposed method.

Chapter 5

A Phasor-Data-Based Method for Harmonic Source Identification

In the previous chapter, a MLR-based method is proposed for harmonic source identification. The method is cost effective and practically sound. However, as discussed in Section 4.4, assumptions in the algorithm, such as the neglect of the load impedance and the constant background harmonic voltage, may limit its application for some cases. In view of the rapid evolvement in measurement technology, this chapter further studies the harmonic source identification problem by considering some advanced functions in modern power quality instruments such as synchronized phasor measurement.

This chapter is organized as follows. Section 5.1 explains the synchronized phasor measurement technology. Section 5.2 presents the proposed phasor-data-based method. The basic idea is to separate the contribution of each harmonic source by exploring their independency feature. Simulation verification and lab experiment test are documented in Section 5.3 and Section 5.4, respectively.

5.1 Synchronized Phasor Measurement

In recent decades, the measurement technology is evolving rapidly in order to achieve the desired functionalities in the metering infrastructure. One of the greatest achievements is the synchronized phasor measurement (SPM). SPM measures the electrical waveforms on an electricity grid using a common time source, such as global positioning system (GPS). As a result, the phasors measured at different system locations can be synchronized. The introduction of the phasor information in power systems significantly improves the monitoring and remedial action capability, which allows the network operators to utilize the

existing power system in a more efficient way. For this purpose, utilities around the world have started to install a new generation of monitors, known as phasor measurement units (PMUs), to measure synchronized 50 Hz or 60 Hz phasors since the early 21th century. Nowadays, PMUs have been applied in various applications, including state estimation [64], wide area measurement and control [65], instability prediction [66], and adaptive relaying, etc.

Since adding an GPS module is not costly, many conventional measurement devices, such as power quality monitors and protective relays, also adopted SPM technique. This trend has made the synchronized phasor data easily accessible. In this thesis, a portable power quality analyzer called "PQPro" is used for SPM. As shown in Figure 5.1, PQPro equips a GPS antenna that can receive the GPS time from GPS satellite. The receiving period is every half cycle of the system frequency. Measured waveforms can be transformed into phasors through DFT analysis and each phasor is tagged by its first sample point' GPS time. The phasors at different locations are then time synchronized based on their GPS time. For example, if the GPS time of a phasor at Location A is $t1$ sec. and the closest GPS time of a phasor at Location B is $t2$ sec., the angle of the phasor at Location B should be shifted by $(t1\text{-}t2)*60*360*h$, where h is the harmonic order. With the availability of synchronized phasor data, the harmonic source identification problem can be formulated and analyzed in the phasor domain.

Figure 5.1 Portable power quality analyzer "PQPro"

5.2 ICA-based Method

The harmonic voltage of the concern is linearly correlated with the harmonic

current measured at the PCC of the suspected load (I_{hA}) and the background harmonic voltage (V_{hX0}), as shown in (5.1). In this chapter, the load impedance is considered in the model. Therefore, I_{hA} includes the harmonic current injected by the load as well as the harmonic current absorbed by the load impedance. From another point of view, I_{hA} can be understood as a new harmonic current source that represents the overall injection from Load A, as shown in Figure 5.2.

$$V_{hX} = I_{hA} Z_{hTA} + V_{hX0} \tag{5.1}$$

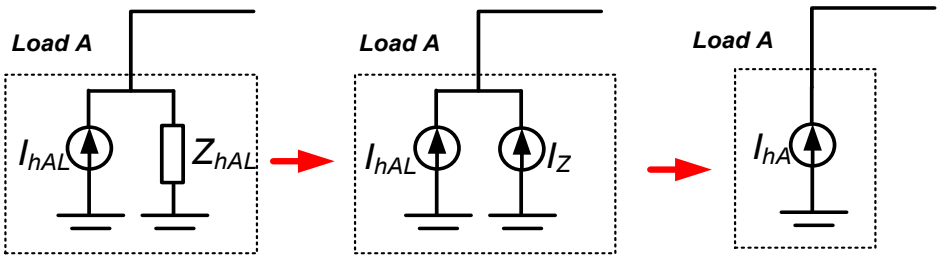

Figure 5.2 Convert customer impedance into equivalent harmonic source.

Since V_{hX} and I_{hA} can be directly obtained from the measurements, the objective is to determine Z_{hTA} or V_{hX0} in order to calculate the harmonic contribution. The MLR-based method solves this problem by studying the magnitude correlation between I_{hA} and V_{hX}, while the idea of this work is to separate the term $Z_{hTA}I_{hA}$ and V_{hX0} by using their statistical independency feature. Recent studies in [67]-[70] have shown that one significant characteristic of different harmonic loads is that their fluctuation is independent. The proposed method explores to utilize this feature to solve the harmonic source identification problem. The proposed method consists of three steps. The first step is to estimate the load harmonic current based on the measurement data at the PCC of the customer. The second step is to estimate the transfer impedance between the customer and the observation bus. The final step is to calculate the harmonic contribution based on its definition.

5.2.1 Load Harmonic Current Estimation

The proposed method attempts to solve (5.1) based on the independent fluctuation of different harmonic loads. However, the fluctuation of I_{hA} and V_{hX0}

are not completely independent due to the load harmonic impedance. According to the Norton circuit shown in Figure 5.3, the harmonic current measured at the PCC of a load (i.e. I_{hA}) is somewhat correlated with the system (i.e. V_{hX0}). Thus, it is necessary to reformulate (5.1) by using the load harmonic current (i.e. I_{hAL}), the current that is truly independent with other harmonic loads in the system. The objective of this subsection is to obtain the load harmonic current by improving the work presented in [68].

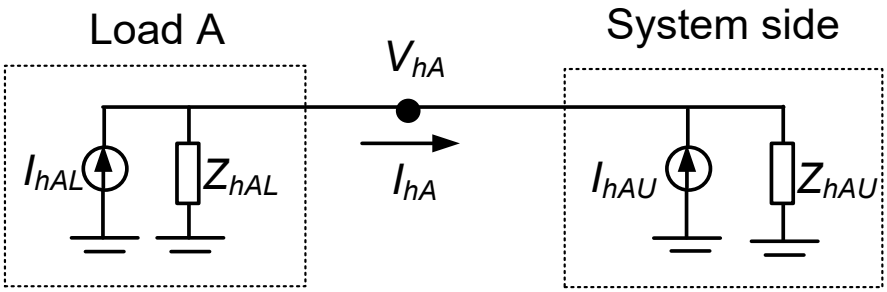

Figure 5.3 Norton equivalent circuit model at the PCC of Load A

Through circuit analysis of Figure 5.3, following equation can be derived.

$$\underbrace{\begin{bmatrix} V_{hA} \\ I_{hA} \end{bmatrix}}_{[M]} = \underbrace{\begin{bmatrix} \dfrac{Z_{hAL}Z_{hAU}}{Z_{hAL}+Z_{hAU}} & \dfrac{Z_{hAL}Z_{hAU}}{Z_{hAL}+Z_{hAU}} \\ \dfrac{-Z_{hAU}}{Z_{hAL}+Z_{hAU}} & \dfrac{Z_{hAL}}{Z_{hAL}+Z_{hAU}} \end{bmatrix}}_{[Z]} \times \underbrace{\begin{bmatrix} I_{hAU} \\ I_{hAL} \end{bmatrix}}_{[I]} \tag{5.2}$$

where V_{hA}=[$V_{hA}(t_1)$,…$V_{hA}(t_n)$] and I_{hA}=[$I_{hA}(t_1)$,…$I_{hA}(t_n)$], are the h-th harmonic voltage and current measured at the PCC, I_{hAU} and I_{hAL} are the h-th system and load harmonic currents, Z_{hAU} and Z_{hAL} are the h-th system and load harmonic impedances seen at the PCC of Load A. Since the fluctuation of I_{hAU} and I_{hAL} are independent, (5.2) represents a linear transformation of two independent signals. The goal is to find these two quantities. This problem is equivalent to a blind source separation (BSS) problem in the statistical field, where [I] is the unknown original independent signals, [Z] is the unknown mixing matrix and [M] is the measured signals. BSS is to separate a set of source signals ([I]) from a set of measured signals ([M]), without the aid of information about the source signals

([*I*]) or the mixing matrix ([*Z*]). One of the effective methods to solve BSS problem is a statistical algorithm called independent component analysis (ICA). The algorithm is explained in Appendix E for detail. In order to utilize ICA to solve (5.2), the conditions of ICA must be satisfied: 1) The third condition is already satisfied as the number of measured signals is equal to the number of source signals. 2) The first and second conditions require the source signals to be statistically independent and non-Gaussian distribution. To meet this condition, a moving average filter should be applied to the data to remove the slow-trend component and remain the random-fluctuation component of the harmonic load [69]. The slow-trend components of different harmonic loads could be similar. For example, many harmonic loads experience heavy load in daytime and light load in nighttime. The independence feature only exists in the random-fluctuation components. Thus, ICA should be applied to random-fluctuation components of [*M*] and the estimation results can be illustrated as (5.3),

$$\underbrace{\begin{bmatrix} V_{hA} \\ I_{hA} \end{bmatrix}}_{[M]} = \underbrace{\begin{bmatrix} w_1 \dfrac{Z_{hAL}Z_{hAU}}{Z_{hAL}+Z_{hAU}} & w_2 \dfrac{Z_{hAL}Z_{hAU}}{Z_{hAL}+Z_{hAU}} \\ w_1 \dfrac{-Z_{hAU}}{Z_{hAL}+Z_{hAU}} & w_2 \dfrac{Z_{hAL}}{Z_{hAL}+Z_{hAU}} \end{bmatrix}}_{[Z_{est}]} \underbrace{\begin{bmatrix} I_{hAU,est} \\ I_{hAL,est} \end{bmatrix}}_{[I_{est}]} \tag{5.3}$$

where [Z_{est}] is the estimated mixing matrix, [I_{est}] is the estimated original sources, $I_{hAU,est}$ is the estimated I_{hAU} and $I_{hAL,est}$ is the estimated I_{hAL}. It should be emphasized there are two indeterminacies in the results of ICA. One is scaling indeterminacy. One row of [*I*] can be multiplied by a factor *k* and the corresponding column of [*Z*] can be divided by *k*, without changing [*M*]. Another is ordering indeterminacy. Permuting two columns of [*Z*] and the two corresponding rows of [*I*] will not affect [*M*]. The cause of these two indeterminacies is that (5.2) is a highly underdetermined equation and only using the independence feature is not sufficient to determine the magnitude and order. As a result, w_1 and w_2 in (5.3) represent the scaling indeterminacy. The order of rows of [I_{est}] is also unknown due to the ordering indeterminacy. This means the order of rows of [I_{est}] in (5.3) may be inversed.

Fortunately, both ordering and scaling indeterminacies can be eliminated through the determination of the system harmonic impedance (Z_{hAU}) and the load harmonic impedance (Z_{hAL}). In (5.3), Z_{hAU} and Z_{hAL} can be calculated by dividing the elements in the second row of [Z_{est}] by the elements in the first row of [Z_{est}], as shown in (5.4), where Z_{est}(i,j) indicates the element in the i-th row and j-th column of the matrix [Z_{est}].

$$Z_{hAU,est} = \frac{Z_{est}(1,2)}{Z_{est}(2,2)}, Z_{hAL,est} = -\frac{Z_{est}(1,1)}{Z_{est}(2,1)} \tag{5.4}$$

If the order of [I_{est}] is inversed, the results should be same as (5.5),

$$Z_{hAU,est} = \frac{Z_{est}(1,1)}{Z_{est}(2,1)}, Z_{hAL,est} = -\frac{Z_{est}(1,2)}{Z_{est}(2,2)} \tag{5.5}$$

Whether the result is (5.4) or (5.5) can be determined by the sign of the real part of $Z_{hAU,est}$ and $Z_{hAL,est}$, both of which should be always positive in real power systems. This means: if the real part of $Z_{est}(1,2)/Z_{est}(2,2)>0$ and $Z_{est}(1,1)/Z_{est}(2,1)<0$, it indicates that the result is (5.4); if the real part of $Z_{est}(1,2)/Z_{est}(2,2)<0$ and $Z_{est}(1,1)/Z_{est}(2,1)>0$, it indicates the result is (5.5). Once Z_{hAL} is estimated, the h-th harmonic current injected by Load A can be calculated using (5.6),

$$I_{hAL,est} = I_{hA} + \frac{V_{hA}}{Z_{hAL,est}} \tag{5.6}$$

Above discussion is based on the assumption that the system and load harmonic impedances are constant. In real power systems, the system side is relatively stable, while the load side is likely to change. Small fluctuation in the load impedance has little impact on the estimation, as the mixing matrix in (5.2) is dominated by the system parameters. However, large load impedance change may still lead to inaccurate results. Here, a statistical method is proposed to check if the load impedance change has significant impact on the estimation result. The idea is that once there is a large load impedance change, the estimated load harmonic current $I_{hAL,est}$ and system harmonic current $I_{hAU,est}$ cannot be completely

independent. Assuming the proposed method is applied to a dataset that has a large load impedance change, the estimated load harmonic current can be represented as (5.7),

$$\begin{aligned} I_{hAL,est} &= I_{hAL,real} - \frac{V_{hA}(I_{hAL,est}, I_{hAU,est})}{Z_{hAL,real}} + \frac{V_{hA}(I_{hAL,est}, I_{hAU,est})}{Z_{hAL,est}} \\ &= a_1 I_{hAL,real} + a_2 I_{hAU,est} \end{aligned} \tag{5.7}$$

where $I_{hAL,real}$ is the real load harmonic current, $Z_{hAL,real}$ is the real load impedance. The estimated load harmonic impedance $Z_{hAL,est}$ cannot equal to $Z_{hAL,real}$ for all sample points since $Z_{hAL,real}$ changes significantly in this dataset. This makes the estimated load harmonic current ($I_{hAL,est}$) includes a function of the estimated system harmonic current ($I_{hAU,est}$). In other words, the random fluctuation of $I_{hAL,est}$ is somewhat correlated with the random fluctuation of $I_{hAU,est}$. $I_{hAU,est}$ can be calculated by the estimated system harmonic impedance as $V_{hA}/Z_{hAU,est}$-I_{hA}. The correlation can be indicated by the correlation coefficient (r). If r is not close to zero (e.g. r>0.1), it indicates a correlation between $I_{hAU,est}$ and $I_{hAL,est}$. Then the result is unreliable and this dataset should be discarded. It is obvious that this method also can be used to check the system side change, even though such cases may not be very frequent. Besides of the proposed index, it should be mentioned that the measured fundamental components can be used to pre-screen the data. To avoid the large change of the system impedance and the load impedance, the fundamental component of I_{hA} and V_{hA} should have small fluctuation in the selected dataset.

5.2.2 Transfer Impedance Estimation

After the harmonic currents of all suspected loads are determined, the harmonic source identification problem can be reformulated using the estimated load harmonic currents if total of three suspected harmonic loads Load A, B and C are considered, as shown in (5.8).

$$\underbrace{\begin{bmatrix} V_{hX} \\ I_{hAL,est} \\ I_{hBL,est} \\ I_{hCL,est} \end{bmatrix}}_{[MM]} = \underbrace{\begin{bmatrix} Z_{hXA} & Z_{hXB} & Z_{hXC} & 1 \\ 1 & 0 & 0 & 0 \\ 0 & 1 & 0 & 0 \\ 0 & 0 & 1 & 0 \end{bmatrix}}_{[ZZ]} \times \underbrace{\begin{bmatrix} I_{hAL,est} \\ I_{hBL,est} \\ I_{hCL,est} \\ V_{hX0} \end{bmatrix}}_{[II]} \tag{5.8}$$

where $V_{hX}=[V_{hX}(t_1),\ldots V_{hX}(t_n)]$ is the h-th harmonic voltage measured at the observation bus, $I_{hAL,est}=[I_{hAL,est}\ (t_1),\ldots I_{hAL,est}(t_n)]$, $I_{hBL,est}=[I_{hBL,est}(t_1),\ldots I_{hBL,est}(t_n)]$ and $I_{hCL,est}=[I_{hCL,est}(t_1),\ldots\ I_{hCL,est}(t_n)]$ are the estimated h-th harmonic currents of Load A, B, and C, Z_{hXA}, Z_{hXB}, Z_{hXC} are the transfer impedances between suspected loads and the observation bus, V_{hX0} is the h-th background harmonic voltage. Since the fluctuation of $I_{hAL,est}$, $I_{hBL,est}$, $I_{hCL,est}$ and V_{hX0} are independent, the new formulation of the harmonic source identification problem in (5.8) is equivalent to a BSS problem, where [*II*] is the unknown original independent signals, [*ZZ*] is the unknown mixing matrix and [*MM*] is the measured signals. Thus, ICA can be adopted to solve the equation. The conditions of ICA are easy to satisfy: 1) the number of measured signals is equal to the number of source signals; 2) the random-fluctuation components of [*II*] are independent and have non-Gaussian distribution. Thus, the mixing matrix ([*ZZ*]) and the original source signals ([*II*]) can be estimated by applying ICA to random-fluctuation components of [*MM*]. Note that the ordering and scaling indeterminacies still exist. The estimation results can be illustrated as (5.9),

$$\underbrace{\begin{bmatrix} V_{hX} \\ I_{hAL,est} \\ I_{hBL,est} \\ I_{hCL,est} \end{bmatrix}}_{[MM]} = \underbrace{\begin{bmatrix} k_1 Z_{hXA} & k_2 Z_{hXB} & k_3 Z_{hXC} & k_4 \\ k_1 & 0 & 0 & 0 \\ 0 & k_2 & 0 & 0 \\ 0 & 0 & k_3 & 0 \end{bmatrix}}_{[ZZ_{est}]} \underbrace{\begin{bmatrix} I_{hAL,est,est} \\ I_{hBL,est,est} \\ I_{hCL,est,est} \\ V_{hX0,est} \end{bmatrix}}_{[II_{est}]} \tag{5.9}$$

where $[II_{est}]$ is the estimated original sources, $[ZZ_{est}]$ is the estimated mixing matrix, $I_{hAL,est,est}$ is the estimated $I_{hAL,est}$, $I_{hBL,est,est}$ is the estimated $I_{hBL,est}$, $I_{hCL,est,est}$ is the estimated $I_{hCL,est}$, $V_{hX0,est}$ is the estimated V_{hX0}, k_1, k_2, k_3 and k_4 represent the scaling indeterminacy. Due to the ordering indeterminacy, the order of rows of $[II_{est}]$, i.e., the order of $I_{hAL,est,est}$, $I_{hBL,est,est}$, $I_{hCL,est,est}$ and $V_{hX0,est}$, is unknown. The

ordering indeterminacy can be eliminated through a linear correlation study. Theoretically, $I_{hAL,est,est}$ is equal to $1/k_1 I_{hAL,est}$, $I_{hBL,est,est}$ is equal to $1/k_2 I_{hBL,est}$ and $I_{hCL,est,est}$ is equal to $1/k_3 I_{hCL,est}$. This indicates that if one row of $[II_{est}]$ has very strong linear correlation with $I_{hAL,est}$ ($I_{hBL,est}$ or $I_{hCL,est}$), this row corresponds to $I_{hAL,est,est}$ ($I_{hBL,est,est}$ or $I_{hCL,est,est}$). The remained row is $V_{hX0,est}$. The linear correlation can be measured by correlation coefficient. Once the order is determined and rearranged as the order in (5.9), the transfer impedances can be calculated by dividing the elements in corresponding rows. For example, the transfer impedance of Load A can be calculated as (5.10),

$$Z_{hXA,est} = \frac{ZZ_{est}(1,1)}{ZZ_{est}(2,1)} \tag{5.10}$$

5.2.3 Harmonic Contribution Calculation

As the phasor data becomes available, the harmonic contribution can be calculated from many other perspectives besides of the projection. In Figure 5.4, the projection of V_{hXA} on V_{hX} are exactly same in two cases. However, mitigating V_{hXA} has much better performance in Case 2. This means only using the projection information is not sufficient in troubleshooting. In this chapter, a new harmonic contribution index is proposed, as shown in (5.11). The new index defines the harmonic contribution of a customer as the harmonic voltage change at the observation bus caused by the connection of a customer.

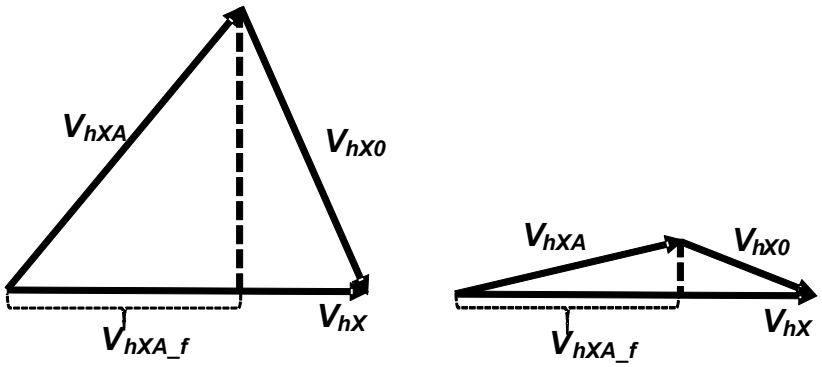

(a) Case 1 **(b) Case 2**

Figure 5.4 Phasor diagram of harmonic voltage at Bus X in two different cases.

$$HC_{Load\ A}^{Bus\ X} = \frac{|V_{hX}| - |V_{hX0}|}{|V_{hX}|} \times 100\% = \frac{|V_{hX}| - |V_{hX} - Z_{hTA} I_{hA}|}{|V_{hX}|} \times 100\% \quad (5.11)$$

In (5.11), V_{hX0} is the harmonic voltage at Bus X without Load A connected to the system and V_{hX} is the harmonic voltage at Bus X with Load A connected to the system. V_{hX} can be obtained from the measurements, while V_{hX0} needs to be estimated based on (5.1). Note the estimated Z_{hXA} in (5.10) is not equal to the required Z_{hTA} in (5.1), as Z_{hXA} includes Load A' load impedance while Z_{hTA} excludes Load A's load impedance. One more step is needed to estimate Z_{hTA} based on Z_{hXA}, as shown in (5.12). Finally, the harmonic contribution can be calculated using (5.13). It is intuitive that the harmonic contribution in (5.13) is not a constant and would change with I_{hA}. In this thesis, the average value is used to represent to overall harmonic contribution. Other statistical indices, such as 95% percentile value, can be developed as well.

$$Z_{hTA,est} = Z_{hXA,est} \frac{Z_{hAL,est} + Z_{hAU,est}}{Z_{hAL,est}} \quad (5.12)$$

$$HC_{Load\ A}^{Bus\ X} = \frac{1}{n} \sum_{i=1}^{n} \frac{|V_{hX}(t_i)| - |V_{hX}(t_i) - Z_{hTA,est} I_{hA}(t_i)|}{|V_{hX}(t_i)|} \times 100\% \quad (5.13)$$

5.2.4 Method Guideline

The procedures of the ICA-based method can be summarized as follows:

1) Measure harmonic voltage phasors (V_{hA}, V_{hB} … V_{hM}) and harmonic current phasors (I_{hA}, I_{hB} … I_{hM}) at the PCC of suspected loads and harmonic voltage phasors (V_{hX}) at the observation bus over the appropriate time interval. All phasors should be time-synchronized.

2) Decompose all phasors into the slow-trend components and random-fluctuation components by using the moving average filter.

3) Estimate the load harmonic currents of each suspected load according to Section 5.2.1.

4) Check if the correlation coefficient r between the random-fluctuation

components of the estimated load harmonic current and the estimated system harmonic current is smaller than 0.1.

5) If yes, estimate the transfer impedances between suspected loads and the observation bus according to Section 5.2.2.

6) Calculate the harmonic contribution according to Section 5.2.3.

5.3 Simulation Verification Using Field Data

In this section, the simulation verification was carried out using IEEE 57 bus system. In this system, large loads at Bus 1, 3, 6, 8, 9, 12 are selected as harmonic producing loads. Among them, Load 1, 8, 9, 12 are suspected harmonic loads. Their harmonic voltages and currents are measured at the PCC. Load 3 and 6 are background harmonic loads. They create background harmonics in the system. The harmonic loads are modeled by the Norton circuit. The injected harmonic currents are 3rd harmonic currents measured at several substations in Alberta, Canada, as shown in Figure 5.5 (a). The purpose of using the harmonic currents in actual power systems is to verify if the independence truly exists in real harmonic loads. The slow-trend components and random-fluctuation components of the harmonic currents obtained by a 10-point moving average filter are also shown in Figure 5.5. According to the correlation coefficient shown in Table 5.1, the slow-trend components are similar for the harmonic currents measured at different substations, while the random-fluctuation components are completely uncorrelated. This is why the random-fluctuation components of the measurements should be used for ICA.

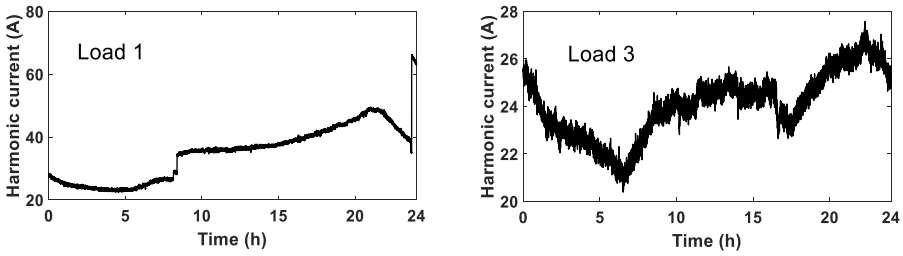

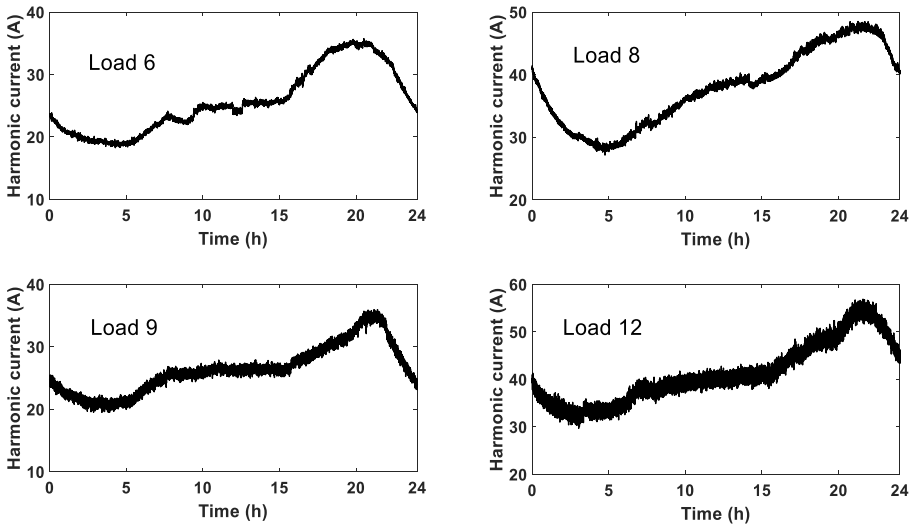

(a) Original measurement data

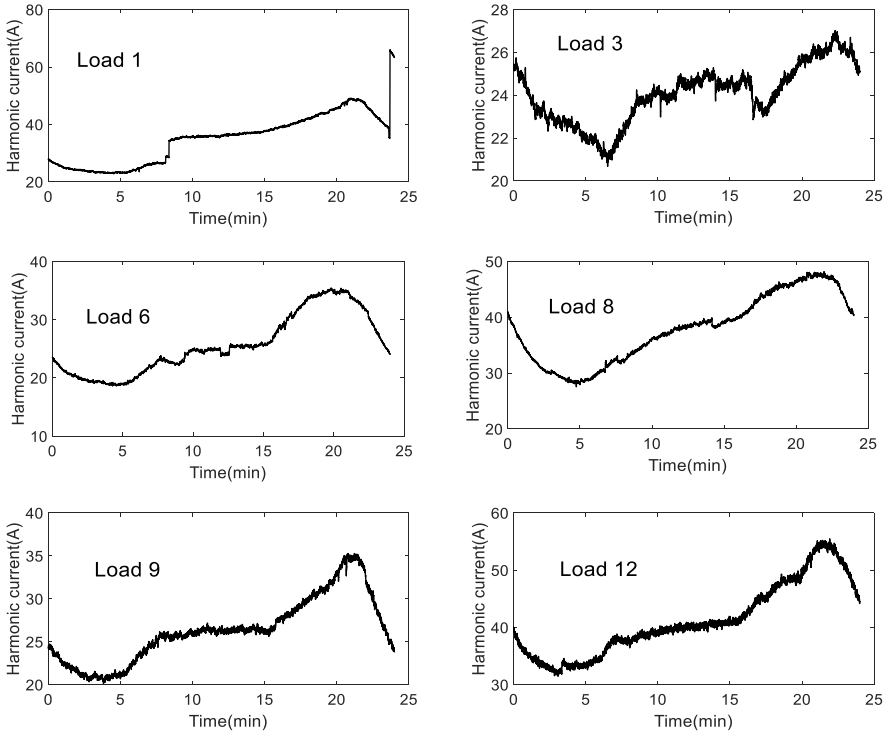

(b) Slow-trend components

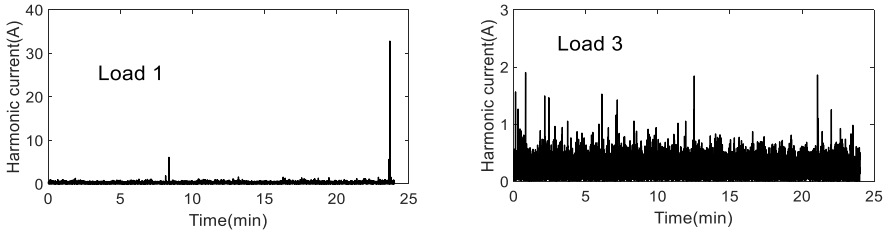

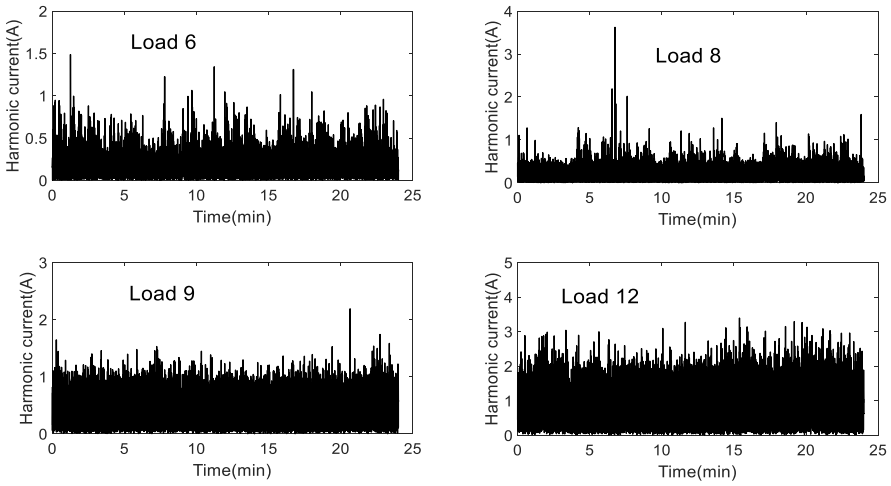

(c) Random-fluctuation components

Figure 5.5 3rd harmonic currents measured at real substations

Table 5.1 Correlation coefficient between slow-trend components (lower left triangle)/random-fluctuation components (upper right triangle)

Load	1	8	9	12	3	6
1		0.00	0.00	0.01	0.01	0.01
8	0.88		0.01	0.01	0.01	0.01
9	0.82	0.91		0.01	0.00	0.00
12	0.86	0.93	0.94		0.01	0.00
3	0.86	0.94	0.93	0.90		0.01
6	0.85	0.95	0.94	0.91	0.94	

Simulations were carried out for four different cases:

1) Case #1: all load impedances are constant and their values are determined by the real load data.

2) Case #2: all load impedances are enlarged ten times.

3) Case #3: all load impedances have 10% random fluctuation.

4) Case #4: large load impedance change occurs in Load 8.

5.3.1 Simulation Case #1

The first step of the proposed method is to estimate the load harmonic current. Table 5.2 shows estimated system and load harmonic impedances, both of which are close to the exact value. Thus, the injected harmonic currents of each

suspected load can be precisely determined using (5.6).

Table 5.2 Case #1 - estimated system and load harmonic impedances

Load	System harmonic impedance		Load harmonic impedance	
	Estimated (ohm)	Exact (ohm)	Estimated (ohm)	Exact (ohm)
1	0.044+0.129j	0.044+0.129j	1.77+0.25j	1.80+0.19j
8	0.055+0.140j	0.050+0.140j	0.65+0.03j	0.67+0.03j
9	0.058+0.111j	0.057+0.112j	0.81+0.03j	0.82+0.06j
12	0.065+0.141j	0.065+0.141j	0.27+0.00j	0.26+0.00j

Bus 10 and Bus 55 are selected as the observation buses. Their harmonic voltages were measured. The estimated transfer impedances between the suspected loads and the observation buses are presented in Table 5.3. The results are in good agreement with the exact value. Finally, the harmonic contribution can be determined accordingly using (5.13). The average harmonic contribution of each suspected load is shown in Table 5.4. The results reveal that: 1) the operation of Load 9 results in +30.9% and +43.4% increase of the harmonic voltages at Bus 10 and 55, respectively; 2) the operation of Load 12 leads to +41.0% and +21.8% increase of the harmonic voltages at Bus 10 and 55, respectively; 3) the operation of Load 8 almost has no impact on the harmonic distortion at these two observation buses; 4) the operation of Load 1 reduces the harmonic distortion at these two observation buses.

Table 5.3 Case #1 - estimated transfer impedances

Load	Bus 10		Bus 55	
	Estimated (ohm)	Exact (ohm)	Estimated (ohm)	Exact (ohm)
1	0.049+0.020j	0.047+0.020j	0.042+0.012j	0.041+0.012j
8	0.051+0.032j	0.050+0.032j	0.062+0.073j	0.061+0.073j
9	0.062+0.054j	0.060+0.055j	0.071+0.104j	0.069+0.106j
12	0.068+0.091j	0.068+0.092j	0.061+0.042j	0.063+0.045j

Table 5.4 Case #1 - estimated average harmonic contribution

Load	Bus 10		Bus 55	
	Est.	Exact	Est.	Exact
1	-32.8%	-31.8%	-25.3%	-24.7%
8	+5.4%	+5.3%	+3.1%	+2.8%
9	+30.9%	+30.7%	+43.4%	+43.5%
12	+41.0%	+41.6%	+21.8%	+22.9%

5.3.2 Simulation Case #2

In many cases, the load harmonic impedance could be way larger than the system harmonic impedance. In general, measuring large load impedances is difficult as it requires large disturbances at the system side. Case #2 investigates the impact of large load impedance on the harmonic contribution determination. The simulation was redone by enlarging all load harmonic impedances ten times. The estimated system and load harmonic impedances are shown in Table 5.5 and the estimated average harmonic contribution is shown in Table 5.6. It is interesting to find that the harmonic contribution still can be accurately determined, even though the estimated load harmonic impedance is not that accurate. The reason is that when the load harmonic impedance is large, its impact on the load harmonic current is very small. Thus, the error in the load harmonic impedance does not reflect in the calculated harmonic contribution.

Table 5.5 Case #2 - estimated system and load harmonic impedances

Load	System harmonic impedance		Load harmonic impedance	
	Estimated (ohm)	Exact (ohm)	Estimated (ohm)	Exact (ohm)
1	0.027+0.206j	0.027+0.207j	19.5+4.5j	18.0+1.9j
8	0.035+0.222j	0.027+0.218j	6.4+0.5j	6.7+0.3j
9	0.035+0.209j	0.032+0.209j	7.6+0.1j	8.2+0.6j
12	0.029+0.231j	0.029+0.231j	2.7+0.1j	2.6+0.0j

Table 5.6 Case #2 - estimated average harmonic contribution with large load impedance

Load	Bus 10		Bus 55	
	Est.	Exact	Est.	Exact
1	-29.4%	-28.5%	-25.4%	-24.7%
8	+5.9%	+5.8%	+7.8%	+7.7%
9	+32.0%	+31.5%	+37.6%	+37.4%
12	+52.2%	+53.0%	+38.3%	+39.4%

5.3.3 Simulation Case #3 and #4

In the real power system, the load harmonic impedance is likely to change with time. This would result in some variations of the mixing matrix in the ICA model. This subsection studies the influence of load fluctuation on the harmonic contribution determination. In case #3, it is assumed that all harmonic load impedances have 10% random fluctuation. The estimated harmonic contribution

is presented in Table 5.7. The results are still accurate as the small fluctuation in the load harmonic impedance has little impact on the mixing matrix.

Table 5.7 Case #3 - estimated average harmonic contribution with 10% load fluctuation

Load	Bus 10		Bus 55	
	Est.	Exact	Est.	Exact
1	-32.8%	-31.8%	-25.3%	-24.7%
8	+6.6%	+5.3%	+2.8%	+2.8%
9	+30.3%	+30.7%	+42.8%	+43.5%
12	+41.0%	+41.6%	+21.9%	+22.9%

An additional scenario was studied in case #4, where Load 8 is assumed to have large load impedance change. The estimated harmonic contribution is shown in Table 5.8. As seen from the table, load impedance change may lead to inaccurate results. Such case can be indicated by the correlation coefficient r between the random-fluctuation components of the estimated load harmonic current and the estimated system harmonic current. In practice, r is suggested to be no greater than 0.1.

Table 5.8 Case #4 - estimated harmonic contribution of Load 8 with different load changes

Load change	Bus 10		Bus 55		r
	Est.	Exact	Est.	Exact	
-20%	+4.6%	+4.8%	+2.0%	+2.2%	0.07
-40%	+2.8%	+4.0%	+0.0%	+1.0%	0.15
-60%	-0.8%	+2.2%	-3.7%	-1.5%	0.26
-80%	-15.7%	-3.0%	-20.8%	-9.3%	0.73

5.4 Experiment Test

To further validate the proposed method, experiments on harmonic source identification problem has been carried out in the laboratory. The equivalent circuit of the test is shown in Figure 5.6, where Vs and Zs are system voltage and impedance, Z_{L1}, Z_{L2}, and Z_{L3} are the cables between power outlets and the loads. Three loads, Load A, B and C, contain both linear loads and the nonlinear loads. The linear loads are the heater and incandescent lamps, while the nonlinear loads are computers and LED lights. Three persons independently switch small parts of the load to simulate the natural random fluctuation of the load. Load A and Load

B are selected as the suspected harmonic loads. Their harmonic voltages and currents are recorded, as shown in Figure 5.7 and Figure 5.8. Since the major harmonics produced by the nonlinear loads in the experiment are 3rd, 5th, and 7th, the harmonic contributions of those harmonic orders are analyzed.

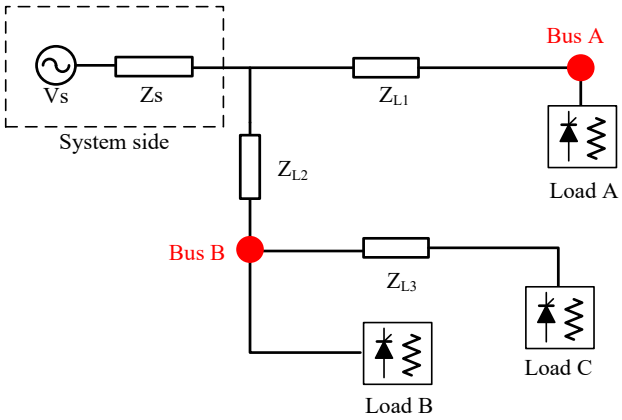

Figure 5.6 The equivalent circuit of the lab experiment.

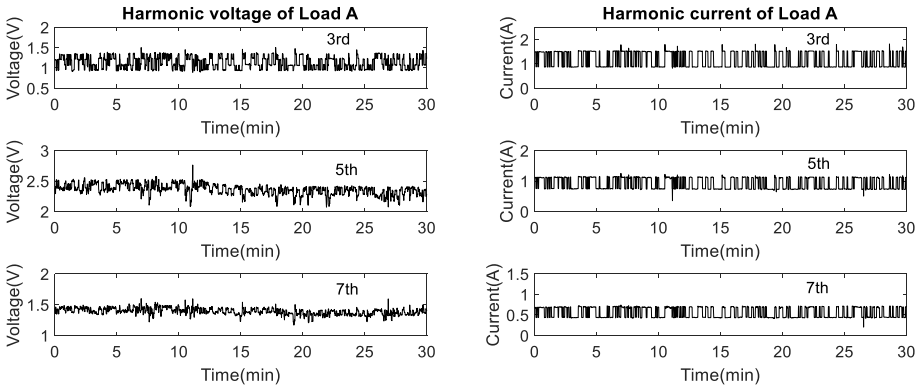

Figure 5.7 Measured harmonic voltages and currents of Load A

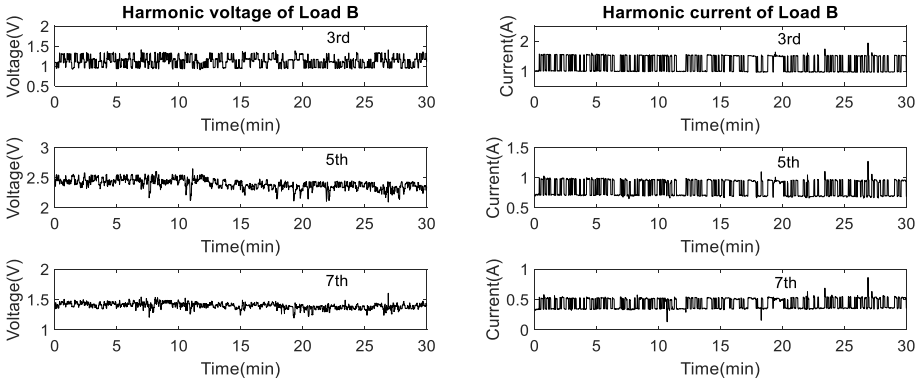

Figure 5.8 Measured harmonic voltages and currents of Load B

The objective of this experiment is to estimate the harmonic contribution of Load A and B on Bus A and B. The estimated system and load harmonic impedances of Load A and B are shown in Table 5.9 and Table 5.10. The reference value is determined by switching a large harmonic load and calculated by $\Delta V / \Delta I$. Since small parts of loads were switching during the experiment, the reference load impedance in the table represents the average value of $\Delta V / \Delta I$ that measured at different states of the load. According to the results, the estimated system harmonic impedance and load harmonic impedances are close to the reference values.

Table 5.9 Estimated system and load harmonic impedances of Load A

Load A	System harmonic impedance		Load harmonic impedance	
	Estimated (ohm)	Reference (ohm)	Estimated (ohm)	Reference (ohm)
3rd	0.429+0.046j	0.422+0.050j	3.2-5.4j	3.2-5.4j
5th	0.440+0.087j	0.430+0.086j	2.2-3.0j	1.8-3.3j
7th	0.469+0.115j	0.464+0.128j	1.8-2.6j	1.9-2.3j

Table 5.10 Estimated system and load harmonic impedances of Load B

Load B	System harmonic impedance		Load harmonic impedance	
	Estimated (ohm)	Reference (ohm)	Estimated (ohm)	Reference (ohm)
3rd	0.390+0.049j	0.392+0.048j	3.3-5.0j	3.2-5.4j
5th	0.399+0.084j	0.400+0.090j	2.5-3.7j	2.5-3.6j
7th	0.419+0.126j	0.419+0.126j	1.4-2.8j	1.7-2.4j

The estimated transfer impedance is shown in Table 5.11. Similarly, the reference value is determined by a large harmonic load switching. It can be seen that the estimation results are close to the reference value. As a comparison, the transfer impedances were also estimated without load harmonic current estimation, i.e., directly using the measured harmonic currents. The results are shown in Table 5.12. For 3rd harmonic, the estimation results in Table 5.12 are still acceptable. The reason is that the background 3rd harmonic voltage is small and the load's 3rd harmonic impedance is large. Thus, the measured harmonic currents are almost independent with the system. However, for 5th and 7th harmonics, directly using the measured harmonic currents lead to large estimation error. Finally, the average harmonic contribution was calculated and the results are shown in Table 5.13. It can be observed that Load A results in +41% increase of 3rd harmonic voltage at

Bus A and +23% increase of 3rd harmonic voltage at Bus B. For 5th and 7th harmonics, Load A has relatively small impact on two observation buses. Similar conclusions can be drawn for Load B.

Table 5.11 Estimated transfer impedances

	$Z_{h,AB}$ (Load A to Bus B)		$Z_{h,BA}$ (Load B to Bus A)	
	Estimated (ohm)	Reference (ohm)	Estimated (ohm)	Reference (ohm)
3rd	0.221+0.043j	0.225+0.043j	0.223+0.046j	0.224 + 0.042j
5th	0.242+0.073j	0.237+0.074j	0.231+0.061j	0.238 + 0.068j
7th	0.256+0.113j	0.256+0.111j	0.234+0.103j	0.248+ 0.108j

Table 5.12 Estimated transfer impedances without load harmonic current estimation

	$Z_{h,AB}$ (Load A to Bus B)		$Z_{h,BA}$ (Load B to Bus A)	
	Estimated (ohm)	Reference (ohm)	Estimated (ohm)	Reference (ohm)
3rd	0.231+0.060j	0.225+0.043j	0.229+0.062j	0.224 + 0.042j
5th	0.293-0.050j	0.237+0.074j	0.267-0.026j	0.238 + 0.068j
7th	0.124+0.161j	0.256+0.111j	0.104+0.190j	0.248+ 0.108j

Table 5.13 Estimated average harmonic contribution

Load	Bus A			Bus B		
	3rd	5th	7th	3rd	5th	7th
Load A	+41.1%	-12.5%	+6.2%	+23.4%	-8.5%	+7.1%
Load B	+24.8%	-7.2%	+6.8%	+41.5%	-11.2%	+8.9%

5.5 Comparison with MLR-based Method

In Chapter 4 and Chapter 5, two different methods are proposed for harmonic source identification. One is the MLR-based method and another is the ICA-based method. This section compares the performance of two methods. Since the MLR-based method can only calculate the harmonic contribution defined in (4.8), this section uses that definition for comparison. The comparative studies were carried out using simulation cases in Section 5.3 and lab experiment in Section 5.4.

The comparison of two methods in simulation case #1 is shown in Table 5.14. It can be seen the MLR-based method does not provide very accurate estimation for some loads. This is due to the impact of the load impedance. Table 5.15 shows the correlation coefficients between measured harmonic currents of different loads. As seen from the table, there are some correlations between different loads, indicating the MLR-based method may provide unreliable results

Table 5.14 Harmonic contributions (%) calculated by two methods in simulation case #1

Load	Bus 10			Bus 55		
	ICA	MLR	Exact	ICA	MLR	Exact
1	-29.45	-44.94	-28.59	-23.04	-31.21	-22.44
8	17.77	16.00	17.36	24.11	1.64	23.43
9	33.96	39.25	33.72	47.82	50.15	47.91
12	58.19	45.30	59.22	31.42	27.04	33.09

Table 5.15 Correlation coefficients between different loads in simulation case #1

r	1	8	9	12
1		0.04	0.05	0.15
8			-0.15	-0.12
9				-0.23
12				

In simulation case #2, all load impedances are enlarged ten times. The results are shown in Table 5.16. Since the load impedances are large in this case (can be ignored), the MLR-based method provides satisfactory results. As seen from Table 5.17, the correlation is very small between different loads.

Table 5.16 Harmonic contributions (%) calculated by two methods in simulation case #2

Load	Bus 10			Bus 55		
	ICA	MLR	Exact	ICA	MLR	Exact
1	-28.22	-31.03	-27.40	-24.74	-26.85	-24.10
8	12.93	13.37	12.54	17.83	19.43	17.37
9	32.18	32.04	31.73	38.08	38.24	37.88
12	53.85	54.13	54.77	39.46	40.28	40.70

Table 5.17 Correlation coefficients between different loads in simulation case #2

r	1	8	9	12
1		0.03	0.01	0.02
8			-0.03	-0.06
9				-0.01
12				

In simulation case #3, all load impedances have 10% random fluctuation. The results are shown in Table 5.18. Compared with Table 5.14, it can be concluded that the small fluctuation of the load impedances does not significantly impact the results for both two methods.

Table 5.18 Harmonic contributions (%) calculated by two methods in simulation case #3

Load	Bus 10			Bus 55		
	ICA	MLR	Exact	ICA	MLR	Exact
1	-29.49	-44.85	-28.60	-23.04	-31.22	-22.67
8	17.55	16.13	17.27	24.02	1.51	23.37
9	34.17	39.01	33.72	47.59	49.94	47.89
12	57.99	45.81	59.21	31.86	27.40	33.68

In simulation case #4, a large load impedance change occurs in Load 8. The comparison of two methods is shown in Table 5.19. Both two methods cannot provide reliable results in this case. In practice, such cases can be filtered out by proposed indices.

Table 5.19 Harmonic contributions (%) calculated by two methods in simulation case #4

Load	Bus 10			Bus 55		
	ICA	MLR	Exact	ICA	MLR	Exact
1	-27.53	-41.81	-30.72	-20.16	-30.12	-25.70
8	27.45	28.54	16.60	38.13	1.18	20.48
9	33.13	36.47	36.49	45.74	48.40	53.13
12	57.49	44.68	63.78	31.32	27.51	39.05

The comparison of two methods in lab experiment is shown in Table 5.20. In general, the results of both two methods are consistent with the reference value. The ICA-based method has good performance for all harmonic orders. The MLR-based method has a better performance for the 3rd harmonic, as the 3rd background harmonic voltage is small. r^2 shown in Table 5.21 also indicates the MLR-based method has better estimation for the 3rd harmonic.

Table 5.20 Harmonic contributions (%) calculated by two methods in lab experiment

	Load	Bus A			Bus B		
		3rd	5th	7th	3rd	5th	7th
Load A	Ref	44.3	-7.4	15.9	24.4	-6.6	9.4
	ICA	44.9	-8.8	11.5	23.9	-5.5	10.1
	MLR	44.7	-12.0	12.8	24.6	-7.5	8.7
Load B	Ref	26.5	-4.8	9.1	45.6	-6.2	15.3
	ICA	25.7	-4.8	6.7	46.2	-7.2	12.4
	MLR	26.1	-6.3	7.0	43.8	-8.9	9.0

Table 5.21 r^2 for the MLR based method in lab experiment

r^2	3rd	5th	7th
Bus A	0.98	0.68	0.60
Bus B	0.98	0.59	0.59

When applying these two methods in practice, one issue that needs to be considered is the measurement requirement. Table 5.22 compares the suggested (minimum) measurement requirements of two methods. The ICA based method has higher requirement on the data volume, as the independence feature can be accurately analyzed only if a large amount of data is available.

Table 5.22 Measurement requirements of two methods

	Samples per cycle (up to 15^{th} harmonic)	Cycles per snapshot	Snapshots per minute	Number of snapshots
MLR	64	6	6	>100
ICA	64	6	60	>1000

Through the analysis above, the strength and weakness of two methods can be summarized as Table 5.23.

Table 5.23 Strength and weakness of two methods

	Strength	Weakness
MLR	1) Only the magnitude data is required 2) r^2 and confidence intervals can indicate the estimation accuracy 3) The algorithm is simple.	1) Only can provide reliable results when load impedances can be ignored. 2) Only can provide reliable results when background harmonic voltage is relatively stable. 2) Only the projection information can be obtained
ICA	1) Immune to the background voltage fluctuation 2) Consider the load impedance in the model 3) Harmonic contributions can be calculated in different ways	1) Synchronized phasor measurement is required. 2) The algorithm is complex. The setting of the algorithm may affect the results. 3) A large amount of data is needed.

5.6 Summary

This chapter presented a new phasor-data-based method to quantify the respective harmonic contributions of multiple concentrated harmonic sources to a harmonic problem. The key idea is to use a statistical method called ICA to separate the harmonic contribution of different harmonic sources by exploring their independency feature. Both simulation verification and lab experiment have

demonstrated the effectiveness of the proposed method. Compared with the MLR-based method in Chapter 4, the main advantage of the ICA-based method is that it does not impose assumptions on load impedances and background harmonic voltages; thus, the method is applicable for more cases. However, the ICA-based method is more complex and can only be performed when the synchronized phasor measurement is available.

The ICA-based method, as well as the MLR-based method, are mostly suited for a power quality (PQ) monitoring system or platform as an advanced PQ analysis tool. Nowadays, more utilities are deploying PQ monitoring systems. These systems can record the PQ indices and statistics, and present trends. However, they cannot do cause-effect and other advanced analysis. The proposed techniques push PQ monitoring to a higher level that fully makes use of the data to obtain useful information. For example, two proposed techniques can be added as a subroutine into the existing PQ monitoring system. The data server can use the techniques to identify major harmonic polluters in the system.

Chapter 6

Conclusions and Future Work

This chapter summarizes the main findings of the thesis and provides suggestions for future work.

6.1 Thesis Conclusions and Contributions

This thesis has approached topics related to the investigation, identification, and mitigation of harmonic distortions in power systems. An extensive investigation of harmonic distortion characteristics in residential distribution systems was first conducted. Then, a cost-effective scheme to address the harmonic resonance issue for multiple switchable capacitors was proposed. Finally, two measurement-based methods were proposed for harmonic source identification problem.

The main conclusions and contributions of this thesis are summarized as follows.

- This thesis presented useful findings on the characteristics of harmonic distortions in residential distribution systems based on extensive field measurement results. They are extracted though multifaceted analysis: 1) the bottom up analysis from homes to feeders provide a complete picture on causes and effects of the harmonic distortion in modern residential distribution systems; 2) the statistical analysis of different measurement individuals reveal the general characteristics of residential distribution systems; 3) the comparative study of the harmonic distortion results involving residential, commercial and industrial feeders shows the severity of the power quality issue in residential systems. Such findings have not been reported before and can be very useful to improve existing standards. The thesis also showed the inductive coupling effects of zero sequence harmonics. In addition, it reported

the first ever synchronized measurement results on the harmonic phasor characteristics at two locations.

- This thesis proposed a new scheme to mitigate harmonic resonance for multiple switchable capacitors. In the proposed scheme, multiple switchable capacitors share one damping block. Damping performance can be guaranteed for all capacitor energization scenarios and system impedance conditions. Compared with the conventional scheme that requires each switchable capacitor to equip a damping block, the main advantage of the proposed scheme is therefore to save damping blocks. Comparative analysis on actual capacitor application cases has been conducted. The results demonstrate that the proposed scheme can achieve the same performance as the conventional scheme with lower cost and space requirement. Furthermore, it has been shown that the design results are independent of the system impedances. As a result, a look-up table of component parameters of the damping block has been calculated for direct industry use.

- Two measurement-based methods were proposed for the harmonic source identification problem. The technical merits of these two methods are one of the main contributions of the thesis to this research area. The first method is based on MLR technique. The basic idea is to study the cause-and-effect relationship between the harmonic current magnitude of a customer and the harmonic voltage magnitude of the concern. The second method advances the MLR-based method by including synchronized phasor data and by adopting ICA. It solves the harmonic source identification problem by exploring the independency feature of the harmonic sources. The feasibility of two proposed methods have been thoroughly demonstrated through rigorous verification studies. Additionally, practical issues have been fully considered and addressed. Since both two proposed methods do not require any system network information by only utilizing the measurements at some locations of the system, they are expected to become useful tools for power quality management.

6.2 Suggestions for Future Work

As with any study, something can always be done to extend the research. Several extensions and modifications of this thesis can be explored as follows:

- The future research can take advantage of the useful data provided in Chapter 2. For example, the results of statistical phase angle distribution can help develop an improved and more realistic methods to predict the harmonic current addition effects. The results on harmonic current magnitude distribution $1/h^{\alpha}$, where α=2.0, 2.0, 2.3 for homes, service transformers and feeders respectively, can be useful to study the impact of residential harmonics on power transmission systems or to determine the loading requirements on distribution level harmonic filters.

- The design method shown in Section 3.3 has several modifications. For example, the design condition "cost minimization" can be replaced by "harmonic loss minimization" or "harmonic voltage minimization". If these two design conditions are applied, the system information is then required to calculate the harmonic loss and the harmonic voltage. The resonance-free condition also can be relaxed by using actual harmonic amplification ratio, rather than worst-case harmonic amplification ratio. Moreover, future research may find a more efficient algorithm, instead of exhaustive search method, to solve the design problem.

- The harmonic source identification problem in this thesis can be extended for other steady-state power quality disturbances, such as the unbalance and the flicker. To address those issues, a reasonable index should be proposed first to quantify the contribution of each source. Then similar measurement-based methods can be developed to solve the problem.

References

[1] A. B. Nassif, W. Xu and W. Freitas, "An investigation on the selection of filter topologies for passive filter applications," *IEEE Transactions on Power Delivery*, vol. 24, no. 3, pp. 1710-1718, July 2009.

[2] X. Li, W. Xu and T. Ding, "Damped high passive filter—a new filtering scheme for multipulse rectifier systems," *IEEE Transactions on Power Delivery*, vol. 32, no. 1, pp. 117-124, Feb. 2017.

[3] H. Hu, Z. He and S. Gao, "Passive filter design for china high-speed railway with considering harmonic resonance and characteristic harmonics," *IEEE Transactions on Power Delivery*, vol. 30, no. 1, pp. 505-514, Feb. 2015.

[4] B. Badrzadeh, K. S. Smith, and R. C. Wilson, "Designing passive harmonic filters for an aluminum smelting plant," *IEEE Transactions on Industry Applications*, vol. 47, no. 2, pp. 973–983, Apr. 2011.

[5] A. Dekka, A. R. Beig, S. Kanukollu and M. S. Al Rahis, "Retrofitting of harmonic power filters in onshore oil drilling rigs: challenges and solutions," *IEEE Transactions on Industry Applications*, vol. 50, no. 1, pp. 142-154, Jan.-Feb. 2014.

[6] L. Morán, C. A. Albistur and R. Burgos, "Multimega var passive filters for mining applications: practical limitations and technical considerations," *IEEE Transactions on Industry Applications*, vol. 52, no. 6, pp. 5310-5317, Nov.-Dec. 2016.

[7] "IEEE recommended practice and requirements for harmonic control in electric power systems," *IEEE Std 519-2014 (Revision of IEEE Std 519-1992)*, vol., no., pp.1-29, June 2014.

[8] IEC/TR 61000-3-6, "Electromagnetic compatibility (EMC) – part 3-6: limits – assessment of emission limits for the connection of distorting installations to MV, HV and EHV power systems", *IEC*, Ed 2.0, 2008.

[9] IEC/TS 61000-3-4, "Electromagnetic compatibility (EMC) – part 3-4: limits - limitation of emission of harmonic currents in low-voltage power supply systems for equipment with rated current greater than 16 A", *IEC*, Ed 1.0, 1998.

[10] B. Singh, V. Garg and G. Bhuvaneswari, "A novel T-connected autotransformer-based 18-pulse AC–DC converter for harmonic mitigation in adjustable-speed

induction-motor drives," *IEEE Transactions on Industrial Electronics*, vol. 54, no. 5, pp. 2500-2511, Oct. 2007.

[11] Y. Yang, P. Davari, F. Zare and F. Blaabjerg, "Enhanced phase-shifted current control for harmonic cancellation in three-phase multiple adjustable speed drive systems," *IEEE Transactions on Power Delivery*, vol. 32, no. 2, pp. 996-1004, April 2017.

[12] R. Abdollahi and G. B. Gharehpetian, "Inclusive design and implementation of novel 40-pulse AC–DC converter for retrofit applications and harmonic mitigation," *IEEE Transactions on Industrial Electronics*, vol. 63, no. 2, pp. 667-677, Feb. 2016.

[13] R. C. Fernandes, P. da Silva Oliveira and F. J. M. de Seixas, "A family of autoconnected transformers for 12- and 18-pulse converters—generalization for delta and wye topologies," *IEEE Transactions on Power Electronics*, vol. 26, no. 7, pp. 2065-2078, July 2011.

[14] A. Mansoor, W. M. Grady, P. T. Staats, R. S. Thallam, M. T. Doyle and M. J. Samotyj, "Predicting the net harmonic currents produced by large numbers of distributed single-phase computer loads," *IEEE Transactions on Power Delivery,* vol. 10, no. 4, pp. 2001–2006, Oct. 1995.

[15] A. E. Emanuel, J. A. Orr, D. Cyganski and E. M. Gulachenski, "A survey of harmonic voltages and currents at the customer's bus," *IEEE Transactions on Power Delivery*, vol. 8, no. 1, pp. 411–421, Jan. 1993.

[16] H. Sharma, M. Rylander and D. Dorr, "Grid impacts due to increased penetration of newer harmonic sources," *IEEE Transactions on Industrial Application*, vol. 52, no. 1, pp. 99–104, Jan. 2016.

[17] D. Salles, C. Jiang, W. Xu, W. Freitas and H. E. Mazin, "Assessing the collective harmonic contribution of modern residential loads—part I: methodology," *IEEE Transactions on Power Delivery,* vol. 27, no.4, pp. 1937-1943, Oct. 2012.

[18] J. A. Pomilio and S. M. Deckmann, "Characterization and compensation of harmonics and reactive power of residential and commercial loads," *IEEE Transactions on Power Delivery,* vol. 22, no.2, pp. 1049-1055, Apr. 2007.

[19] K. D. McBee and M. G. Simoes, "Evaluating the long-term impact of a continuously increasing harmonic demand on feeder-level voltage distortion," *IEEE Transactions on Industrial Application*, vol. 50, no. 3, pp. 2142-2149, May 2014.

[20] R. Torquato, Q. Shi, W. Xu and W. Freitas, "A monte carlo simulation platform for studying low voltage residential networks," *IEEE Transactions on Smart Grid*, vol. 5, no. 6, pp. 2766-2776, Nov. 2014.

[21] Y. J. Wang, R. M. O'Connell and G. Brownfield, "Modeling and prediction of distribution system voltage distortion caused by nonlinear residential loads," *IEEE Transactions on Power Delivery*, vol. 16, no.4, pp. 744-751, 2001.

[22] J. Yong, L. Chen, and S. Chen, "Modeling of home appliances for power distribution system harmonic analysis," *IEEE Transactions on Power Delivery*, vol. 25, no.4, pp. 3147-3154, Oct. 2010.

[23] A. Tokić, A. Jukan and J. Smajić, "Parameter estimation of single-phase rectifier-based loads: analytical approach," *IEEE Transactions on Power Delivery*, vol. 31, no. 2, pp. 532-540, April 2016.

[24] N. Zhou, J. Wang, Q. Wang and N. Wei, "Measurement-based harmonic modeling of an electric vehicle charging station using a three-phase uncontrolled rectifier," *IEEE Transactions on Smart Grid*, vol. 6, no. 3, pp. 1332-1340, May 2015.

[25] Q. Shi, H. Hu, W. Xu, and J. Yong, "Low-order harmonic characteristics of photovoltaic inverters," *International Transactions on Electrical Energy Systems*, vol. 26, no. 2, pp. 347–364, Feb. 2016.

[26] S. Munir and Y. W. Li, "Residential distribution system harmonic compensation using PV interfacing inverter," *IEEE Transactions on Smart Grid*, vol. 4, no. 2, pp. 816-827, Mar. 2013.

[27] P. Bagheri, W. Xu and T. Ding, "A distributed filtering scheme to mitigate harmonics in residential distribution systems," *IEEE Transactions on Power Delivery*, vol. 31, no. 2, pp. 648-656, April 2016.

[28] P. Bagheri and W. Xu, "A technique to mitigate zero-sequence harmonics in power distribution systems," *IEEE Transactions on Power Delivery*, vol. 29, no. 1, pp. 215-223, Feb. 2014.

[29] M. S. Munir, Y. W. Li and H. Tian, "Improved residential distribution system harmonic compensation scheme using power electronics interfaced DGs," *IEEE Transactions on Smart Grid*, vol. 7, no. 3, pp. 1191-1203, May 2016.

[30] IEC 61000-3-2, "*Electromagnetic Compatibility (EMC) - part 3-2: limits - limits for harmonic current emissions (equipment input current ≤ 16 A per phase)*", *IEC*, Ed 4.0, 2014.

[31] S. B. Gin, J. H. Sawada and T. R. Treasure, "BC Hydro harmonic resonance experience," *2000 Power Engineering Society Summer Meeting* (Cat. No.00CH37134), Seattle, WA, 2000, pp. 1088-1093 vol. 2.

[32] R. K. Varma, S. A. Rahman, T. Vanderheide and M. D. N. Dang, "Harmonic contribution of a 20-MW PV solar farm on a utility distribution network," *IEEE Power and Energy Technology Systems Journal*, vol. 3, no. 3, pp. 89-98, Sept. 2016.

[33] G. M. Minamizaki, S. U. Ahn, G. L. Torres, L. E. Borges and N. C. Jesus, "Technical solutions for harmonic resonance at MV: relocatable capacitor bank technique," *2010 IEEE/PES Transmission and Distribution Conference and Exposition: Latin America* (T&D-LA), Sao Paulo, 2010, pp. 99-103.

[34] C. Boonseng, C. Chompoo-Inwai, V. Kinnares, K. Nakawiwat and P. Apiratikul, "Failure analysis of dielectric of low voltage power capacitors due to related harmonic resonance effects," *2001 IEEE Power Engineering Society Winter Meeting. Conference Proceedings* (Cat. No.01CH37194), Columbus, OH, 2001, pp. 1003-1008 vol.3.

[35] "IEEE guide for the application of shunt power capacitors," *IEEE Std 1036-2010 (Revision of IEEE Std 1036-1992)*, vol., no., pp.1-88, Jan. 17 2011.

[36] G. Lemieux, "Power system harmonic resonance-a documented case," *IEEE Transactions on Industry Applications*, vol. 26, no. 3, pp. 483-488, May/Jun 1990.

[37] S. H. E. Abdel Aleem, A. F. Zobaa and M. Mamdouh Abdel Aziz, "Optimal C-type passive filter based on minimization of the voltage harmonic distortion for nonlinear loads," *IEEE Transactions on Industrial Electronics*, vol. 59, no. 1, pp. 281-289, Jan. 2012.

[38] R. Horton, R. Dugan and D. Hallmark, "Novel design methodology for C-type harmonic filter banks applied in HV and EHV networks," in *Proc. 2012 IEEE PES T&D Conf. and Expo.*, May 2012, pp. 1-6.

[39] W. Xu, T. Ding, X. Li and H. Liang, "Resonance-free shunt capacitors—configurations, design methods and comparative analysis," *IEEE Transactions on Power Delivery*, vol. 31, no. 5, pp. 2287-2295, Oct. 2016.

[40] J. Játiva-Ibarra, G. Navarro-Méndez, F. L. Quilumba and W. J. Lee, "Field measurements, modeling, and analysis of power system harmonics caused by industrial customers," *2014 IEEE Industry Application Society Annual Meeting*, Vancouver, BC, 2014, pp. 1-13.

[41] P. Doyle, O. Burke and W. Phang, "Field measurements, modelling and simulation for harmonic analysis of a large industrial power system," *CIRED 2009 - 20th International Conference and Exhibition on Electricity Distribution - Part 1*, Prague, Czech Republic, 2009, pp. 1-4.

[42] W. Xu, R. Bahry, H. E. Mazin and T. Tayjasanant, "A method to determine the harmonic contributions of multiple loads," *2009 IEEE Power & Energy Society General Meeting*, Calgary, AB, 2009, pp. 1-6.

[43] M. Schael, C. Sourkounis, A. Rogat and C. Neumann, "Industrial electric grid evaluation regarding harmonics based on measurement data," *2016 International Symposium on Power Electronics, Electrical Drives, Automation and Motion (SPEEDAM)*, Anacapri, 2016, pp. 282-287.

[44] G. W. Chang, Y. J. Liu, H. M. Huang and S. Y. Chu, "Harmonic analysis of the industrial power system with an AC electric arc furnace," *2006 IEEE Power Engineering Society General Meeting*, Montreal, Quebec, 2006.

[45] K. Yu, N. Watson, and J. Arrillaga, "An adaptive Kalman filter for dynamic harmonic state estimation and harmonic injection tracking," *IEEE Transactions on Power Delivery*, vol. 20, no. 2, pp. 1577–1584, Apr. 2005.

[46] A. Kumar, B. Das, and J. Sharma, "Robust dynamic state estimation of power system harmonics," *International Journal of Electrical Power & Energy Systems,* vol. 28, no. 1, pp. 65-74, Jan. 2006.

[47] H. Liao, "Power system harmonic state estimation and observability analysis via sparsity maximization," *IEEE Transactions on Power Systems*, vol. 22, no. 1, pp. 15–23, Feb. 2007.

[48] C. F. M. Almeida and N. Kagan, "Harmonic state estimation through optimal monitoring systems," *IEEE Transactions on Smart Grid*, vol. 4, no. 1, pp. 467-478, Feb. 2013.

[49] D. Saxena, S. Bhaumik, and S. Singh, "Identification of multiple harmonic sources in power system using optimally placed voltage measurement devices," *IEEE Transactions on Industrial Electronics*, vol. 61, no. 5, pp. 2483–2492, May 2014.

[50] T. Pfajfar, J. Meyer, P. Schegner, and I. Papic, "Influence of instrument transformers on harmonic distortion assessment," *IEEE Power and Energy Society General Meeting,* San Diego, pp. 1-6, 22-26 July 2012.

[51] J. Hui, H. Yang, S. Lin and M. Ye, “Assessing utility harmonic impedance based on the covariance characteristic of random vectors,” *IEEE Transactions on Power Delivery,* vol. 25, no. 3, pp. 1778-1786, Jul. 2010.

[52] CSA C22.3 No.6-13, “Principles and practices of electrical coordination between pipelines and electric supply lines,” 2013.

[53] M. Ladjavardi and M. A. S. Masoum, "Genetically optimized fuzzy placement and sizing of capacitor banks in distorted distribution networks," *IEEE Transactions on Power Delivery*, vol. 23, no. 1, pp. 449-456, Jan. 2008.

[54] A. A. Eajal and M. E. El-Hawary, "Optimal capacitor placement and sizing in unbalanced distribution systems with harmonics consideration using particle swarm optimization," *IEEE Transactions on Power Delivery*, vol. 25, no. 3, pp. 1734-1741, July 2010.

[55] Y. Baghzouz and S. Ertem, "Shunt capacitor sizing for radial distribution feeders with distorted substation voltages," *IEEE Transactions on Power Delivery*, vol. 5, no. 2, pp. 650-657, Apr 1990.

[56] S. Segura, L. C. P. D. Silva, R. Romero and D. Salles, "Strategic capacitor placement in distribution systems by minimisation of harmonics amplification because of resonance," *IET Generation, Transmission & Distribution*, vol. 6, no. 7, pp. 646-656, July 2012.

[57] Y. Xiao, J. Zhao and S. Mao, "Theory for the design of C-type filter," *2004 11th International Conference on Harmonics and Quality of Power* (IEEE Cat. No.04EX951), 2004, pp. 11-15.

[58] ftp://www.pjm.com/planning/project-queues/arr-facilities-studies/s10_arr-fac.pdf

[59] P. Sinha, S. K. Goswami, S. Nath, “Wavelet-based technique for identification of harmonic source in distribution system,” *International Transactions on Electrical Energy Systems*, vol. 26, no. 12, pp. 2552-2572, Dec. 2016.

[60] E. Gursoy and D. Niebur, "Harmonic load identification using complex independent component analysis," *IEEE Transactions on Power Delivery*, vol. 24, no. 1, pp. 285-292, Jan. 2009.

[61] H. E. Mazin, W. Xu and B. Huang, "Determining the harmonic contributions of multiple harmonic-producing loads," *IEEE Transactions on Power Delivery*, vol. 26, no. 2, pp. 1187-1195, April 2011.

[62] X. Yan. Linear Regression Analysis: Theory and Computing. World Scientific, 2009.

[63] https://www2.ee.washington.edu/research/pstca/pf57/pg_tca57bus.htm

[64] P. Yang, Z. Tan, A. Wiesel and A. Nehorai, "Power system state estimation using PMUs with imperfect synchronization," *IEEE Transactions on Power Systems*, vol. 28, no. 4, pp. 4162-4172, Nov. 2013.

[65] M. Chenine and L. Nordstrom, "Modeling and simulation of wide-area communication for centralized PMU-based applications," *IEEE Transactions on Power Delivery*, vol. 26, no. 3, pp. 1372-1380, July 2011

[66] J. Yan, C. C. Liu and U. Vaidya, "PMU-based monitoring of rotor angle dynamics," *IEEE Transactions on Power Systems*, vol. 26, no. 4, pp. 2125-2133, Nov. 2011.

[67] J. Hui, W. Freitas, J. C. M. Vieira, H. Yang and Y. Liu, "Utility harmonic impedance measurement-based on data selection," *IEEE Transactions on Power Delivery*, vol. 27, no. 4, pp. 2193-2202, Oct. 2012.

[68] X. Zhao and H. Yang, "A new method to calculate the utility harmonic impedance based on FastICA," *IEEE Transactions on Power Delivery*, vol. 31, no. 1, pp. 381-388, Feb. 2016.

[69] F. Karimzadeh, S. Esmaeili and S. H. Hosseinian, "A novel method for noninvasive estimation of utility harmonic impedance based on complex independent component analysis," *IEEE Transactions on Power Delivery*, vol. 30, no. 4, pp. 1843-1852, Aug. 2015.

[70] Y. M. Liu, Li-Hong Wang, Xian-Yong Xiao, Ying Wang and Fei-Yu Chen, "Complex blind source separation based harmonic contribution assessment," *2016 17th International Conference on Harmonics and Quality of Power* (ICHQP), Belo Horizonte, 2016, pp. 176-180.

[71] https://nepsi.com/resource/Cost%20per%20kvar.pdf

[72] M. Ramalinga Raju, K.V.S. Ramachandra Murthy, K. Ravindra, “Direct search algorithm for capacitive compensation in radial distribution systems,” *International Journal of Electrical Power & Energy Systems*, vol. 42, no. 1, pp. 24-30, Nov. 2012.

[73] Nocedal J, Wright S J. Sequential quadratic programming. Springer New York, 2006.

[74] E. Bingham, A. Hyvarinen, “A fast fixed-point algorithm for independent component analysis of complex valued signals,” *International Journal of Neural Systems*, vo. 10, no.1, Feb. 2000.

Appendix

Appendix A Comparison of Design Methods

The resonance-free scheme proposed in Chapter 3 is built on the previous work in [39]. The improvement is not only a novel topology that saves one damping block, but also a new design method. Comparing the design method in Section 3.3 and the one in [39], it can be found two methods have three same design conditions and one different design condition. The same design conditions are 1) reactive power support, 2) resonance-free condition and 3) fundamental frequency loss minimization. The fourth condition in [39] is "condition of the inductive impedance". This condition is based on the following consideration: since the system impedance is more likely to be inductive than capacitive at various frequencies, it is advantageous to have a C-type filter that exhibits inductive impedance above its tuning frequencies. However, the guarantee of the inductive impedance does not mean that the resonance-free capacitor can behave like a filter. For example, if the resonance-free capacitor is equivalent to a very large resistor, it cannot significantly reduce the system harmonic distortion. Therefore, this design condition may not be mandatory as its actual performance on harmonic reduction is unknown. Instead, the proposed design method selects the fourth condition more flexibly, i.e., application dependent. In this thesis, the fourth design condition is chosen to be "cost minimization" as the cost is always an important concern for both the utility and the customer. Following two tables compares the performance of two design methods using the case described in Section 3.4.1. Table A.1 compares the voltage THD at substation SX when two different design methods are applied. As seen from the table, the design method in [39], i.e. condition of the inductive impedance, does not lead to a lower voltage THD. Table A.2 compares the cost of C-type damping blocks when two different design methods are applied. Using the proposed design method leads to 17% cost saving in case #1 and 29% cost saving in case #2. Hence, it can be concluded that

the proposed design method is more advantageous.

Table A.1 Comparison of resultant voltage THD using different design methods

voltage THD	Case #1		Case #2		
Scenario	#1	#2	#3	#4	#5
The proposed design method	2.9%	2.8%	3.2%	3.0%	3.0%
Design method in [39]	3.1%	3.0%	3.3%	3.3%	3.3%

Table A.2 Comparison of C-type damping block cost using different design methods

Cost ($)	Case #1	Case #2
The proposed design method	96,413	115,453
Design method in [39]	115,560	163,160

The future research may consider other design conditions, such as “harmonic loss minimization” and “harmonic voltage minimization”, in the proposed design method. If these two design conditions are applied, the system impedance information is required to calculate the harmonic loss and the harmonic voltage.

Appendix B Derivation of Design Equations

This section of appendix presents the derivations of the design procedure developed in Section 3.3.

B.1 Frequency to Rach Maximum HAR_{worst}

This subsection presents the method to find the frequency that reaches the maximum HAR_{worst}. If the maximum HAR_{worst} is below the defined limit, the resonance-free performance can be guaranteed.

Let

$$F(\omega) = X_Z(\omega) / R_Z(\omega) \tag{B.1}$$

According to (3.7), $HAR_{\text{worst}}(\omega) = \sqrt{1+F^2(\omega)}$. It is straightforward that $HAR_{worst}(\omega)$ reaches the maximum when $F(\omega)$ achieves one of its extrema. Therefore, the solve of the frequency to reach maximal HAR_{worst} is transformed

into the solve of the frequency to reach extrema of $F(\omega)$. According to (3.12), $F(\omega)$ equals to

$$F(\omega) = (a_1\omega^4 + b_1\omega^2 - 1) / (\omega RC_1(\omega^2 LC_2 - 1)^2) \tag{B.2}$$

The derivative of $F(\omega)$ with respect to ω is given by

$$F'(\omega) = (d\omega^6 + e\omega^4 + g\omega^2 - 1) / (\omega^2 RC_1(\omega^2 LC_2 - 1)^3) \tag{B.3}$$

where

$$\begin{cases} d = L^3C_2^3 - R^2L^2C_2{}^3C_1 \\ e = 3R^2LC_2{}^3 - 3L^2C_2{}^2 \\ g = R^2C_2{}^2 + R^2C_1C_2 + 3LC_2 \end{cases}.$$

As can be seen from (B.3), the denominator of $F'(\omega)$ is always larger than zero and the $F(\omega)$ achieves its extrema when the numerator of $F'(\omega)$ is zero. So, the frequency that reaches the maximum HAR_{worst} can be obtained by solving the following equation,

$$G(p) = dp^3 + ep^2 + gp - 1 = 0 \tag{B.4}$$

where $p = \omega^2$. This is a cubic equation and its analytical root can be easily obtained by using Cardano's method. There must be three roots with either one or three real roots. Once p is obtained, ω can be calculated as $\sqrt{p}$. The root of ω should be abandoned if it is a complex number or a real number but smaller than ω_T. The remained roots are defined as the set ω_e. Since ω_T is a boundary point, it should be included in ω_e as well. Once ω_e is obtained, the resonance-free performance can be guaranteed if $HAR(\omega_e)$ is smaller than the HAR_{limit}.

B.2 Establish of Search Range

This section develops a method to establish the search range of L and R in order to improve the search efficiency. The range is defined based on the frequency response at the tuning frequency (e.g. 5th harmonic). This is due to the

consideration that a C-type damping block provides better damping performance at high frequencies. As a result, the range established by the low-order tuning frequency is relatively narrow.

According to (3.12), the worst-case amplification ratio at the tuning frequency ω_T is

$$HAR_{worst}(\omega_T) = \sqrt{1+(\frac{R^2T - S(R^2+T^2)}{RT^2})^2} \tag{B.5}$$

where $T = \omega_T L - \omega_F^2 L/\omega_T$ and $S = 1/(C_1\omega_T)$. If the HAR_{limit} is selected to be λ, (B.5) must be smaller than λ, which leads to (B.6).

$$|\frac{R^2T - S(R^2+T^2)}{RT^2}| \le \delta \tag{B.6}$$

where $\delta = \sqrt{\lambda^2 - 1}$. Eq. (B.6) is equivalent to the condition (B.7) and (B.8).

$$(T-S)R^2 - \delta T^2 R - ST^2 \le 0 \tag{B.7}$$

$$(T-S)R^2 + \delta T^2 R - ST^2 \ge 0 \tag{B.8}$$

By solving (B.7) and (B.8), the search range of R can be established as following,

$$\begin{cases} \dfrac{\delta T^2 - \sqrt{\Delta_1}}{2(S-T)} \le R \le \dfrac{\delta T^2 + \sqrt{\Delta_1}}{2(S-T)} & \text{if } T < S, \\ \dfrac{-\delta T^2 + \sqrt{\Delta_2}}{2(T-S)} \le R \le \dfrac{\delta T^2 + \sqrt{\Delta_2}}{2(T-S)} & \text{if } T > S, \\ R \ge \dfrac{S}{\delta} & \text{if } T = S. \end{cases} \tag{B.9}$$

where $\Delta_1 = \delta^2 T^4 - 4ST^2(S-T)$ and $\Delta_2 = \delta^2 T^4 + 4ST^2(T-S)$. The search range of L can be established by the condition of $\Delta_1 \ge 0$ (Δ_2 is always greater than zero), which lead to

$$L \geq \frac{-2S + \sqrt{4S^2 + 4S^2\delta^2}}{\delta^2(\omega_T - \omega_F^2 / \omega_T)} \tag{B.10}$$

Since S has more than one values due to multiple capacitor energization scenarios, multiple ranges of R and L can be obtained. The final range of R can be determined as the intersection of those ranges and the final search range of L can be defined as,

$$L_{\min} = \frac{-2S_{\max} + \sqrt{4S_{\max}^2 + 4S_{\max}^2\delta^2}}{\delta^2(\omega_T - \omega_F^2 / \omega_T)} \tag{B.11}$$

Appendix C Cost Estimation for RLC components

The capacitor cost is assumed to be directly proportional to its capacity, as the HV capacitor is normally constructed by numbers of basic capacitor units. The per MVar cost is assumed to be $5,000 [56][71][72].

The inductor and resistor at the HV level are always custom-made. Their cost cannot be assumed to be proportional to the capacity. Instead, we quoted the cost of the inductor and resistor from the manufacturers. Table C.1 shows the quotations of four dry-type air-core inductors. It is clear the cost of the inductor is not proportional to its capacity. For example, the capacity of "150mH-120A" inductor is four times of "150mH-60A" inductor, but the cost of the former one is only 50% higher.

Table C.1 Quotations of inductors from the manufactures

Inductor	1st	5th	7th	11th	13th	17th	19th	Cost ($)
150mH-60A	60A	11A	4.2A	2.3A	1.5A	1.0A	1.2A	10350
150mH-120A	120A	8A	3.5A	2.2A	1.4A	0.8A	1.1A	15150
240mH-40A	40A	7.5A	3.1A	1.6A	1.1A	0.7A	0.8A	9950
240mH-120A	120A	4.1A	2.1A	1.4A	1.0A	0.6A	0.7A	19660

Based on the quotations above, it is useful to establish the correlation between the capacity of the inductor and its cost. There are three different definitions of the

reactive power when harmonic currents are considered. The first one is the fundamental reactive power, defined as $Q_1 = V_1 I_1$. The second one is the total reactive power, defined as $Q = \sum_{h=1,2..} V_h I_h$. It adds up the reactive powers at different frequencies. The third one is the nonactive power, defined as $N = V_{rms} I_{rms}$. This power lumps together both fundamental and nonfundamental nonactive components. According to Table C.2, the coefficient of determination (r^2) is one for all three correlation studies. This indicates all three definitions of reactive powers can be used to estimate the cost. This thesis uses the total reactive power Q to estimate the inductor cost.

Table C.2 Correlation study between inductors' reactive power and cost

Inductor	Q_1(MVar)	Q(MVar)	N(MVar)
150mH-60A	0.2036	0.2552	0.3342
150mH-120A	0.8143	0.8436	0.9166
240mH-40A	0.1448	0.1821	0.2443
240mH-120A	1.3028	1.3178	1.3627
Correlation	Cost=8336*Q_1+8639	Cost=8539*Q+8236	Cost=8702N+7561
r^2	1.0	1.0	1.0
Sum of Residuals	554.8	659.6	1011.2

Table C.3 shows the quotation of three damping resistors. It is clear the cost of the resistor is also not proportional to its capacity. For example, the capacity of "500ohm-15A" resistor is roughly four times of "500ohm-8A" resistor, but the cost of the former one is only slightly higher. The correlation between the resistor's capacity and the resistor's cost is Cost=61005*P(MW)+11356. The coefficient of determination (r^2) is 0.95.

Table C.3 Quotations of resistors from the manufactures

Resistor	1000ohm-5A	500ohm-8A	500ohm-15A
Cost ($)	12180	14070	18158

Appendix D Alternative Topology – 3rdHP Damping Block

This section of appendix investigated the performance of the 3rdHP damping block in the proposed resonance-free scheme (Chapter 3). Section D.1 develops the design method. Comparative studies are conducted in Section D.2. Finally, sample lookup tables of component parameters are calculated in Section D.3.

D.1 Design Method

A 3rdHP damping block in Figure D.1 has three components: the auxiliary capacitor C_2, the tuning inductor L and the damping resistor R. Its configuration is similar as the C-type damping block. Instead of tuning L and C_2 at the fundamental frequency to reduce the loss, the 3rdHP damping block inserts C_2 into R branch, which increases the impedance of that branch at the fundamental frequency and thus reduces the fundamental frequency loss of R. The design conditions of the proposed scheme using 3rdHP damping block are listed below.

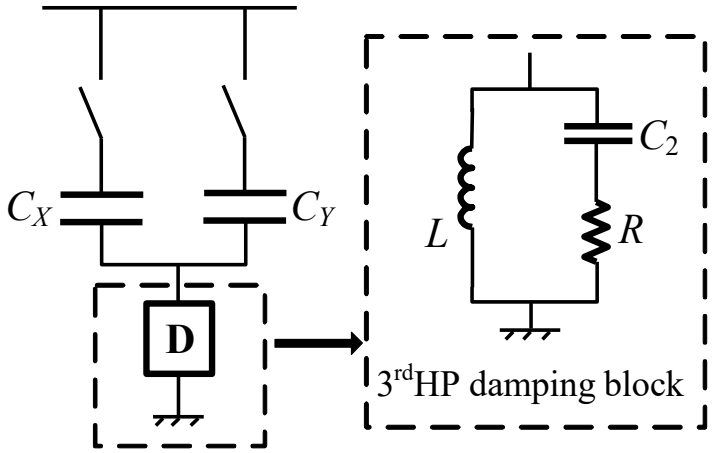

Figure D.1The proposed resonance-free scheme with 3rdHP damping block

- **Condition 1:** reactive power support

At the fundamental frequency, the equivalent impedance of the entire shunt device is dominated by the main capacitors. Hence, the reactive power output of

the entire shunt device is mainly determined by C_X and C_Y. This feature yields the first design equation (D.1):

$$C_X = Q_{FX} / (\omega_F V_r^2), C_Y = Q_{FY} / (\omega_F V_r^2) \tag{D.1}$$

where ω_F is the fundamental angular frequency, V_r is the rated system voltage, Q_{FX} and Q_{FY} are the required reactive power for C_X and C_Y, respectively.

- **Condition 2:** resonance-free condition

The 3rdHP damping block should guarantee all capacitor energization scenarios (i.e. C_X on, C_Y on and C_X & C_Y both on) to be resonance free. This condition leads to the second design equation (D.2).

$$HAR_{\text{worst}}(\omega, C_1, C_2, L, R) \le HAR_{\text{limit}}, \quad \text{for } \omega \ge \omega_T \tag{D.2}$$

where C_I=[C_X, C_Y, C_X||C_Y], ω_T is the tuning frequency which normally can be selected as 3rd or 5th harmonic, and

$$HAR_{worst}(\omega, C_1, C_2, L, R) = \sqrt{1 + (\frac{a_2\omega^4 + b_2\omega^2 - 1}{RL^2C_2^2C_1\omega^5})^2} \tag{D.3}$$

$$\begin{cases} a_2 = R^2LC_2^2C_1 - L^2C_2C_1 - L^2C_2^2 \\ b_2 = LC_1 - R^2C_2^2 + 2LC_2 \end{cases} \tag{D.4}$$

- **Condition 3:** fundamental frequency loss limit

To reduce the operating cost, the fundamental frequency loss of the entire shunt device should be limited under a certain level, as shown in (D.5). In this section, P_{limit} is set to be 1% of the total reactive power.

$$P_{Floss}(C_1, C_2, R, L) = \frac{V_r^2 R_F(\omega_F)}{R_F(\omega_F)^2 + X_F(\omega_F)^2} \le P_{\text{limit}} \tag{D.5}$$

where ω_F is the fundamental angular frequency and

$$\begin{cases} X_F(\omega) = \dfrac{a_2\omega^4 + b_2\omega^2 - 1}{(\omega^2(RC_2)^2 + (\omega^2 LC_2 - 1)^2)\omega C_1} \\ R_F(\omega) = \dfrac{RL^2 C_2{}^2 \omega^4}{\omega^2(RC_2)^2 + (\omega^2 LC_2 - 1)^2} \end{cases} \tag{D.6}$$

- **Condition 4:** cost minimization

Above three conditions are the basic requirements for the proposed scheme with 3rdHP damping block. If only those three constraints are applied, there would be thousands of solutions. As a result, one more constraint is required to select the final parameter. The fourth design condition can be application dependent. To be consistent with the design method of the C-type damping block (Section 3.3), we adopt the cost minimization as the fourth design condition. Regarding a 3rdHP damping block, the fundamental current mainly flows through L, thus the capacity of L is much larger than C_2 and R. When the reactive power requirement of the main capacitor is given, the larger inductance of L, the greater of its capacity. If the inductance of L can be reduced to the minimum, the total investment of the block is assumed to be the least. Thus, the cost minimization function is to minimize the inductance of L.

$$\text{Cost minimization:} \quad \min(L) \tag{D.7}$$

- Design procedure

Among the four design conditions, only C_X and C_Y can be determined using (D.1). The problem is a three-variable (L, C_2 and R) optimization problem, which tries to find the minimum L that satisfies HAR_{limit} with acceptable fundamental frequency loss. The formulation of the design problem, complying with the previous constraints, is presented as follows

Objective function: $F = \min_{L, C_2, R}(L)$

Subject to:

- $C_X = Q_{FX} / (\omega_F V_r^2), C_Y = Q_{FY} / (\omega_F V_r^2)$

- $P_{Floss}(C_1, C_2, R, L) = \dfrac{V_r^2 R_F(\omega_F)}{R_F(\omega_F)^2 + X_F(\omega_F)^2} \le P_{\text{limit}}$

- $HAR_{\text{worst}}(\omega, C_1, C_2, L, R) \le HAR_{\text{limit}}$, for $\omega \ge \omega_T$

Since there are three variables in this optimization problem, scanning all feasible values could be time-consuming. Instead, advanced optimization algorithms are suggested. In this thesis, sequential quadratic programming (SQP) [73] is adopted to solve this problem.

D.2 Comparative Case Study

In this section, comparative case studies are presented for evaluating the effectiveness of the proposed scheme. Detailed system description and case illustration can be found in Section 3.4.1.

D.2.1 Performance and Cost Comparison of Case #1

In case #1, two 15MVar capacitors are connected to substation SX. There are two capacitor energization scenarios in this case.

1) Scenario #1 – one 15MVar capacitor on,

2) Scenario #2 – two 15MVar capacitors on.

The proposed design methods are applied to determine the parameters for the conventional scheme and the proposed scheme. The resonance-free condition is selected as HAR_{limit}=1.2 and the tuning frequency is f_T=300Hz (i.e., 5th harmonic). This study compares the resonance-mitigation performance, power loss and cost.

a) Resonance-mitigation performance

Figure D.2 shows the harmonic voltage amplification caused by two schemes. As can be seen from the figure, the proposed scheme with 3rdHP damping block can guarantee the resonance-free performance for both two capacitor energization scenarios and its actual HARs for most harmonic orders are below 1.0.

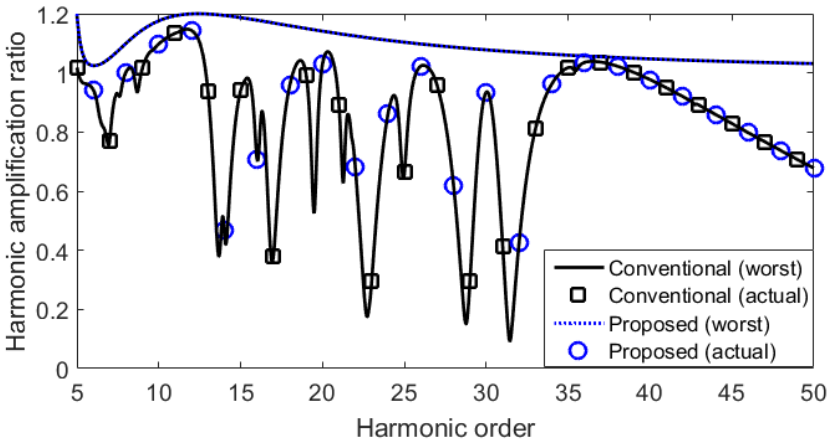

(a) Scenario #1

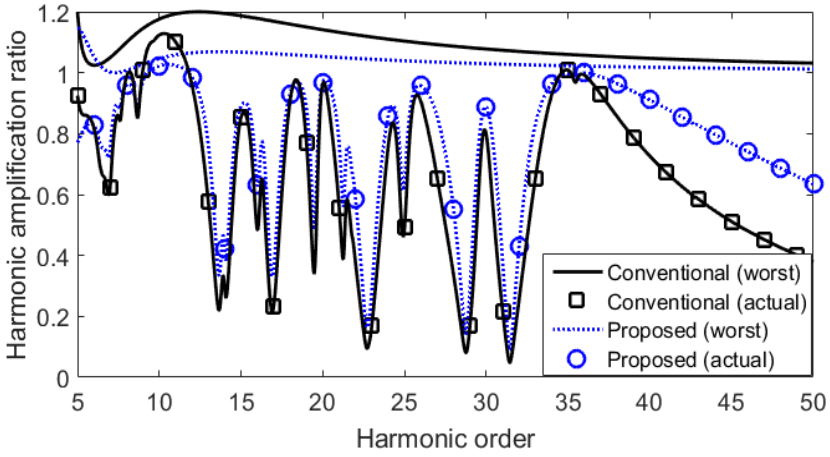

(b) Scenario #2

Figure D.2 HARs of two schemes with 3rdHP damping block (case #1)

Figure D.3 gives the voltage spectra at substation SX for installation scenarios: 1) no capacitor; 2) pure capacitors; 3) the conventional scheme (3rdHP damping block); and 4) the proposed scheme (3rdHP damping block). According to the results, the pure capacitor could cause significant voltage distortion at this substation, while using the proposed scheme would lead to a slight decrease of the harmonic voltages. The harmonic reduction performance of the proposed scheme is comparable with that of the conventional scheme.

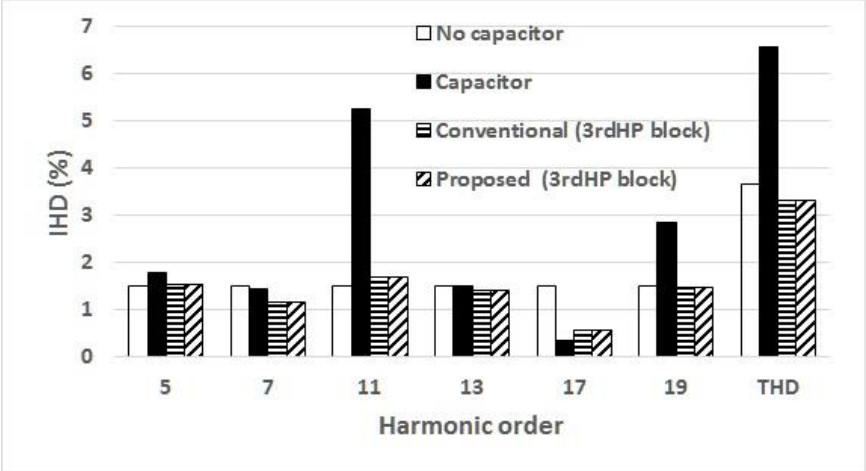

(a) Scenario #1

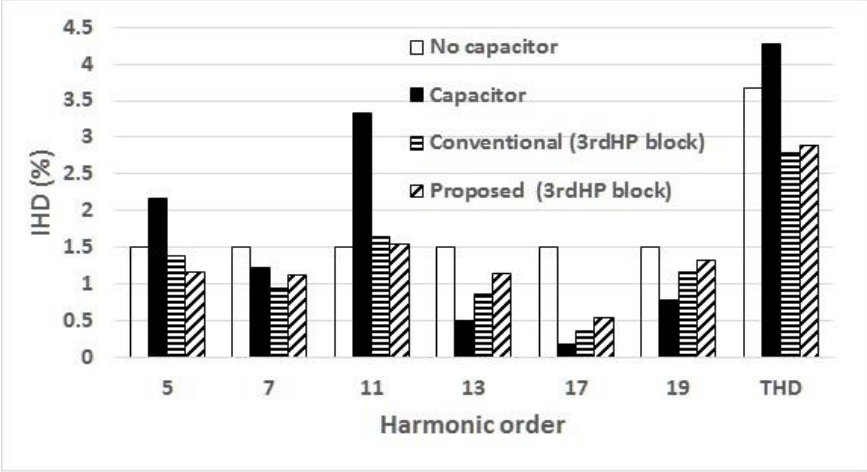

(b) Scenario #2

Figure D.3 Voltage spectra at SX for different installation scenarios (case #1).

b) Cost comparison

Table D.1 compares the parameters and loadings of two schemes with 3rdHP damping block. The conventional scheme has two same 3rdHP damping blocks, denoted as DP #1 and DP #2 that designed for two15MVar capacitors (C_X and C_Y). The proposed scheme only needs one 3rdHP damping block, denoted as DP #3. According to the table, the values of R, L, C_2 are exactly same in two schemes. This finding confirms the conjecture in Section 3.2 that the parameters of the damping block of the proposed scheme are mainly determined by the smallest main capacitor (15MVar). In terms of the loading conditions of two schemes, the

fundamental current flowing through the 3rdHP damping block is determined by the main capacitor (C_X & C_Y), so the current flowing through L in DP #3 is roughly double of that in DP #1 (or DP#2). The harmonic current flowing through the 3rdHP damping block is mainly determined by the 3rdHP damping block itself. Therefore, the current flowing though C_2 and R in DP #1 is almost equal to that in DP #1 (or DP #2).

Table D.1 Comparison of parameters and loadings of two schemes with 3rdHP damping block (case #1)

Main capacitor		Conventional (C_X or C_Y)	Proposed (C_X or C_Y)
C_1	Value (uF)	1.92	1.92
	Voltage (kV)	147.17	150.33
	Current (A)	63.14	63.14
3rdHP damping block		Conventional (DP #1 or DP #2)	Proposed (DP #3)
C_2	Value (uF)	2.47	2.47
	Voltage (kV)	4.88	7.06
	Current (A)	15.65	15.65
L	Value (mH)	75.00	75.00
	Voltage (kV)	6.15	7.90
	Current (A)	65.30	129.65
R	Value (Ω)	137.88	137.88
	Voltage (kV)	3.74	3.74
	Current (A)	15.65	15.65

With the information of parameters and loadings, the cost is then compared for each component:

- C_1: The loading and cost of C_1 are same for two schemes.
- C_2: The capacity of C_2 in the proposed scheme is smaller than that of the conventional scheme, so the cost of C_2 in the proposed scheme is lower.
- L: The inductance of L in DP #3 is equal to that in DP #1 (or DP #2), but the current rating of L in DP #3 is doubled. At the HV level, the increase of the inductor's capacity does not significantly increase its cost. According to the quotations of manufacturers, the cost of the inductor in the proposed scheme is lower than two inductors in the conventional scheme.

- *R*: The loading of *R* in DP #3 is exactly equal to that in DP #1 (or DP #2). The proposed scheme saves one resistor, so its expense on *R* is half.

Table D.2 shows the expenses of two schemes on 3rdHP damping blocks based on the quotations from the manufacturers. As can be seen from the table, the component cost of the proposed scheme is roughly half of the conventional scheme.

Table D.2 Cost of 3rdHP damping blocks in two schemes (case #1)

	Conventional ($)	Proposed ($)	Relative cost (p.u.)
C_2	1,002	547	0.55
L	57,640	37,647	0.65
R	80,494	40,247	0.50
Total	139,134	78,440	0.56

c) Power loss comparison

Table D.3 compares the power loss of two schemes with 3rdHP damping block. Two schemes have the same loss in scenario #1 due to the same 3rdHP damping block parameters. In scenario #2, the proposed scheme has higher fundamental frequency loss. The reason is as following. When C_X and C_Y are both on, the fundamental current flowing through *R* of the proposed scheme becomes double, so the fundamental frequency loss is four times of that in scenario #1. Regarding the conventional scheme, the fundamental frequency loss in scenario #2 is doubled with one more capacitor and 3rdHP damping block switched on. This finding suggests that the fundamental frequency loss of the proposed scheme increases exponentially with the reactive power output, while the fundamental frequency loss of the conventional scheme increases linearly with the reactive power output. The harmonic loss is lower for the proposed scheme in scenario #2. This is because the equivalent harmonic impedance of the entire shunt device is mainly determined by the 3rdHP damping block. In scenario #2, the conventional scheme with two paralleled 3rdHP damping blocks has smaller harmonic impedances. A smaller shunt impedance results in higher harmonic loss.

Additionally, it can be found that the reactive power output of the proposed

scheme is slightly larger than the required amount. This is because Q_{FX} and Q_{FY} in (D.1) are assumed as the reactive power of the main capacitor rather than the entire shunt device. The reactive power of the entire shunt device, therefore, is slightly larger than the required amount due to L.

Table D.3 Power loss comparison of two schemes with 3rdHP damping block (case #1)

		Conventional		Proposed	
Scenario		I	II	I	II
Reactive power (MVar)		15.76	31.47	15.65	32.69
Power loss (kW)	Fundamental frequency	1.12	2.23	1.12	4.69
	Harmonic frequencies	100.16	140.46	100.16	86.25
	Total	101.28	142.69	101.28	90.94
	% loss (of total MVar)	0.31	0.45	0.31	0.28

d) Summary of case #1 study

Through the comparison of resonance-mitigation performance, economic performance and power loss performance, some key findings are summarized for case #1 study.

- The proposed scheme has comparable resonance-mitigation performance as the conventional scheme.
- Compared with the conventional scheme, the proposed scheme has clear advantages in cost.
- The proposed scheme has lower harmonic loss but higher fundamental frequency loss than that of the conventional scheme.

D.2.2 Performance and comparison of Case #2

In case #2, one 10MVar capacitor and one 20MVar capacitor are connected to substation SX. There are three capacitor energization scenarios in case #2.

1) Scenario #3 – 10MVar capacitor on,

2) Scenario #4 – 20MVar capacitors on.

3) Scenario #5 – both 10MVar capacitor and 20MVar capacitor on.

The proposed design methods are applied to determine the parameters for the conventional scheme and the proposed scheme. The resonance-free condition is selected as HAR_{limit}=1.2 and the tuning frequency is f_T=300Hz (i.e., 5th harmonic). This study compares the resonance-mitigation performance, power loss and cost.

a) Resonance-mitigation performance

Figure D.4 shows the harmonic voltage amplification caused by two schemes with 3rdHP damping block. The proposed scheme can guarantee the resonance-free performance for all three capacitor energization scenarios and its actual HARs for most harmonic orders are below 1.0.

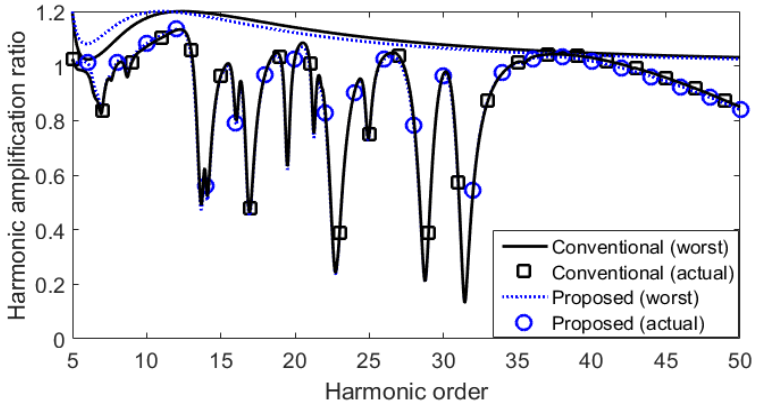

(a) Scenario #3

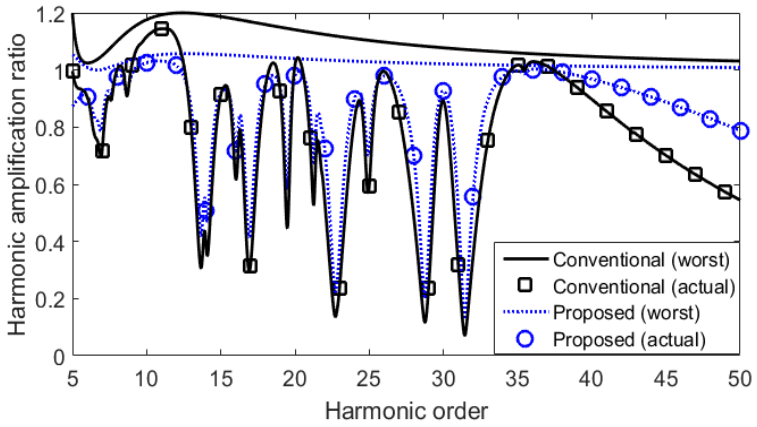

(b) Scenario #4

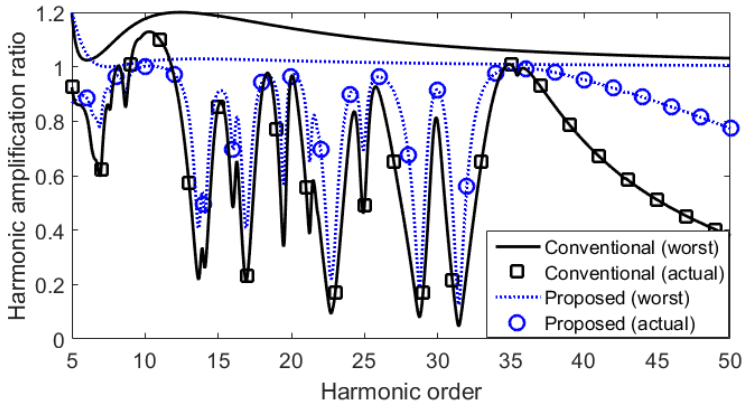

(c) Scenario #5

Figure D.4 HARs of two schemes with 3rdHP damping block (case #2)

Figure D.5 gives the voltage spectra at substation SX for different installation scenarios. As can be seen from three figures, the proposed scheme and the conventional scheme have similar harmonic reduction performances.

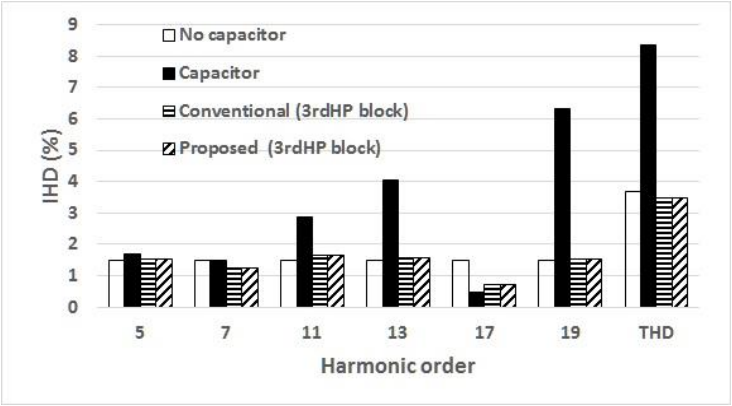

(a) Scenario #3

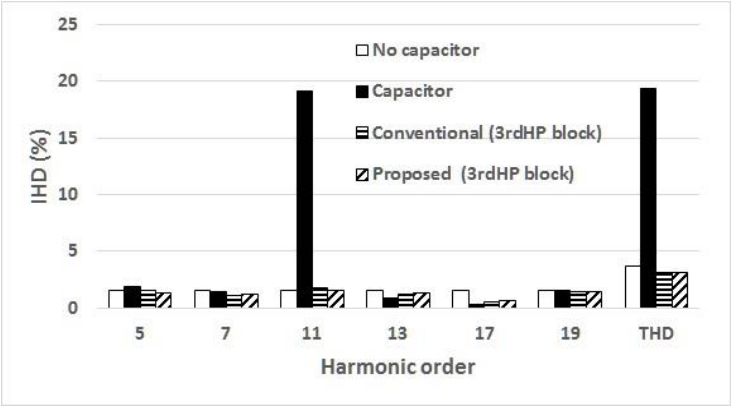

(b) Scenario #4

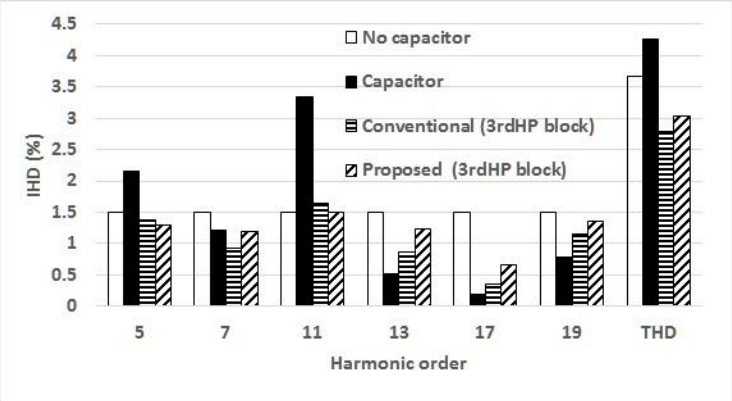

(c) Scenario #5

Figure D.5 Voltage spectra at SX for different installation scenarios (case #2)

b) Cost comparison

Table D.4 shows the parameters and loading conditions of two schemes. In case #2, the conventional scheme requires two different 3rdHP damping blocks, denoted as DP #4 and DP #5 that designed for the 10MVar capacitor (C_X) and the 20MVar capacitor (C_Y), respectively. The proposed scheme only needs one 3rdHP damping block, denoted as DP #6. According to the table, the parameters of DP #4 and DP #6 are very close. This finding, again, confirms the conjecture that the parameters of the damping block of the proposed scheme are mainly determined by the smallest main capacitor. In terms of the loading condition, the current flowing through L in DP #6 is three times of that in DP #4, as L in DP #6 need to carry the current of both main capacitors. The harmonic current flowing through R and C_2 is mainly determined by the 3rdHP damping block itself. Consequently, the loading condition of R and C_2 in DP #6 is close to that in DP #4.

Table D.4 Comparison of parameters and loadings of two schemes with 3rdHP damping block (case #2)

Main capacitor		Conventional		Proposed	
		C_X	C_Y	C_X	C_Y
C_1	Value (uF)	1.28	2.56	1.28	2.56
	Voltage (kV)	147.18	147.17	154.00	154.00
	Current (A)	42.18	83.97	42.99	85.97
3rdHP damping block		Conventional		Proposed	
		DP #4	DP #5	DP #6	
C_2	Value (uF)	1.64	3.29	1.92	

	Voltage (kV)	4.96	4.78	10.29
	Current (A)	10.88	19.78	11.03
L	Value (mH)	112.50	56.30	115.30
	Voltage (kV)	6.31	5.95	11.04
	Current (A)	43.59	86.90	132.97
R	Value (Ω)	206.83	103.41	210.00
	Voltage (kV)	3.90	3.54	4.01
	Current (A)	10.88	19.78	11.03

With the information of parameters and loadings, the cost is then compared for each component.

- C_1: The loading and cost of C_1 in the proposed scheme is slightly higher due to the overcompensation caused by L.
- C_2: The capacity of C_2 in the proposed scheme is smaller than that of the conventional scheme, so the cost of C_2 is lower for the proposed scheme.
- L: The capacity of L in the proposed scheme is approximately three times of that in the conventional scheme, while this ratio is roughly two in case #1. Therefore, the relative cost of L becomes higher in case #2.
- R: The loading of R in DP #6 is roughly equal to that in DP #4. The proposed scheme saves one resistor, so its expense on R is roughly half.

Table D.5 shows the expenses of two schemes on 3rdHP damping blocks based on the quotations from the manufacturers. As can be seen from the table, the total cost of the proposed scheme increases from $78,440 to $84,174 due to the higher rating of L. Nevertheless, the total cost of the proposed scheme is still 40% lower than that of the conventional scheme.

Table D.5 Cost of 3rd HP damping blocks in two schemes (case #2)

	Conventional ($)	Proposed ($)	Relative cost (p.u.)
C_2	972	578	0.59
L	57,572	44,851	0.78
R	80,017	38,745	0.48
Total	138,561	84,174	0.61

c) Power loss comparison

Table D.6 compares the power loss of two schemes. Two schemes have comparable loss in scenario #3 due to the similar 3rdHP damping block parameters. In scenario #4 and scenario #5, the proposed scheme has higher fundamental frequency loss. The reason has been explained in case #1. Harmonic loss is lower for the proposed scheme in scenario #4 and scenario #5, as the proposed scheme has larger equivalent harmonic impedances in these two scenarios.

Table D.6 Power loss comparison of two schemes with 3rdHP damping block (case #2)

		Conventional			Proposed		
Scenario		#3	#4	#5	#3	#4	#5
Reactive power (MVar)		10.43	20.87	31.30	10.45	21.85	34.31
Power loss (kW)	Fundamental frequency	0.74	1.49	2.23	1.09	4.54	10.69
	Harmonic frequencies	72.6	119.9	140.5	70.8	70.9	66.0
	Total	73.4	121.4	142.7	71.9	75.5	76.7
	% loss (of total MVAr)	0.25	0.40	0.48	0.24	0.25	0.26

d) Summary of case #2 study

Through the comparison of resonance-mitigation performance, economic performance and power loss performance, some key findings are summarized for case #2 study.

- In case #2, the proposed scheme still has comparable resonance-mitigation performance as the conventional scheme.
- Compared with case #1, the cost of the proposed scheme in case #2 becomes slightly higher due to the higher rating of L.
- In case #2, the proposed scheme still has higher fundamental frequency loss and lower harmonic loss than that of the conventional scheme.

D.2.3 Sensitivity Study

The subsection presents the sensitivity study results. The studies are related to

following parameters: HAR_{limit}, tuning frequency and background voltage distortion. Since the resonance-free performance must be guaranteed by the proposed scheme, this sensitivity study focuses on the cost performance, the power loss performance and the overcompensation performance.

a) HAR_{limit}

The impact of HAR_{limit} selection on the cost, the power loss and the overcompensation are presented in Figure D.6. According to those three figures, all performances (except for the harmonic loss) become worse with the decrease of HAR_{limit}. It is not very feasible to select HAR_{limit} lower than 1.1 due to the high fundamental frequency loss and the severe overcompensation.

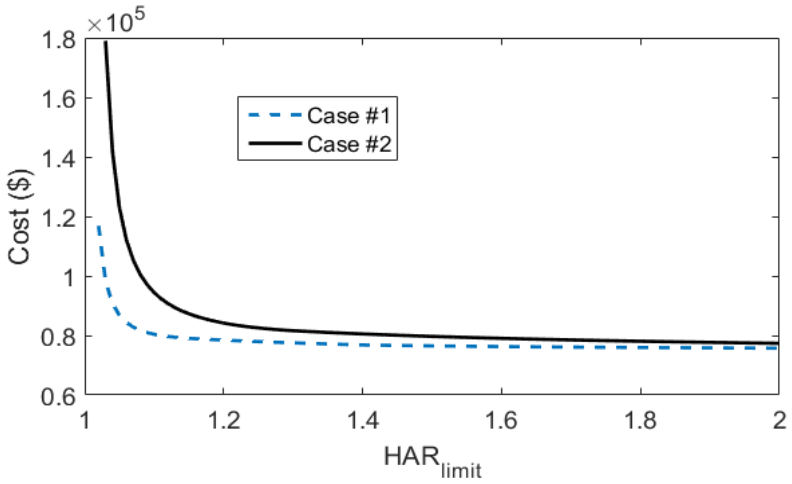

(a) Cost

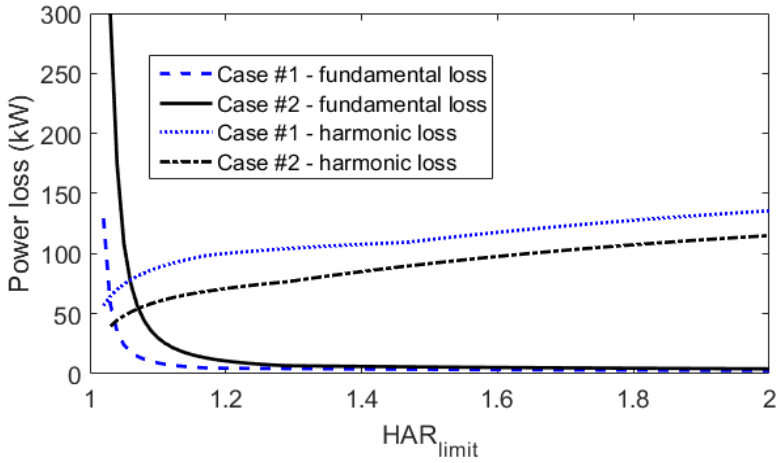

(b) Power loss

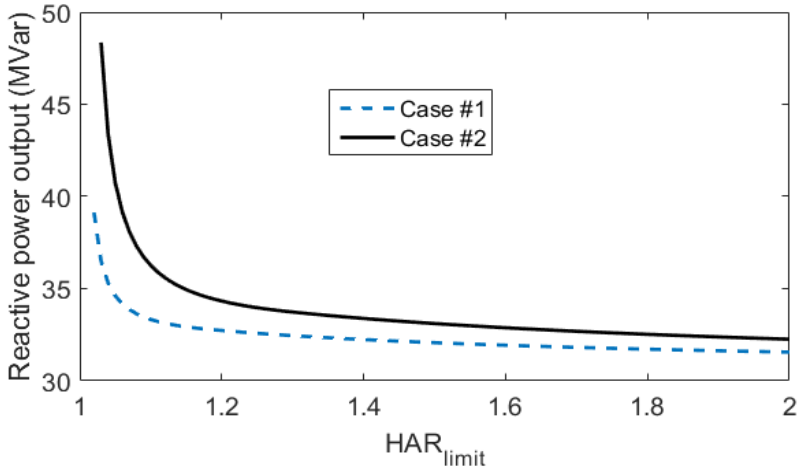

(c) Reactive power output (rated at 30MVar)

Figure D.6 The impact of HAR_{limit}

b) Tuning frequency

Table D.7 shows the performances of two schemes with different tuning frequencies. According to the table, the fundamental frequency loss becomes high and the overcompensation issue becomes severe when the capacitor is tuned to the 3rd harmonic instead of the 5th harmonic. Therefore, if the capacitor has to be tuned to the 3rd harmonic, the C-type damping block is a better option.

Table D.7 Performance comparison with different tuning frequencies

	Case #1		Case #2	
Tuning frequency	3rd	5th	3rd	5th
Cost ($)	113,243	78,440	158,956	84,174
Fundamental frequency loss (kW)	76.00	4.67	196.49	10.69
Harmonic loss (kW)	65.85	100.16	50.23	70.90
Overcompensation (MVar)	8.94	2.73	15.76	4.33

c) Background voltage distortion

In case #1 and case #2, the background voltage distortion is assumed to be 1.5% from 5th to 19th harmonics according to IEEE 519 limit. It is straightforward that the component cost and the harmonic loss will increase with the background voltage distortion. The correlation is shown in Figure D.7. The results in these two figures are obtained by simultaneously changing the voltage

distortion at each harmonic frequency.

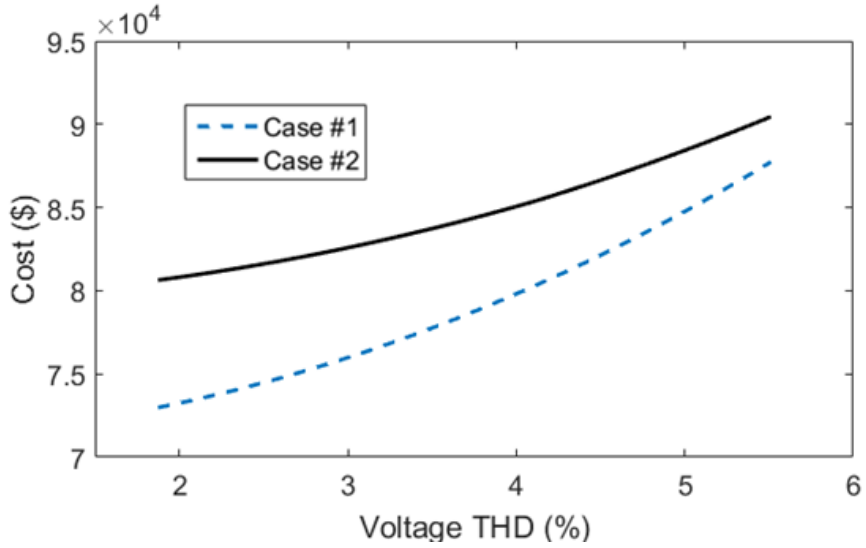

(a) Component cost

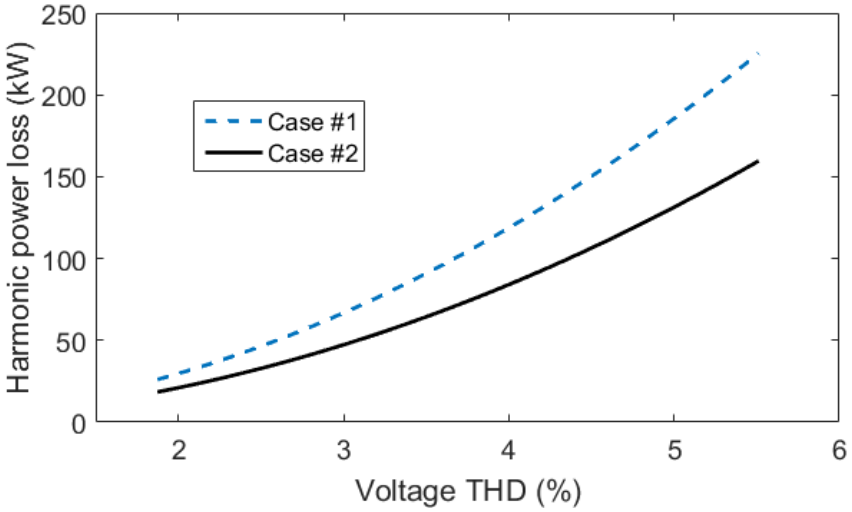

(b) Harmonic loss

Figure D.7 The impact of background harmonic voltage

D.2.4 Comparison with C-type damping block

Through the case studies and sensitivity studies, the performances of the 3rdHP damping block in the proposed scheme have been evaluated. Its performance is compared with that of the C-type damping block in this subsection, as shown below.

1) Both two topologies can guarantee the resonance-free performance for multiple switchable capacitors. According to the comparison in Table D.8, using C-type damping block leads to slightly lower voltage THD.

Table D.8 Comparison of voltage THD at substation SX

THD	Case #1		Case #2		
	Scenario #1	Scenario #2	Scenario #3	Scenario #4	Scenario #5
C-type	2.95%	2.79%	3.17%	3.04%	3.03%
3rdHP	3.33%	2.88%	3.46%	3.11%	3.03%

2) The component cost is lower for the 3rdHP damping block, as shown in Table D.9. This is due to the smaller parameter of 3rdHP damping block.

Table D.9 Comparison of the cost of two damping blocks

Cost ($)	Case #1	Case #2
C-type	96,413	115,453
3rd HP	78,440	84,174

3) C-type damping block has better performance in power loss. According to Table D.10, the fundamental frequency loss and the harmonic loss are both lower for C-type damping block in all cases and scenarios.

Table D.10 Comparison of the power loss of two damping blocks

		Case #1		Case #2		
	Scenario	#1	#2	#3	#4	#5
Fundamental loss (kW)	C-type	0	0	0	0	0
	3rd HP	1.12	4.69	1.09	4.54	10.69
Harmonic loss (kW)	C-type	70.62	55.24	52.7	47.8	42.4
	3rd HP	101.28	90.94	71.9	75.5	76.7

4) Using 3rdHP damping block brings the overcompensation issue. It is necessary to check if the design parameters would lead to an unacceptable reactive power output. If yes, one may consider to adjust the value of the main capacitor to reduce the reactive power. This would make the design process more complicated.

5) There are some limitations for the application of the 3rdHP damping block. For the case that the capacitor needs to be tuned to the 3rd harmonic or HAR_{limit} needs to be very small, it is not attractive to use the 3rdHP damping block due

to high fundamental frequency loss and the severe overcompensation.

In summary, C-type damping block has better performance while the component cost of 3rdHP damping block is lower.

D.3 Lookup Table for Component Parameters

Sample lookup tables for normalized component parameters have been created and are shown in Table D.11 and Table D.12. Two tables list the parameters for the tuning frequency f_T=300Hz (i.e., 5th harmonic) and f_T=180Hz (i.e., 3rd harmonic) under three HAR_{limit} values, respectively. The capacity ratio (Cap_{ratio}) in tables indicates the ratio of the capacity of two capacitors. The value of C_1 in tables is the value of the capacitor with smaller capacity. The usage of the lookup table can be found in Section 3.5.

Table D.11 Lookup table for per-unit component parameters (tuning frequency f_T=300Hz)

			Capacity Ratio (Cap_{ratio})		
			1.0	1.5	2.0
HAR_{limit}	1.1	C_1	1.0000	1.0000	1.0000
		C_2	1.2873	1.4259	1.4972
		L	0.0246	0.0268	0.0288
		R	0.1308	0.1366	0.1421
	1.2	C_1	1.0000	1.0000	1.0000
		C_2	1.2846	1.3896	1.4976
		L	0.0205	0.0206	0.0210
		R	0.0998	0.1000	0.1013
	1.5	C_1	1.0000	1.0000	1.0000
		C_2	1.9164	1.9157	1.9150
		L	0.0154	0.0154	0.0154
		R	0.0630	0.0630	0.0630

Table D.12 Lookup table for per-unit component parameters (tuning frequency f_T=180Hz)

			Capacity Ratio (Cap_{ratio})		
			1.0	1.5	2.0
HAR_{limit}	1.1	C_1	1.0000	1.0000	1.0000
		C_2	1.2873	1.4660	1.6336
		L	0.0684	0.0723	0.0734
		R	0.2180	0.2214	0.2171
	1.2	C_1	1.0000	1.0000	1.0000
		C_2	1.2843	1.3896	1.4976
		L	0.0568	0.0571	0.0583
		R	0.1662	0.1667	0.1687

1.5	C_1	1.0000	1.0000	1.0000
	C_2	1.9174	1.9165	1.9156
	L	0.0428	0.0428	0.0428
	R	0.1051	0.1051	0.1051

Appendix E Independent Component Analysis

ICA is a powerful algorithm for BSS problem, which can extract independent original signals from the measured signals. The linear mixing model of ICA is given as [74],

$$x_{M\times T} = A_{M\times N} s_{N\times T} \tag{E.1}$$

where x is the measured signals, s is the original signals, A is the linear mixing matrix, N denotes the dimensional of unknown source signals, M denotes the dimensional of measured signals, T denotes the number of samples.

What ICA can do is to estimate both the mixing matrix A and the original signals s by using the measured signals x. Since ICA is based on the statistical properties of signals, some requirements for the original and measured signals need to be satisfied: 1) the original signals s are statistically independent; 2) at most one of the original signals is Gaussian distributed; 3) the number of measured signals M is greater or equal to the number of original signals N.

In this work, one most popular ICA algorithm called Complex FastICA is utilized. The algorithm is illustrated in Figure E.1. This procedure shows an iterative process to maximum the non-gaussianity of the original sources, which can be understood as the independence of the original sources. The non-gaussianity is measured by a smooth even function G. The explanation of other symbols in Figure E.1 are as follows: E denotes the statistical expectation, w_p for p=1,…,M are the columns of matrix W, an w^H is the hermitian transpose of vector w, $g(y)=dG(y)/dt$ and $g'(y)=dg(y)/dt$. A more detailed description of Complex FastICA can be found in [74].

1). Start from p=1.

2). Set a random vector for w_p

3). Calculate w_p:

$$w_p = E\left\{x(w^H x) * g(|w^H x|^2)\right\} - E\left\{g(|w^H x|^2) + |w^H x|^2 \; g'(|w^H x|^2)\right\} w$$

4). Orthogonalize w_p:

$$w_p = w_p - \sum_{j=1}^{p} (w_p w_j^H) w_p$$

5). Normalize w_p:

$$w_p^{new} = w_p / \| w_p \|$$

6). If not converged ($\sum \| w_p^{new} | - | w_p \| > \varepsilon$), set $w_p = w_p^{new}$ and go back to step 3. If converged, set p=p+1 and go back to step 2.

Figure E.1The procedure of Complex FastICA algorithm